UNIVERSITY OF CALGARY

Human Patellofemoral Kinematics and Related Joint Surface Geometry

by

Marilyn Joy Powers

A THESIS

SUBMITTED TO THE FACULTY OF GRADUATE STUDIES

IN PARTIAL FULFILLMENT OF THE REQUIREMENTS FOR THE

DEGREE OF MASTER OF SCIENCE

DEPARTMENT OF MECHANICAL AND MANUFACTURING ENGINEERING

CALGARY, ALBERTA

SEPTEMBER, 1999

Abstract

Abnormal patellofemoral tracking has been implicated in the presence of patellofemoral pain syndrome and osteoarthritis. However, results from normal PF studies indicate large inter-limb variability. It is speculated that this variability may be explained with detailed knowledge of the underlying surface geometries. This study presents an externally loaded, dynamic in-vitro leg extension model to collect continuous kinematic data through a range of motion. Cartilage surface data were collected using the multi-station digital photogrammetry (MDPG) technique and represented using a thin plate spline algorithm. Kinematics and surface plots were input into a mathematical model to investigate joint contact. The patellae rotated and shifted laterally with increasing knee flexion with varying magnitudes. Patellar tilt was variable with most limbs exhibiting medial then lateral tilt. Abnormal PF tracking was not always correlated with abnormal contact characteristics. The complex joint contact mechanics were governed by both joint surface geometries and kinematics.

Acknowledgements

I would like to express my sincere thanks to:

My supervisor, Dr. Janet Ronsky, for her support, guidance and enthusiasm for research.

Dr. Ron Zernicke and Dr. Bob Bray for taking the time to serve on my examining committee.

Zubin Canteenwalla for his extensive assistance in preparing the experiments and collecting the data.

Kent Paulson, Jessica Maurer, Rebecca Moss, Nicole Baker, Barbara Kralovic, Carol Scovil, Jeff Smithanik and Claire Davies for their help during those long days of data collection.

Derek Lichti for his help with the photogrammetry and bundle adjustment protocols and programs.

Steve Boyd and Barbara Kralovic for their help in understanding the digitizing and surface fitting programs.

Byron Tory for his help with all my computer problems.

Warren Lyons in the anatomy lab for accomodating my requests and Sam, for teaching me 'old Indian tricks'.

Nicole Baker, Daniel Sennhauser, Romona Corbiell and Jessica Maurer for their help in preparing this manuscript.

Rebecca Moss, Jessica Maurer, Nicole Baker, Jennifer Henderson, Sandee , Joe Lafort, Romona Corbiel and Daniel Sennhauser for creating a fun office environment.

Janos for his love and encouragement and for conviently leaving town when I really needed to get work done.

My parents for their understanding and encouragement.

Jessica Barnes for giving me an image to live up to and trying to understand why anyone would go to school for this long.

Table of Contents

List of Tables

List of Figures

List of Abbreviations

ACL	Anterior Cruciate Ligament
ACS	Anatomical Coordinate System
AKP	Anterior Knee Pain
CMM	Coordinate Measurement Machine
DLT	Direct Linear Transformation
EM	Extensor Mechanism
EVA	Expert Vision Analysis (software)
FCS	Femur Coordinate System
JCS	Joint Coordinate System
LCL	Lateral Collateral Ligament
LCS	Lab Coordinate System
MAS	Motion Analysis System
MCL	Medial Collateral Ligament
MDPG	Multi-Station Digital Photogrammetry
MRI	Magnetic Resonance Imaging
MTS	Materials Testing System
PCL	Posterior Cruciate Ligament
PCS	Patella Coordinate System
PF	Patellofemoral
PFPS	Patellofemoral pain syndrome
RCS	Ring Coordinate System
rms	Root Mean Square
ROM	Range of Motion
RSA	Roentgen Stereophotogrammetric Analysis
RSP	Roentgen Stereophotogrammetry
SCS	Segment Coordinate System
TCS	Tibia Coordinate System
TPS	Thin Plate Spline

1 Introduction

Characterization of normal and abnormal patellofemoral joint mechanics has been the goal of an abundance of research over the past century. If fact, 163 years ago, Malgaigne stated that "When one searches among the past or present authors for the origins of the doctrines generally accepted today concerning dislocation of the patella, one is surprised to find among them such disagreement and such a dearth of facts with such an abundance of opinions." (Reider et al., 1981). The complexity of the knee joint has presented a plethora of clinical disorders including patellofemoral pain syndrome, patellar instability and complete degeneration of the articular cartilage due to osteoarthritis requiring total joint replacement. (Fulkerson and Hungerford, 1990)

Anterior knee pain (AKP) is one of the most common musculoskeletal disorders affecting adults (Bray and Roth, 1987). The term AKP is used to describe pain arising from the anterior aspect of the knee that may be caused by any of the surrounding structures of the knee as well as the patella itself and includes such problems as patellofemoral pain syndrome and patellar instability. The etiology of AKP is however unclear, making diagnosis and treatment difficult. Possible etiologic pathologies could be divided into four groups: 1) abnormalities in the quadriceps muscle and other soft tissue surrounding the knee joint such as quadriceps tendinitis and fat pad syndrome, (2) abnormalities of the knee alignment (Q-angle, varus/ valgus angle), (3) abnormalities of the shape of the patella and (4) abnormalities of the shape of the femoral condyles (Reider et al., 1981). An underlying commonality amongst these abnormalities is the presence of altered patellofemoral tracking (Reider et al., 1981). Therefore, an understanding of the mechanics of the normal knee joint function and the interaction of the mechanics and joint surface geometries, is necessary for the diagnosis of

abnormal patellofemoral tracking.

In-vivo analysis of patellofemoral tracking through traditional gait analysis with skin mounted markers is not feasible due to inaccuracies associated with skin marker movement. Some researchers have quantified in-vivo knee kinematics (Koh et al. 1992, Lafortune et al. 1992) using invasive bone pin techniques. This method is not feasible for a larger number of subjects which is necessary for characterizing general patellofemoral kinematics. MRI provides a non-invasive, in-vivo alternative to accurately quantify joint surfaces (Ronsky 1994), but incorporation of dynamic loading remains difficult and it remains expensive. Recently, Sheehan et al. (1999) presented a method of quantifying patellofemoral joint kinematics in a dynamic motion using the MRI. However, this technique did not provide sufficient resolution to quantify the joint surface geometry. Due to these limitations most patellofemoral kinematic information and insights to date have been obtained from in-vitro approaches.

Patella movement relative to the femur has been characterized in three dimensions (3D). Four classifications are used to describe this motion: patellar flexion (rotation about the medial/lateral axis), patellar tilt (rotation about the longitudinal axis), patellar rotation (rotation about the anterior/posterior axis) and patellar shift (translation along the medial/ lateral axis) (Reider et al., 1981, van Kampen and Huiskes, 1990). The remaining two degrees of freedom are patellar anterior/posterior translation and inferior/superior translation. These translations are predominantly prescribed by the femoral condylar anatomy and can generally be described by patellar flexion. Therefore they are not reported individually in this study.

Several studies have quantified the normal 3D, in-vitro, patellofemoral kinematics with

variable results (Reider 1981, van Kampen and Huiskes 1990, Hefzy 1992). Reider et al. (1981) reported two distinctly different types of tracking in a study of 20 limbs taken through a quasi-static range of motion from 90° flexion to full extension. Type I (17 limbs) knees exhibited lateral shift and tilt as well as medial rotation, whereas type II knees (3 limbs) exhibited medial patella shift, almost no tilt (slightly medial) and medial rotation.

Van Kampen and Huiskes (1990) were the first to quantify the effects of tibial rotation on 3D patellar tracking in an in-vitro human model. Roentgen stereophotogrammetry was used to measure the relative bone positions of the knee, which was mounted in a six-degree-of-freedom device. The knee joints were taken through a quasi-static range-of-motion from full extension to 140° of flexion at increments of 15°. Four specimens were tested, of which at least three demonstrated similar trends in each variable. They found that the patella exhibited a wavering tilt, medial rotation and lateral patellar shift with increasing knee flexion, and that tilt and shift were most influenced by tibial rotations. They suggested that patellar shift was coupled with patellar tilt and that patellar rotations were coupled with the varus/valgus rotations of the tibia.

Hefzy and coworkers (1992) investigated the effects of tibial rotation on patellofemoral motion and contact areas. They tested four specimens in a quasi-static knee extension motion through approximately 90°, using force applied to the quadriceps tendon. They found that the patella tilted more medially and rotated medially with internal tibial rotation and tilted more laterally and rotated laterally with external tibial rotation. The patella exhibited very little shift but was slightly lateral. Like van Kampen and Huiskes (1990) they found that tibial rotations affected tilt in the first 30° of knee flexion and rotation between 60-90° of knee flexion.

Nagamine et al. (1995) tested eleven cadaver limbs using a mechanical measurement and loading apparatus. The sensitivity of patellar kinematics due to alterations of coordinate axis orientation, quadriceps force and direction of pull, and tibial rotations were tested all while keeping the varus/valgus rotation of the tibia within 1°. They also found two types of tracking patterns. However, in the two that they classed abnormal, pre-test evaluation showed that they had a laterally placed tibial tubercle. They found that the magnitude of the quadriceps force had no influence on patellar tracking patterns. Their results were in agreement with those of van Kampen and Huiskes (1990) and Reider (1981).

These studies have provided some important insights into normal patellar tracking, however, there still exist some discrepancies in what is characterized as 'normal' patellar tracking. Limitations of these studies include: quasi-static movement of the knee joint angle, and an unloaded knee joint, which does not reflect the physiologic condition. Nonetheless, there is good agreement in the literature that tibial rotations influence patellar tracking patterns.

Joint surface geometries may play an important role in the interaction between the patella and the femur. This interaction is a function of the congruity (i.e. similarity of surface curvatures) between the two surfaces. Similar curvatures of the two opposing surfaces allow load through the joint to be distributed over a larger region corresponding to contact area. For surfaces with very different curvatures, load may be transmitted through a localized area, resulting in higher stresses on the articular surfaces and possibly greater inherent instability.

The ability of the patella to articulate freely with the femur depends largely on the curvatures of the two surfaces. A highly curved trochlea would constrain a similarly curved patella. However, if the trochlea were relatively flat, the patella would be free to rotate and

shift throughout knee flexion, placing larger demands on the surrounding soft tissues to actively stabilize the patella. This could lead to strain and weakness of the tissues, further compromising their ability to stabilize the joint. Detailed knowledge of the surface geometries and articulation of the patella and femur, through all flexion angles, may be important factors when understanding the intricate puzzle of patellofemoral kinematics.

Characterizing surface geometries requires several steps: 1) experimental acquisition of surface data points, 2) mathematical representation of the surface and 3) mathematical modelling to determine curvature, contact area and articular sulcus angles.

The experimental acquisition of surface data has been done using both mechanical and optical methods (e.g. Hefzy et al. 1992, Ateshian et al. 1991, Ronsky et al., 1999). Optical methods are advantageous in comparison to mechanical methods because the surface remains unaltered during data collection. Huiskes et al. (1995) used analytical, close-range photogrammetry to obtain surface measurements of the femoral condyles and tibial plateau. This method involved the acquisition of 2D images of the surfaces which were later digitized and reconstructed into 3D space. Ateshian et al. (1991) developed this method further, obtaining an accuracy of 90 μm. Boyd (1997) introduced multi-station digital photogrammetry, based on similar principles to stereophotogrammetry, obtaining surface data of the cat patellofemoral joint with an accuracy of 25 μm. This method is easily adaptable to any joint size and permits a short (<30 min.) data acquisition time.

Mathematical representation of the articular surface requires fitting experimental data points to a theoretical model (section 2.6.4). Limitations involved in this process are a direct result of the distribution of the experimental data points. B-splines (Ateshian et al., 1993) allow the representation of all the data points in a single equation, unlike bi-cubic surface

patches (Huiskes et al., 1985). However, this method requires equally spaced data points in a complete grid form. The thin plate spline (Boyd, 1997) utilizes a cloud of randomly spaced data points to create a continuous surface, which is ideal for calculating further surface characteristics such as curvatures.

Combining the kinematic data with the surface geometries, results in a mathematical joint model. This model can then be manipulated to determine specific curvatures, contact characteristics and topological features. Several authors (e.g. Ateshian et al., 1994, Boyd, 1997, Ronsky, 1999) have successfully employed joint surface models to quantify joint contact areas, cartilage thickness and joint congruity.

Specific geometry is an intrinsic component of the mechanics of patellofemoral tracking. It is hypothesized that abnormal contact areas will relate to abnormal patellofemoral kinematics and that external axial loading will significantly alter the kinematics of the patellofemoral joint. It is further hypothesized that abnormal tracking characteristics can be directly associated with unique features of the articulating joint surface geometry. The incorporation of patellofemoral kinematics, specific joint geometry and contact area characteristics into a model, will allow the specific features of tracking to be correlated with the articulating surface geometry at a precise location.

Therefore the objectives of this study are to 1) relate geometry characteristics, e.g. curvatures, articular sulcus angles, to kinematic variables of patellar tracking throughout a range of knee joint motion, and 2) to relate contact area and centroid of contact area location to specific joint surface geometries.

The specific aims of this study are to:

1) Obtain 3D patellofemoral kinematics for normal healthy joints.

2) Develop a method of loading the knee to emulate external loading.

3) Determine the articular surface geometries of the patella and femur.

4) Use contact models to relate the surface geometries of the patella and femur to the patellofemoral kinematics determined in Specific Aims 1 and 2.

This thesis begins with a review of literature relevant to the quantification of human patellofemoral kinematics and surface geometries. The methods used for data collection, processing and analysis are then presented followed by the results found in this study. Finally the discussion will summarize the results and discuss their relevancy and significance.

2.0 Review of Literature

The articulation of the patella with the femur is controlled by several mechanisms. Muscle forces, ligamentous constraints, neurological control, synovial fluid lubrication and bony articulations are just a few of the factors that affect the motion of the knee joint. All of these factors work together in a complex system to maintain a healthy balance. Breakdown or damage of these factors alters the normal function of the knee. This could result in pain, a change in kinematics and possibly degeneration of the articular surfaces. This thesis will examine the mechanical aspects of knee joint motion and more specifically, the relationship between patellar tracking and the underlying joint geometry.

The following review of literature provides a generalized background for three main aspects for this study. Firstly, a brief overview of the patellofemoral joint anatomy and biomechanical function will be presented. Secondly, relevant studies involving patellar tracking will be examined. Finally, current methods of acquiring specific joint geometries will be discussed.

2.1 The Knee Joint

Knee joint motion is prescribed by the interaction of several biological structures; bone, cartilage, ligaments, tendons, muscle and other soft tissues such as the retinaculum and IT band. The articulating surfaces of the femur, patella and tibia consist of articular cartilage which in combination with synovial fluid, permit a relatively frictionless contact surface. Extreme range of motion of the tibia relative to the femur is constrained by four ligaments. The medial collateral ligament (MCL) and the lateral collateral ligament (LCL) prevent the femur from translating medially or laterally with respect to the tibia and prevent varus/valgus

motion of the knee. The anterior cruciate ligament (ACL) prevents the posterior translation of the femur with respect to the tibia whereas the posterior cruciate ligament (PCL) prevents the anterior motion of the femur relative to the tibia. The patella, a sesamoid bone which articulates with the femur, is controlled by two tendonous structures attached to the superior pole (the quadriceps tendon) and the inferior pole of the patella (the patella tendon). The patella tendon inserts into the tibial turbercle just below the proximal central end of the tibia. The patella articulates only with the femur. However, patellar motion is influenced by motion of the tibia, through the tibial insertion. The quadriceps muscle group (rectus femoris, vastus lateralis, vastus medialis and the vastus intermedius) converges at the quadriceps tendon working as a whole to extend the knee (Figure 2-1). Its main direction of pull is through the rectus femoris which inserts continuously from the superior pole of the patella over the entire anterior surface. The rectus intermedius inserts over the largest area of the superior edge of the patella. The vastus medialis inserts on the superior medial end of the patella and vastus lateralis along the superior lateral edge of the patella. (Fox and Del Pizzo, 1993)

The articular surface geometry of the patella and femur are of primary interest in this study. The retropatellar surface consists of four main areas (Figure 2-2). There are two main facets, the medial facet and the lateral facet. These facets are separated by a distinct ridge that runs along the longitudinal axis of the patella. Some patellae have equal sized facets, however, most patellae exhibit a larger lateral facet (Fulkerson and Hungerford, 1990). The medial facet also has an odd facet which is a much smaller facet that runs along the medial border of the patella. It can be distinguished by a secondary ridge, smaller than that between the medial and lateral facets, that is mainly cartilagenous. Thus, this secondary ridge is not apparent on the bone surface. This facet also varies greatly between individuals (Fulkerson

and Hungerford, 1990).

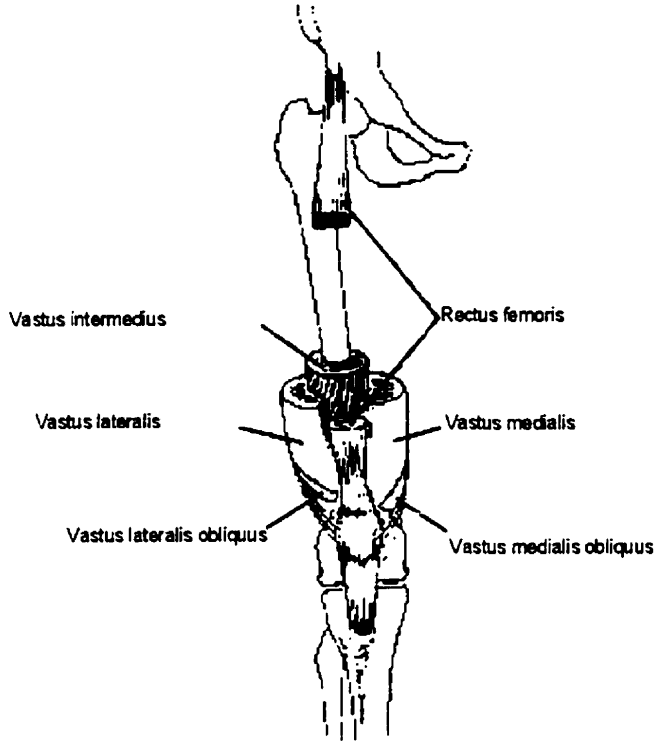

Figure 2-1 The anatomy of the knee joint. Adapted from Fox and Del Pizzo, 1993.

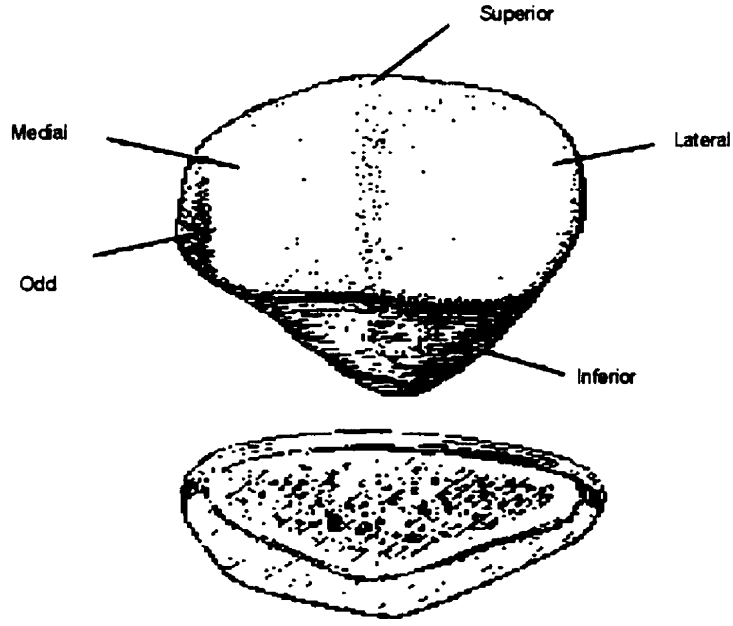

Figure 2-2 General topology of the patella articular cartilage surface. Adapted from Fox and Del Pizzo, 1993.

The articular surface of the femur consists mainly of the trochlea, which is also referred to as the patellar groove or femoral sulcus. This groove is situated between the two condylar facets of the femur, the medial and lateral condylar facets. The groove eventually deepens posteriorly to become the intercondylar notch. The lateral facet of the femur commonly extends further anteriorly than the medial facet (Fulkerson and Hungerford, 1990). A lateral notch or fat pad forms beyond the cartilage surface of the proximal femur which the patella articulates with during full extension.

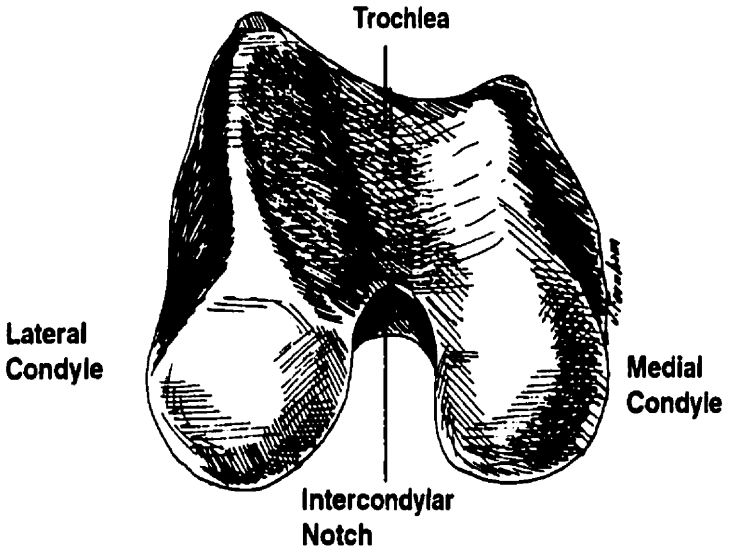

Figure 2-3 Femoral Articular Surface Anatomy adapted from Norkin and Levangie (1983).

2.2 The Function of the Patella in Joint Mechanics

The function of the patella in patellofemoral joint biomechanics is complex and its importance has been subject to debate (Fox and Del Pizzo,1993). The primary function of the patella is to transmit extension forces from the femur to the tibia (Fulkerson and Hungerford, 1990). The quadriceps muscle group converges on the superior end of the patella. This

centralizes the muscle forces and allows the patella to function as a guide in transmitting those forces to the patella tendon.

The patella also acts as a fulcrum to effectively increase the moment arm of the quadriceps tendon (Fox and Del Pizzo,1993). In order to extend the knee joint, a force must be generated from the femur and transferred to the tibia. An efficient force would pull anteriorly on the tibia. The patella achieves this by increasing the angle at which the patella tendon inserts into the tibia. This effectively increases the moment arm of the force vector created by the quadriceps muscle. As the joint angle changes so does the joint centre and therefore the moment arm. At full extension it has been shown that the patella contributes roughly 31% to the extension moment arm force. Between 90° and 120 °of flexion however, it contributes to only 13% of the extension moment arm (Kaufer 1979).

The patella also functions as protection for the patella tendon. Tendons, being very capable of transmitting tensile load, respond poorly to friction and compression. The patella, with its morphology consisting of trabecular bone and articular cartilage, is capable of distributing compressive loads while retaining a low coefficient of friction (Fulkerson and Hungerford, 1990).

The function of the patella became more apparent when patellectomies were readily performed for diseased patellae. Patients with patellectomies often presented with several problems including quadriceps atrophy, instability, extension lag, decreased flexion range, decreased stance phase flexion, decreased knee extension power and chronic effusion (Kaufer 1979). Thus, it is evident that the patella plays an essential role in maintaining an efficient extensor mechanism and adequate stability of the knee joint.

2.3 Clinical Problems of the Patellofemoral Joint

The patellofemoral joint is the site of many disorders such as subluxation, excessive lateral pressure syndrome and patellofemoral pain syndrome. Causes of these various pathologies are diverse. Abnormalities of patellar and trochlear topology or shape, termed dysplasia, are often associated with patellofemoral pain. However, not all dysplasias present with pain, and having normal morphology does not guarantee freedom from disease (Fulkerson and Hungerford, 1990). Wiberg's (1941) work classified three types of patellofemoral joints of which type III is considered dysplastic although there was no evidence to suggest that chondromalacia occurred more frequently in this type. Deformations of the trochlear contours have been associated with patellar instability and chondromalacia (Fulkerson and Hungerford, 1990). Patella tilt/compression is characterized by chronic lateral tilt of the patella. This pathology often leads to arthrosis on the lateral facet within the first 30° of flexion. Patellar subluxation is a condition in which the patella shifts off the lateral condyle causing pain and instability. Permanent lateral subluxation could arise from several conditions such as: dysplastic anatomy, abnormal mechanics which repetitively stretch or injure the medial stabilizers, or from trauma (Fulkerson and Hungerford, 1990). Anterior knee pain is often associated with malalignment of the patella (Fulkerson and Hungerford, 1990). However, the distinction between normal alignment and malalignment is not well characterized in the literature.

Abnormal mechanics as a result of these clinical problems could lead to the degeneration of the articular cartilage. In several cases, Fulkerson and Hungerford (1990) cite malalignment or abnormal tracking as a likely cause of cartilage degeneration, resulting in soft tissue stretching or shortening. It is speculated that altered patellar tracking results in

altered patellofemoral contact areas, which, under the same loading conditions, would lead to altered stress on the cartilage. It is unclear however, what causes the patella to become malaligned. It is important therefore, to characterize the normal tracking of the patella and the interaction of mechanical components that may influence tracking (i.e. specific joint geometry).

2.4 Quantifying Joint Kinematics

Knowledge of joint kinematics may provide important insights into the role of the patella in patellofemoral (PF) mechanics. Quantifying joint kinematics requires three steps. First, the motion data of the patella and tibia relative to the femur must be accurately acquired. Next the data must be represented in a coordinate system that allows representation of relative segment movement. This coordinate system also provides a standardized approach which will allow comparison of kinematics across several limbs. Finally, joint motion or relative movement of segmental coordinate systems must be quantified.

2.4.1 Data Acquisition

Acquisition of PF joint kinematic data has been performed using a variety of methods. Reider et al. (1981) used an orthogonal grid system in combination with four bone pins inserted directly into the patella and one into the tibial tubercle, to evaluate patellar kinematics. Veress et al. (1979), van Kampen and Huiskes (1990), Blankevoort et al. (1988) and Heegaard et al. (1994) all used roentgen stereophotogrammetric analysis (RSA) to quantify the kinematics. This system involved taking two x-rays at different angles and subsequently, using reference markers, to reconstruct the hand-digitized images into a three-dimensional image. Nagamine et al. (1995) used an externally mounted block attached to the

patella and a protractor to measure its movement throughout a range of motion. Hefzy et al. (1992) used a magnetic-tracking device consisting of magnetic sensors to determine the discrete motions of the patellofemoral joint. In-vivo studies (e.g. Koh et al, 1992, Lafortune, 1984, Reinschmidt et al.1996) used motion analysis video camera technology in combination with bone mounted reflective markers, to obtain relative bone movement. The use of video motion analysis in recording the dynamic loading of the patella and tibia relative to a fixed femur was applied in-vitro by Barnes (1998) to quantify patellofemoral movement. This method provided several advantages over previous techniques: automated marker digitization, marker position coordinates were readily obtained (2 minutes to track one trial), continuous data collection allowed for a dynamic motion capture and no environmental influences, such as ferrous materials in the case of magnetic-tracking devices. This method also permitted concurrent capture of anatomical coordinate system with kinematic data collection. Other methods require post-experiment digitization of bony landmarks to create anatomical coordinate systems. This introduces a longer collection time as well as requiring further coordinate system transformations. In addition, motion analysis equipment is readily available in most biomechanical laboratories.

2.4.2 Relative Motion Quantification

Several studies have presented standardized proposals for the description of knee joint motion (e.g. Grood and Suntay, 1983, Cole et al. 1993, Woltring, 1994). Two commonly used methods in biomechanics for describing relative motion are: Cardan/Euler angles and the Joint Coordinate System (JCS). Cardan/Euler angles are the traditional method of describing relative motion. In this system, the rotation matrix consists of an ordered sequence

of rotations about the three orthogonal axes of the embedded Cartesian coordinate system. A joint coordinate system is a non-orthogonal coordinate system consisting of one axis embedded in the proximal segment, a second embedded in the distal joint and the third axis, or floating axis resulting from the cross product of the other two (Nigg, 1994). Mathematically the advantages and disadvantages of the two systems are virtually the same; anatomical representation of body segments, sequence dependent rotations (solved by standardizing the sequence) and gimbal lock (a mathematical singularity that occurs when the second rotation equals 90°). The major difference between the two systems is merely conceptual (Nigg, 1994). The visualization of joint orientation is more practical using the JCS. For example, in the knee joint, when the femur is held fixed, the tibia rotates about the medial/lateral axis of the femur and the longitudinal axis of the tibia. Therefore, the JCS is used in this thesis.

2.4.3 Mathematical Description of a Body in space

Description of a body in space requires an understanding of vector and rotation matrix representation. A brief overview, as well as introduction to the nomenclature used in this thesis, is presented in this section. A more detailed description may be found in section 3.1.3.

To describe a point in space, three coordinates [x,y,z] are needed in order to create a position vector with respect to a universal or fixed coordinate system {A}. Two position vectors can describe a plane, and three orthogonal position vectors describe a coordinate system {B}. The orientation of a body in space can be described through the use of a coordinate system that is attached in a known way to that body. The position of one coordinate system (e.g. {B}) with respect to another (e.g. {A}) can be described by

expressing the unit vectors of the principal axes of {B} written in {A}. Arranging these principal vectors in columns in a 3x3 matrix, results in a rotation matrix ${}^{A}R_{B}$.

$$ {}^{A}R_{B} = \left[{}^{A}\hat{X}_{B} \; {}^{A}\hat{Y}_{B} \; {}^{A}\hat{Z}_{B} \right] = \begin{bmatrix} X_x & Y_x & Z_x \\ X_y & Y_y & Z_y \\ X_z & Y_z & Z_z \end{bmatrix} \qquad 2.1 $$

where ${}^{A}\hat{X}_{B}$ is the unit vector describing the x-axis of {B} written in {A} and

$\begin{bmatrix} X_x \\ X_y \\ X_z \end{bmatrix}$ are the x, y, z components of ${}^{A}\hat{X}_{B}$ written in column form.

This rotation matrix, ${}^{A}R_{B}$ is also referred to as the direction cosine matrix. Dividing each component of a vector in the matrix by the length of that vector will result in the cosine of the angle that vector makes with each of the corresponding universal coordinate system axes (X Y Z). From above, each of the columns of the rotation matrix are the position vectors of {B} written in {A}. Further investigation shows that the rows of this matrix are the unit vectors of {A} written in {B}. Therefore, ${}^{A}R_{B} = {}^{B}R_{A}{}^{T}$ where T is the transpose. A matrix with orthonormal (perpendicular) columns has an inverse equal to its transpose.

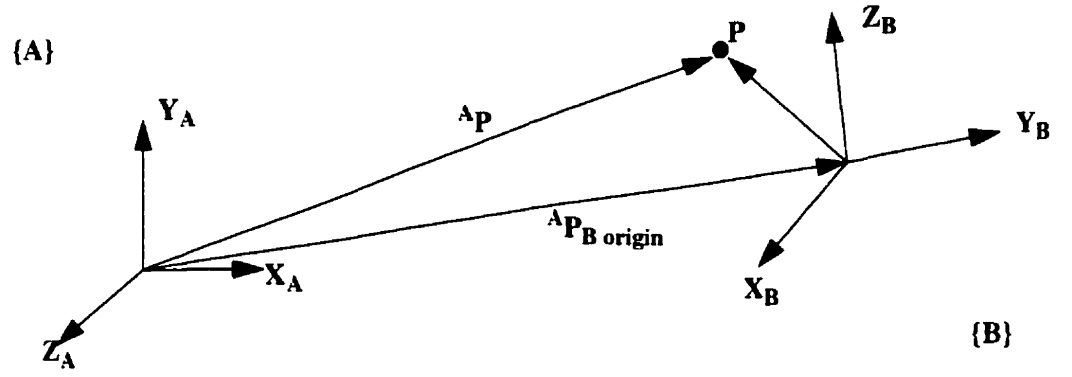

Figure 2-4 Mapping of a point in one coordinate system to another coordinate system.

Figure 2-4 demonstrates graphically the calculation or mapping of a point in one coordinate system to another coordinate system. The vector dot product of the rotation matrix ${}^{A}R_{B}$ and the vector ${}^{B}P$ results in a vector ${}^{A}P$ describing the point/vector in coordinate system {A}.

$$ {}^{A}P = {}^{A}R_{B} \cdot {}^{B}P \qquad 2.2 $$

This essentially rotates the coordinate system but does not take into consideration the translation. Inclusion of translation of the coordinate system origin is quantified by adding the vector describing the new origin position ${}^{A}P_{Borigin}$ which is the position of the origin of {B} written in {A}.

$$ {}^{A}P = {}^{A}R_{B} \cdot {}^{B}P + {}^{A}P_{Borigin} \qquad 2.3 $$

For clarity the position vector (often the origin of the coordinate system) is written in the fourth column of the rotation matrix. This new 4x4 matrix is a transformation matrix ${}^{A}T_{B}$.

$$[{}^{A}T_{B}] = \left[\begin{array}{c|c} {}^{A}R_{B} & {}^{A}P_{Borigin} \\ \hline 0\ 0\ 0 & 1 \end{array}\right]\left[\begin{array}{c} {}^{B}P \\ \hline 1 \end{array}\right] \qquad 2.4$$

For an additional coordinate system, {C}, with position only known relative to {A}, another transformation matrix ${}^{A}T_{C}$ can be determined. If the transformation of an object of {C} into {B} is desired, this transformation matrix can be calculated using the other two known transforms, i.e. ${}^{C}T_{B} = [{}^{C}T_{A}][{}^{A}T_{B}] = [{}^{A}T_{C}]^{-1}[{}^{A}T_{B}]$

The theory presented in this section will be used in this thesis to calculate the relative motion of segment coordinate systems and the reorientation of surfaces in the mathematical knee joint model presented in section 2.6.6.

2.5 Patellar Tracking

Patellar tracking is a term used to describe the movement of the patella relative to the femur during knee motion. Abnormal patellar tracking (a term commonly used clinically, but not well described or defined in the scientific literature) is associated with many pathologies including patellofemoral pain syndrome (van Kampen and Huiskes, 1990), which have unknown sources and often result in degeneration of the articular cartilage. Numerous researchers have quantified patellar tracking (e.g. Reider at al., 1981, van Kampen and Huiskes, 1990, Hefzy et al., 1992) in an attempt to determine the normal function of the patella. Quantifying patellar tracking involves classifying the movement of the patella relative to the femur. In one commonly utilized system for movement description (Reider et al. 1981, van Kampen and Huiskes 1990, Hefzy et al. 1992), the rotations can be described as flexion about the medial/lateral axis of the patella, patella rotation about the anterior/ posterior axis of the patella and internal/external rotation about the long axes of the patella

(Figure 2-5). Medial patellar rotation is defined as the rotation of the apex of the patella towards the medial condyle. The patella can also translate along its medial/lateral axes which is termed patella shift. Anatomical constraints allow very little movement along the anterior/ posterior axes of the patella and any translation along the long axes is incorporated into patella flexion. Therefore patella shift, rotation, tilt and flexion can describe the predominant three-dimensional tracking of the patella.

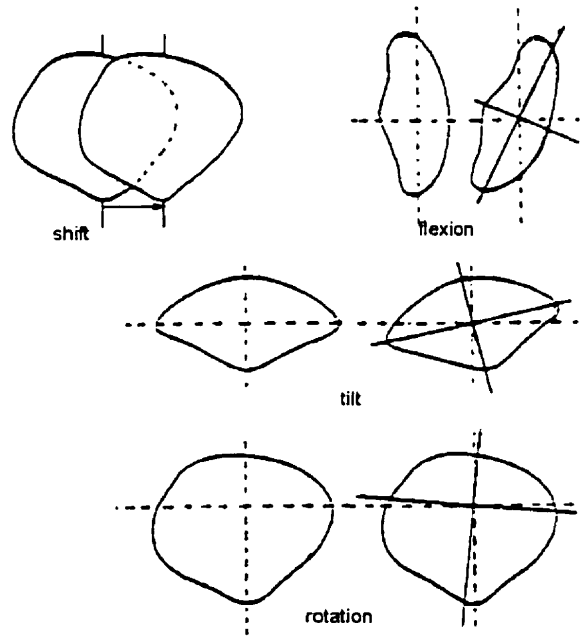

Figure 2-5 Patella motion classifications. Adapted from van Kampen and Huiskes, 1990.

2.5.1 Three-Dimensional Patellar Tracking - In vitro

Reider et al. (1981) were among the first to measure patellar tracking in three-dimensions. Using a projected orthogonal grid and four bone pins inserted into the anterior surface of the patella and one into the tibial tubercle, the position of the patella was measured. The experimental setup consisted of a fixed tibia with a free moving femur that would allow for the 'screw home' mechanism. The 'screw home' mechanism is used to describe the external

rotation of the tibia relative to the femur as the knee joint reaches full extension. Although this is a characteristic arising from the geometry of the tibiofemoral joint, the effects of this tibial rotation could influence the patellar tracking near full extension. The femur could be held at any angle between 90° of flexion and full extension. In order to load the patella, all four quadriceps muscles were loaded to 9.2 kg and kept in line with the predominant fibres of each muscle. The limb was taken through a range of motion quasi-statically in 15° increments.

This study characterized two different types of patellar tracking. Seventeen of the twenty limbs tested exhibited a medial shift, medial tilt and medial rotation (Type I). The second type of knee demonstrated a lateral shift between 90° and 30° of flexion and then shifted medially during the last 30° of extension (Type II). Medial tilt was relatively small and rotation was not significantly different from the Type II knees. Patellar rotation was not significantly different between the two types of knees. The pathological ratings of the Type II knees did not differ significantly from the Type I knees.

This was a very important study which introduced a higher level of quantification to further understand the tracking of the patella in normal knees as well as the potential influence of surgical procedures on this tracking. Great care was taken in loading each of the quadriceps muscles at an angle close to the physiological line of action. However, the question of physiological validity is uncertain. The limb was not loaded through the tibia to emulate loading during locomotion and the femur was positioned in a quasi-static movement. Loading could alter the tracking of the patella, as could a dynamic motion. Additionally, the experimental apparatus could have constrained the knee in such a way that the tibiofemoral and patellofemoral joint would behave differently than in-vivo. There is no evidence that

performing surgery on normal knees will have the same effect as it would on a pathological knee.

Blankevoort et al. (1988) proposed a study to examine and quantify the role of passive joint structures on the knee joint. The movement of the knee joint was separated into two major contributors: the passive motion characteristics and the external loads. Passive motion results directly from bony and ligamentous constraints. External loads result from the muscle activity and external forces. Roentgen stereophotogrammetry (RSP) was used for quantification of tibiofemoral and patellofemoral joint kinematics. A six-degree-of-freedom device was used to load and move the limb. The motion was quantified by sequence dependent rotations, cardan angles, about each of these axes in the order of flexion, tibial rotation and ab/adduction.

All soft tissues surrounding the knee were left intact. The femur angle was moved through 5° increments with the loading apparatus allowing freedom of motion in the other 5 rotational and translational directions. Axial forces were applied through the femur and rotational and anterior-posterior torques were applied through the tibia.

Although this study did not include patellar tracking, important characteristics of tibiofemoral motion were quantified. This study found no evidence of the screw-home mechanism in passive knee joint motion, but it was observed when external loads were applied. It was concluded that knee joint motion patterns were highly susceptible to small changes in the load configuration. The application of small axial loads to the tibia were reported to rotate the tibia internally. This could have further implications to patella movement which may be even more susceptible to small changes in applied load. Lastly, the RSP method produces a high degree of accuracy (50 μm) at the cost of being very time-

consuming and requiring unique, expensive optical equipment and technical expertise.

Van Kampen and Huiskes (1990) extended the study completed by Blankevoort et al. (1988) and investigated the three-dimensional tracking of the patella. The RSP method was used along with the loading apparatus of Blankevoort et al. (1988). Patellar motion was tested on four specimens in three tibial alignment conditions: neutral, internal rotation and external rotation. The four quadriceps muscles were sutured to guide wires which were aligned along the direction of the muscle fibres over pulleys and were attached to weights. The coordinate system of the patella originated in the centre of the patella with the flexion axis directed medially, the longitudinal axis directed proximally and the third axis directed anteriorly. Rotations about these axes were used to define the patella flexion, tilt, rotation and shift, as defined at the beginning of this section.

Patellar flexion was found to lag tibial flexion by roughly 20° and was not influenced by tibial rotations. Patellar tilt wavered from medial to lateral in 3 of the 4 limbs and was highly influenced by tibial rotations. Patellar rotation was medial as flexion angle increased and was reduced with external rotation of the tibia. Patellar shift moved laterally with increasing flexion angles after an initial medial shift in the first 30° of flexion.

All four limbs demonstrated similar tracking of the patella. This is in contrast to the two distinct types described by Reider et al. (1981). They also suggest that patella shift is coupled with patella tilt and the rotation is coupled with the varus-valgus movement of the tibia. A possible explanation of the difference in this study may be attributed to the movement frame of reference. Reider et al. (1981) measured the patella movement relative to the tibia, whereas van Kampen and Huiskes (1990) measured patella movement relative to the femur.

This study highlights several key issues affecting the normal tracking of the patella, most

notably that tibial rotations influence patellar tracking. The model presented was quasi-static and the effects of dynamic loading on the patellofemoral joint were not investigated.

Hefzy et al. (1992) used a three-space magnetic tracking device to measure the movement of the patella with respect to the femur, in-vitro. The experimental set-up consisted of clamping the femur to a table and allowing the tibia to hang freely at about 90°. The quadriceps tendon was exposed and sutured to a clamp which would pull the knee into extension. A joint coordinate system was used to describe the motions of the patella and tibia with respect to the femur. During the experiments, the tibial alignment was altered from neutral in both internal and external rotation to allow for direct comparisons with the results of van Kampen and Huiskes (1990).

Patellar flexion was found to lag tibiofemoral flexion and tibial rotations did not significantly affect patellar flexion. Patella tilt was medial in the first part of flexion but then tilted laterally after about 30°of flexion. The average tilt range was about 8°. An internally rotated tibia caused the patella to tilt more medially and this was found to be statistically significantly different from neutral tibial rotation (α=0.05) in the first 30°of flexion. Patella rotation averaged between 3° medially and 5° laterally, but remained almost constant at 1° lateral rotation for the first 40°of flexion. Tibial rotations caused a significant (α=0.05) difference (comparing internal tibial rotation to external tibial rotation) in patellar rotations between 60° and 90°of flexion. Internal tibial rotation produced medial patella rotations while external tibial rotation resulted in lateral patella rotation. Lateral patella shift occurred with increasing knee flexion and was also significantly different (α=0.05) between internal and external tibial rotations in the first 30° of knee flexion. External tibial rotations resulted in an average increase in lateral patella shift of 3 mm.

Heegaard et al. (1994) investigated the effects of soft tissues on the three-dimensional tracking of the patella, using the loading device described in van Kampen and Huiskes (1990). Two normal intact knees were tested and then all soft tissues excluding the cruciate ligaments were resected and the joint motion retested, using the experimental protocol of van Kampen and Huiskes (1990). The effects of tibial rotation on the intact knee were comparable to those presented by van Kampen and Huiskes (1990). In the dissected knee, shift and tilt motion of the patella near full extension were altered by as much as 20° from those for the intact knee. This indicates that patella motion is controlled primarily by soft tissue near full extension, and that patellofemoral geometry plays a key role at increasing flexion angles (e.g. larger than 30°). It was also found that dissection of soft tissue structures resulted in more pronounced patellar motion with the application of internal or external applied torques.

Nagamine et al. (1995) tested eleven cadaver limbs in four different conditions to establish the influence of the following variables: 1. location of the reference axis (femur or tibia), 2. rotation of the femoral axis (6° internal), 3. direction of pull of the quadriceps force, and 4. magnitude of the quadriceps forces (111N and 500N). The femur and tibia were mounted in a device which consisted of two pivoting mechanisms to simulate the hip and ankle joints. The hip mechanism could be locked into position and the flexion angle was measured using potentiometers. A 30N axial force was applied to the tibia and the quadriceps tendon was also loaded to 30 N. The motion of the patella was measured by an externally applied measuring block and protractor. Patellar shift was measured by the medial/lateral movement of the measurement block, which was attached to the anterior surface of the patella. Tilt was observed through a measuring rod that was inserted medial/laterally through

the patella. Finally, rotation was measured by the free rotation of the measurement rod about its long axis. The measurements were done visually by use of a protractor attached to the patella measuring device. The estimated accuracy of this method was reported to be 100 μm.

Nine of the eleven specimens exhibited similar patellar mechanics. The two exceptions were evaluated to have an "extremely laterally placed tibial tubercle" (Nagamine et al., 1995). Throughout knee flexion (5° to 90°) the patella shifted medially (5° to 15°) then laterally, tilted medially then laterally (45° to 90°) and rotated medially. Comparison of results with abnormally lateral tibial tubercles and internally or externally rotated tibias is presented in Table 1. It was also found that the direction of the quadriceps pull did not alter the patellar tracking patterns. This study also fixed the amount of varus/valgus movement of the tibia to less than 1°, in order to eliminate the introduction of an additional unknown in the evaluation of results.

The key results of the most relevant studies on patellar tracking are compared in Table 1. General patellar movements occurring between 0° and 90° of knee joint flexion can be grouped into in-vitro tibial rotation investigations. For neutral tibial rotations, 26 knees exhibited lateral patellar shift (ranging from 4.5 to 21 mm), medial patellar rotation (ranging from 2° to 11°) and lateral patellar tilt (ranging from 4° to 21°) whereas 5 knees exhibited medial shift (ranging from 4 to 12 mm), medial rotation (ranging from 2° to 7.5°); and medial tilt (ranging from 0° to 10°). Studies evaluating internal tibial rotations (16 knees) report lateral patellar shift (2-20 mm), medial patellar rotation (5°-18°) and lateral tilt (4°-16°) with increasing knee flexion to 90°. External tibial rotations, tested in 17 knees, resulted in lateral patellar shift (0 to 18 mm) and either lateral tilt (2 -6°) or medial tilt (2°-10°) and lateral rotation (2°-12°) or medial rotation (4°) during knee flexion to 90°.

Table 1 Combined Results of Previously Published Patellar Tracking Studies

Authors	No. of Specimens		Quad. Tendon loading	Measurement	Tibia	Average Patella Movements		
	in-vivo	in-vitro		Range (degrees)	Rotation	Shift (mm)	Rotation (degrees)	Tilt (degrees)
Veress et al. (1979)	4		Isometric	0-90	Neutral	Lateral	Unknown	not conclusive
Sikorski et al. (1979)	12		Isometric	60-90	Neutral	Unknown	Lateral	Medial
Reider at al. (1981)		type I - 17	92 N	0-90	Fixed	Lateral, 14mm	Medial, 6°	Lateral 12°
		type II - 3	92 N	0-90	Fixed	Medial, 7 mm	Medial, 6°	Neutral, 0°
Fujikawa at al. (1983)		8	20-30 N	25-130	Unknown	Unknown	Lateral, 6.2°	Medial, 11°
van Kampen at al.(1990)		4		0-150	Internal, 3 Nm	Lateral, 10 mm	Medial, 13°	1 Medial, 4° 3 Lateral, 15°
		4		0-150	External, 3 Nm	Lateral, 8 mm	2 Medial, 10° 2 Lateral, 2°	1 Medial, 4° 3 Lateral, 12°
Hefzy et al. (1992)		4	0-250 N		Internal	Lateral, 2 mm	Medial, 5°	Lateral, 8°
		4	0-250 N		External	Neutral	Lateral, 6°	Lateral 4°
Nagamine et al (1995)		9 2	30 N	0-90	Neutral	Lateral, 4.5 mm Medial, 6 mm	Medial, 4° Medial, 7.5°	Lateral, 4° Medial, 10°
		9	30 N	0-90	Internal	Lateral, 5 mm	Medial, 6°	Lateral, 5°
		9	30 N	0-90	External	Lateral, 3 mm	Medial, 2°	Lateral, 2°
Koh et al. (1992)	1		seated	0-50	Neutral	Lateral, 9mm	Medial, 1°	Lateral, 10°
			squat	0-50	Neut / Ext.	Lateral, 10 mm	Lateral, 2°	Lateral, 10°

2.5.2 Three-Dimensional Patellar Tracking - In vivo

Cadaveric studies have obvious limitations, perhaps most importantly the non-physiological environment in which evaluation is performed. The contributions of blood flow, neurological muscle stimulation and physiologic loading can not be overlooked.

Two different studies have been completed with the use of intra-cortical bone pins to measure accurate movement of the femur, tibia and patella. Lafortune et al. (1992) reported tibial-femoral kinematics using intra-cortical traction pins in five healthy male subjects. The pins were placed in the cortices of the right femur and tibia and the centre of the patella. They reported that tibiofemoral motions other than flexion/extension were relatively small, 5° for ab/adduction and 10° for internal/external rotation, over the entire gait cycle. Patellofemoral motions (Lafortune, 1984) over the gait cycle were averaged as 40.8° patellar flexion, 9.5° patellar rotation. Inconsistency across subjects for patellar tilt omitted the calculation of a mean value. An average lateral shift of approximately 7.2 mm was observed during the stance phase of the gait cycle with a medial displacement during the swing phase.

Koh et al. (1992) inserted bone pins into the patella, femur and tibia of one subject. Four conditions were tested. The subject performed a flexion/extension exercise while seated. A maximal electrical stimulation of the vastus medialis obliqus was performed at 0°and 30 °of knee flexion. The subject also did a maximal voluntary contraction at 0° and 30°of flexion. Lastly, a squatting motion was performed from an initial standing position. Patellar flexion was seen to lag behind knee flexion by about 20°, which was greater than that reported by van Kampen and Huiskes (1990). A larger lateral tilt of 12° and shift of 10 mm were also reported. Patella rotation was reported at only 1°. The squatting flexion/extension exercise showed that, the tibia externally rotated and the knee demonstrated a varus rotation as the

knee flexion angle increased. The measured movements however, did not differ much (less than 1°) in shift or rotation compared to those values measured for the sitting flexion/ extension exercise. Stimulation of the vastus medialis oblique, at 0° and 30° of knee joint flexion, produced medial shift of 1.99 mm and 0.32 mm, medial tilt of 2.16° and 0.43° and medial rotation of 1.4° and 0.3° respectively. Isometric contraction of the quadriceps at 0° and 30° knee joint flexion, produced shift of 1.61mm lateral and 0.07 mm medial, tilt of 0.62° lateral and 0.99° medial and lateral rotation of 4.5° and 1.5° respectively. Although an important study, it was only performed on one subject due to the invasive aspects of the technique. Determination of how representative these results are requires application to larger sample sizes, especially due to the known variability of in-vitro results.

Imaging techniques using MRI have also been used to quantify joint kinematics (Ronsky 1994 and Sheehan et al. 1999). Ronsky (1994) used MRI and a quasi-static loading apparatus to record patellofemoral kinematics and joint contact at three different knee flexion angles. Results from this study indicated that joint geometry had direct influence on patellar tracking.

Sheehan et al. (1999) has reported preliminary results from a study which quantified patellofemoral kinematics through a dynamic range of motion under loading. This technique shows comparable magnitudes for patellar flexion and tilt with other studies. However, in order to record dynamic motion, sufficient resolution of cartilage images for contact modelling purposes was not possible.

In conclusion, non-invasive, in-vivo quantification of patellofemoral kinematics is possible. Quantification of joint contact area has also been done. However, the ability to obtain simultaneous patellofemoral kinematics and joint contact area in-vivo is not yet feasible.

2.6 Quantifying Joint Geometry

Intuitively, joint geometry plays a significant role in kinematics. It is speculated that abnormal femoral condylar geometry is the cause of patellofemoral problems such as patellar subluxation (Fulkerson and Hungerford, 1990). Current concepts in the literature speculate that osteoarthritis is initiated as a result of abnormal joint loading. Abnormal joint loading could be related to abnormal contact characteristics.

Congruence can be defined as the goodness-of-fit of one surface against the opposing surface of a joint. Good congruity leads to larger contact areas. A larger contact area employed under the same loading conditions leads to lower stresses. Obtaining detailed knowledge of the surface geometry and its surface characteristics, e.g. curvature, contact area, is a first step toward the classification of normal and abnormal contact in the knee joint.

There are three components involved in obtaining detailed surface geometries. Firstly, 3-dimensional surface point data must be measured in order to describe the surface. Secondly, these data points need to be described as a mathematical surface. Finally, the surface geometry can be characterized mathematically for example, with surface normals and curvatures. Details of each of these components will be provided in the following paragraphs.

Early attempts at quantifying joint geometry involved two dimensional analysis from roentgenograms (e.g. Erkman and Walker, 1974), photos of sliced specimens (Rehder, 1983) and contour measurements on multiple sliced mouldings of the knee joint (Seedhom et al., 1972). Three-dimensional methods can be classified as mechanical or optical. Optical methods involve either invasive or non-invasive techniques. Invasive techniques include Moire contourgraphy, introduced by Wijk (1980) and rasterstereography (Frobin and Hierholzer, 1983). Ghosh (1983) introduced close range photogrammetry which was further

developed by Huiskes (1985), Ateshian (1991) and Ronsky et al. (1999). Haut et al. (1998) introduced a laser technique for measuring joint surface topography. Non-invasive techniques include MRI (Ronsky, 1994 and Eckstein, 1996), CT (Cohen, 1997) and ultrasound (Rushfeldt et al., 1981).

2.6.1 Surface Data Acquisition

Mechanical techniques involve disrupting the natural contour of the joint. Dial gauges (Wismans et al. 1980) and three dimensional probing of the cartilage contour (Hefzy et al. 1992) involve contact and to some extent indentation of the articular surface. The major limitation of these methods is that they all require contact with the cartilage surface to obtain measurements. Because cartilage is a visco-elastic tissue, a finite amount of deformation will occur upon contact. This deformation upon contact is not typically measured or reported with these contact techniques (Boyd, 1997). Therefore a non-contacting technique would be more desirable.

Optical techniques hold a strong advantage over mechanical techniques by allowing quantification of geometry without disruption of the natural cartilage surface. These methods can also be divided into invasive, in-vitro (SPG, MDPG) and non-invasive, in-vivo (MRI) techniques. In recent years, with the advance of computers to aid in data acquisition and processing, photogrammetry has become a more widely used and applicable measurement tool. In order to obtain accurate measurements from photography, basic photogrammatic principles must be understood. The following section will give a general overview of these principles to provide a basic understanding of the methods used in biomechanics.

2.6.2 Photogrammetry

Close range photogrammetry is based on the central perspective theory. This theory states that a point A in object space will be projected onto a projection plane (in the camera) resulting in point a (Figure 2-6). These points will lie in a line that passes through the principal perspective centre O.

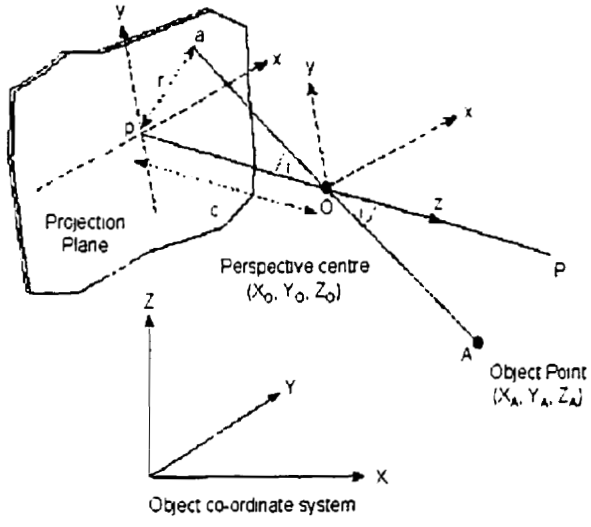

Figure 2-6 Schematic of the central perspective theory. Adapted from Atkinson, 1996.

If two coordinate systems are considered, one based in the camera and one based in the object space, equations can be defined to determine the projected image coordinates of a point a. Consider point A in object space to have coordinates (X_A, Y_A, Z_A). The perspective centre has the coordinates (X_O, Y_O and Z_O). Point a is described in image coordinates as (x_a, y_a) and the principal distance is described as c. The resulting equations for image coordinates for point a in space would be:

$$x_a = \frac{-c[r_{11}(X_0 - X_A) + r_{12}(Y_0 - Y_A) + r_{13}(Z_0 - Z_A)]}{[r_{31}(X_0 - X_A) + r_{32}(Y_0 - Y_A) + r_{33}(Z_0 - Z_A)]} \quad 2.5$$

$$y_a = \frac{-c[r_{21}(X_0 - X_A) + r_{22}(Y_0 - Y_A) + r_{23}(Z_0 - Z_A)]}{[r_{31}(X_0 - X_A) + r_{32}(Y_0 - Y_A) + r_{33}(Z_0 - Z_A)]} \quad 2.6$$

where r_{ij} are elements of the rotation matrix R between the object space coordinate system and the image space coordinate system and c is the principal distance. These equations are referred to as the collinearity equations. (Atkinson, 1996)

In reality, the theory can never truly be realized due to lens distortions in the camera. As light rays pass through the lens of a camera, they bend and form an angle of incidence with the principal axis. Since each ray has a slightly different angle of incidence, the principal distance for focus varies. This variation is proportional to the radial distance from the principal point and thus is called radial lens distortion. It is described mathematically as:

$$\delta r = K_1 r^3 + K_2 r^5 + K_3 r^7 \quad 2.7$$

where: δr is the radial displacement of an image point,

K1, K2, K3 are coefficients that depend upon the camera focal setting,

$r^2 = ((x - x_o)^2 + (y - y_o^2))$ and (x,y) are the fiducial coordinates of the image point and (x_o, y_o) is the principal point.

Radial lens distortion can be incorporated into the collinearity equations. Errors are also introduced due to a misalignment of the lens components. This results in a displacement of the image point referred to as a tangential lens distortion. The displacement is described in both the x (δx) and y (δy) directions by use of polynomial equations:

$$\delta x = P_1[r^2 + 2(x - x_o)^2] + 2P_2(x - x_o)(y - y_o) \quad 2.8$$

$$\delta y = P_2[r^2 + 2(y - y_o)^2] + 2P_1(x - x_o)(y - y_o) \quad 2.9$$

P1 and P2 are coefficients based on the camera and the focal length used. These equations can also be included in the collinearity equations.

In order to solve the collinearity equations, the interior orientation coordinate c, x_a and y_a, the coordinates of A (X_A,Y_A and Z_A) measured in object space and the exterior orientations which are the rotations ω,φ and κ and the perspective centre coordinates X_O,Y_O and Z_O are required. A process called resection and intersection can be used to calculate these parameters. Resection solves for the exterior orientations of the camera. In order to do this, three non-collinear control points are needed as input into the collinearity equations above. For more accurate results, more than three control points are recommended and iterative least squares estimation can be used to solve the system. Intersection uses the collinearity equations to find point A in object space. This gives 3 unknowns for four equations and also requires a least square estimation. The advantage of this technique is that it is relatively fast computationally (requires inversion of 6x6 matrices). However, the main disadvantage is the low number of degrees of freedom, which produces low reliability results, as there are only two cameras. Multi-station photogrammetry uses more than two images, therefore greatly increasing the number of degrees of freedom of the solution and hence the solution accuracy.

Direct linear transformation (DLT) was developed by Abdel-Abiz and Karara (1971) for use in non-metric cameras. Unlike the above collinearity equations, the DLT does not require approximate values for the transformation (between the camera and object space) parameters. The DLT uses the following equations:

$$x = \frac{L_1 X + L_2 Y + L_3 Z + L_4}{L_9 X + L_{10} Y + L_{11} Z + 1} \qquad 2.10$$

$$y = \frac{L_5X + L_6Y + L_7Z + L_8}{L_9X + L_{10}Y + L_{11}Z + 1} \qquad 2.11$$

where x and y are the coordinates in the image coordinate system, (X,Y,Z) are the object space coordinates of the target and L_1 - L_{11} are coefficients of the camera parameters, assumed to be independent. These equations are also solved using an iterative least squares estimation.

Multistation photogrammetry uses multiple cameras and/or images to solve for the target points in object space. The original collinearity equations (2.5 and 2.6) can be altered and rewritten as follows:

$$x_{ij} = \frac{-c_j[r_{j,11}(X_{oj} - X_i) + r_{j,12}(Y_{oj} - Y_i) + r_{j,13}(Z_{oj} - Z_i)]}{[r_{j,31}(X_{oj} - X_i) + r_{j,32}(Y_{oj} - Y_i) + r_{j,33}(Z_{oj} - Z_i)]} \qquad 2.12$$

$$y_{ij} = \frac{-c_j[r_{j,21}(X_{oj} - X_i) + r_{j,22}(Y_{oj} - Y_i) + r_{j,23}(Z_{oj} - Z_i)]}{[r_{j,31}(X_{oj} - X_i) + r_{j,32}(Y_{oj} - Y_i) + r_{j,33}(Z_{oj} - Z_i)]} \qquad 2.13$$

where c is the principal distance, r_j are the components of the rotation matrix and j is the camera number. For example, $r_{1,13}$ indicates the value in the first row and third column of the rotation matrix for camera 1.

Equations 2.12 and 2.13 can also be altered to include radial and tangential lens distortion parameters introduced in equations 2.7, 2.8 and 2.9.

2.6.3 Photogrammetry in Biomechanics

Ghosh (1979 and 1983) introduced the use of close-range photogrammetry to the medical field. Its advantages were that the specimen could be viewed and reconstructed in its original form. Through the use of two cameras and a stereocomparator restitution instrument (device which combines the two images into a 3D image), the surface contours of the knee joint were

reproduced on the computer.

Huiskes et al.(1985) used analytical, close-range photography to obtain surface measurements of the knee joint. Analytical photogrammetry involves digitizing two separate (2D) images followed by a computer reconstruction to obtain the 3D surface. The method used by Huiskes et al. (1985) involved mounting the specimen inside a frame containing precisely calibrated control points (posts of known position and height) (Figure 2-7). Using a slide projector, a grid was projected onto the surface and photographs of the surface were acquired using a camera placed in two separate positions. The photographs of the control frame and specimen, in each camera position, were then digitized on a two-dimensional coordinate digitizer. The digitized points and control points, whose 3D values are known a priori, were then used as inputs into a mathematical reconstruction algorithm, similar to that described in section 2.6.2.

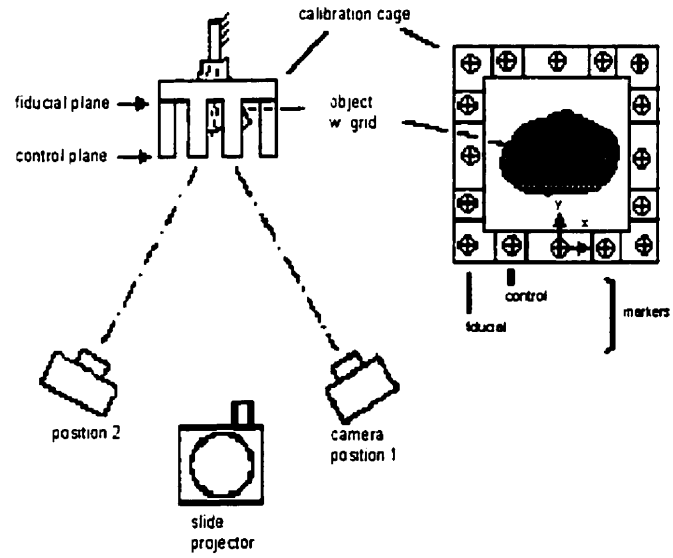

Figure 2-7 Experimental setup for stereophotogrammetry. Adapted from Huiskes, 1985.

In order to test the accuracy of this system, a cylinder engraved with a grid was photographed in two orientations; firstly with the long axis oriented horizontally and secondly oriented vertically. The intersections of the grid were measured using a coordinate measuring machine with an accuracy of ±2μm. The results showed that the better accuracy was achieved with the cylinder oriented horizontally and that the largest errors occurred at the peripheral points. The resultant cylindrical fit accuracy lies between 150 and 200 μm.They also performed a precision test where the same points were digitized several times. Comparing the precision test results from the cylindrical test and those done on the tibia surface, provided an estimate of the accuracy of the reconstructed surface points. The overall accuracy of this set-up, for the specimen surfaces, was estimated to be between 140 - 270 μm. This indicated slightly less accuracy could be obtained with the surface measurements. The reduced sharpness of the grid on the specimen surface compared to that of the engraved grid on the cylinder is believed to be the largest contributor to this decreased accuracy. These accuracies could be improved upon with the addition of non-linear lens distortion algorithms to the reconstruction procedure.

Ateshian et al. (1991) used the stereophotogrammetric (SPG) technique presented by Huiskes et al. (1985) to describe surface geometries of cartilage, bone and menisci. The set-up was identical to Huiskes et al. (1985) and the same cylinder and error calculation methods were used to estimate the accuracy of the system. They improved the accuracy reported Huiskes et al. (1985) from 150-200μm, in the cylindrical calibration test, to 90μm. They reported a measurement precision of 68μm for bone surfaces and 116μm for cartilage surfaces, in the least favourable coordinate direction.

Stereophotogrammetry provides an increased advantage over previous mechanical

techniques with an improved accuracy. However, there are still many factors that contribute to its inaccuracy that can be improved upon. One type of error results from distortion in photographic paper and its grain resolution (Ateshian et al. 1991). Another is the convergence or parallax error produced with only two camera angles. Additional camera angles would yield more results to add to redundancy of inputs with the reconstruction algorithm. Both of these problems can be alleviated by the use of multi-station digital photogrammetry (MDPG). The multi-station format will increase the accuracy of the reconstruction by adding redundant measurement inputs. The digital camera produces digital images that can be downloaded directly into the computer for subsequent digitization. Boyd (1997) used this technique to measure the patellofemoral surface of a cat knee joint. MDPG presented several advantages over SPG in addition to the improved accuracy of redundant measurement inputs. The digital format of the images enabled the development of semi-automated edge detection and pattern fitting algorithms. This decreased the subjectivity involved in the digitizing process, thus increasing the accuracy of the 2D image points. Accuracy for this system was estimated to be 25μm compared to the 90μm accuracy reported by Ateshian et al. (1991).

Haut et al. (1998) introduced a laser technique to obtain the 3D surface geometry of a joint. The setup consists of a laser mounted on a planar positioning arm with the specimen mounted directly perpendicular to the laser beam. A computer controlled step-up motor moved the laser through a programmed x-y grid coordinate system while the laser emitted a 0.5 mm beam onto the surface. The reflection was then recorded and converted to the z-direction coordinate of the surface.The accuracy of this system was reported to be 0.1μm in the Z-direction and 1.4μm in the X and Y directions resulting in an overall root mean square

accuracy of 8μm when the slope of the specimen surface is below 45°. The acquisition time for this system was reported to be 25 minutes to scan both the menisci and the adjoining articular surface. In order to accommodate steep slopes, i.e. the femoral condyles, the system required rotation to reorient the desired surface perpendicular to the laser. This would increase the time of data acquisition, presumably another 20-25 minutes, and require post hoc patching of the two scans.

2.6.4 Surface Modelling

The data acquisition systems described above provide 3D coordinate data of the specific surface of interest. In order to make any quantitative observations with these data, they must be combined to describe a surface. Numerous mathematical modelling approaches can be employed. The selection of the most appropriate model to create the surface model is influenced by the format in which the data were collected. For example, data points can be either uniformly distributed (e.g. Haut et al., 1998) or non-uniformly distributed.

Once an equation for the surface is found, many measurements to characterize the surface are possible. For example, surface curvatures can be calculated, cartilage thickness (based on both the cartilage and underlying bone surface) and contact area between two cartilage surfaces can be measured.

A surface can be described as a function of an x-y grid. This function can represent z, e.g. $z = f(x,y)$. This function is continuous, if for every (x,y) combination there exists a value for z. An example where this is not true would be for the function $z=x/y$. When $y=0$, z does not have a solution. However, a curve that is continuous is not necessarily smooth. Smoothness is determined by taking the derivative of a function. If the curve of interest has a sharp corner,

there will be no definable derivative at that point, resulting in a discontinuous derivative. When a function has a definable slope for every (x,y), it has C^1 continuity, where C^1 refers to the first derivative of the function. To test for the smoothness of a surface, a second derivative is calculated. If this is definable for every (x,y), the surface will have C^2 continuity. For the purposes of describing joint surfaces in biomechanics, it is imperative that the surface model be both continuous and smooth (i.e. C^1 and C^2 continuity).

Scherrer and Hillberry (1979) presented the use of Coon's bicubic surface patches for representing articular surfaces. This method is piecewise continuous across its surface patches, having C^1 continuity over its boundary curves and C^2 continuity at the corner nodes (measured data points). These surface patches go through each data point with no smoothing. Huiskes et al. (1985) and Ateshian et al (1991) also used this technique to describe the surface of the human knee joint. Ateshian (1993) introduced the use of a B-Spline least-squares surface-fitting technique that would be able to describe the entire surface with a single equation. The technique does not interpolate the data point but smooths the experimental surface data. This approach appears rational as the articular surface measurement does contain some error and we know the surface is smooth and continuous. The primary limitation of this method is that it requires the data to be placed in a grid with rows and columns that form a complete rectangle. This is not always possible with experimental data as joints are not rectangular. Boyd (1997, 1999) presents the thin plate spline (TPS) surface model, which can deal with sparsely and randomly distributed data points.

2.6.5 Thin Plate Spline

The thin plate spline uses a bi-variate function, or radial basis function, which allows it to

describe complex surfaces (Lancaster and Salkauskas, 1986). It does not require patches, so data may be input in a random order and missing data will not present a problem. In order to fit the data, the bending energy of the surface is minimized, where the bending energy is

$$J(s) = \int_{R^2}\int \left\{ \left[\frac{\partial^2 s}{\partial x^2}\right]^2 + 2\left[\frac{\partial^2 s}{\partial x \partial y}\right]^2 + \left[\frac{\partial^2 s}{\partial x y^2}\right]^2 \right\} dxdy \qquad 2.14$$

where J is the approximation of the bending energy

R^2 is the surface area

x and y are the projected planar positions

s is a function of x and y

If bending energy is equal to zero, the surface is flat. This method has two main assumptions: the deformation is assumed to be only in bending with no shear, and deflections are small.

2.6.6 Surface Characterization

The mathematical description of a surface as an equation, allows further surface characterization such as curvature and contact areas. The following sections outline the techniques used to quantify surface normals, curvature and the distance between two surfaces (Mortenson, 1985).

2.6.7 Surface Normals

For discrete points on a curve, a normal vector can be described that is perpendicular to the tangent of the curve at that point. For a surface, the normal vector is perpendicular to all tangents of the surface at that point. This normal is described vectorily as:

$$\bar{n} = \left[S^x \; S^y \; -1 \right] \qquad 2.15$$

where

S^x and S^y are the derivatives $\frac{\partial S}{\partial x}$ and $\frac{\partial S}{\partial y}$

and $\bar{n}$ is normalized by dividing by its magnitude $\sqrt{(S^x)^2 + (S^y)^2 + (-1)^2}$

The surface normal is necessary for further characterization of the surface and quantification of curvatures and proximity between two surfaces.

2.6.8 Surface Curvatures

If a surface is continuously differentiable, a normal to the surface can be found at any point. This normal lies in a plane that slices through the surface, intersecting it along a curve C. The radius of curvature is defined as $\rho = 1/\kappa$ where κ is the curvature. For every point on a surface there exists two principal curvatures, κ_{min} and κ_{max}, which are oriented orthogonal to one another (Ateshian et al, 1992).

The determination of the principal curvatures involves solving for the roots of the two equations that are based on the coefficients of the first and second fundamental forms for the intrinsic properties of a surface. (Mortenson, 1985)

$$(EG - F^2)\kappa^2 - (EN + GL - 2FM)\kappa^2 + (LN - M^2) = 0 \qquad 2.16$$

$$(FN - GM)h^2 - (EN - GL)h + (EM - FL)) = 0 \qquad 2.17$$

where $E = S^x \bullet S^x$ $\qquad L = S^{xx} \bullet n$

$F = S^x \bullet S^y$ $\qquad M = S^{xy} \bullet n$

$G = S^y \bullet S^y$ $\qquad N = S^{yy} \bullet n$

where S^{xx}, S^{xy} and S^{yy} are the partial derivatives of S.

In biomechanics, surface curvatures have been used for congruence evaluation (Ateshian et al. 1992) and for identification of joint surface topological features (Kwak et al, 1997 and Kralovic et al., 1998). There are three main methods of describing surface curvatures; Gaussian curvature, average principal curvature and rms curvature (Ateshian et al., 1992). Gaussian curvature is the product of the two principal curvatures, $K = \kappa_{min}\kappa_{max}$. If K>0, the surface is ovoid and if K<0, the surface is sellar or saddle-shaped. At K=0 the surface is cylindrical or ruled (Ateshian et al., 1992). The average principal curvature is described as $H = (\kappa_{min} + \kappa_{max})/2$. However, average principal curvature does not provide any information about the intrinsic characteristics of the surface (Ateshian et al., 1992). The root mean square curvature, reported by Ateshian et al. (1992), indicates the flatness of a curve. It is defined as: $\kappa_{rms} = \sqrt{(\kappa_{min}^2 + \kappa_{max}^2)/2}$. If κ_{rms}=0, the surface is flat.

2.6.9 Proximity

Proximity, in biomechanical literature, is described as the distance between two surfaces. It has been used to calculate cartilage thickness (Ateshian et al, 1991, Boyd, 1997) and contact area (Soslowsky et al, 1992, Ateshian et al., 1994, Luo et al, 1996, Boyd and Ronsky, 1998). Proximity is calculated as the distance along the surface normal, from an original surface to a destination surface. Because the surface normals of the originating surface may not be perpendicular to the destination surface, proximity values are dependant on the relative curvatures of the opposing surfaces. If this method were used for determining contact area, the contact area would be dependent on the choice for the original surface. For cartilage thickness calculations, the surfaces typically have relatively similar curvature and therefore

the surface normals would be similar on the original and destination surfaces.

2.6.10 Contact Area

It is speculated that abnormal contact area patterns or contact areas of high pressure can lead to degenerative disease such as osteoarthritis. Numerous researchers have used various approaches to investigate joint contact area. Radiographic techniques were perhaps the first attempt at measuring contact (Steindler, 1955). Injecting radio-opaque solution into the joint before taking a radiograph was used by Kettelkamp and Jacobs (1972) and Maquet et al. (1975). These techniques provide only one region of contact in two dimensional space. Wiberg (1941) sectioned frozen cadaver knees to determine the joint contact at a particular joint angle. Dye staining is a technique that allows the investigator to examine contact throughout the entire surface (3D), although only at one joint angle (Greenwald and O'Connor, 1971, Goodfellow et al., 1976, Moran et al., 1985). This method involves the absorption of a chemical into the articulating cartilage surfaces prior to loading. Once the joint is loaded, a second chemical is injected into the joint capsule. This agent reacts with the first chemical, resulting in a coloured stain on the surfaces where no contact occurred. Matthews et al. (1977) employed another staining technique for contact analysis. The retropatellar surface was soaked with methylene blue and the joint was loaded, forcing the patella to stain the contact area on the trochlear groove of the femur.

Casting techniques have also been widely used in biomechanics for contact analysis (e.g. Walker & Hajeck, 1972). This method involves injecting a casting liquid (usually methylmethacrylate or silicone rubber) into the desired joint either prior to and/or during loading. The material hardens leaving a mould of the joint devoid of material where the two

joints contacted. Yao and Seedhom (1991) presented a similar technique which they term the'3S' technique. It involved the use of silicone oil-carbon black powder suspension that was applied to the articular surfaces, and subsequently squeezed out of regions where contact occurred.

Contact areas have also been estimated using contact pressure measurements. Pressensor pressure-sensitive film has been used by many investigators to determine contact pressures and areas (e.g. Huberti and Hayes, 1984, 1988, Singerman et al., 1987, Ronsky et al. 1995). This method involves inserting a thin (250-300μm) film into the joint and applying subsequent loading. The film contains miniature ink bubbles that burst upon a certain force level. The intensity of the stain correlates to contact pressure allowing pressure maps to be determined.

The method of surface proximity is the most recent development in contact area assessment. Scherrer et al. (1979) introduced this method combining joint kinematics with mathematical surface models to determine the joint interaction throughout a range of motion. The method involves realigning the surface models using kinematics. Contact occurs when the proximity is zero, or where the two surfaces overlap. This method has been used by Soslowsky et al. (1992), Kwak et al. (1993) and Boyd (1997).

Ateshian et al. (1994) compared the contact area results using four different methods: silicon rubber casting, dye staining, Fuji-pressure-sensitive film (0.5-2.5 MPa) and SPG in combination with the proximity model on bovine tibiofemoral and glenohumeral joints. Dye staining resulted in the largest contact area with silicone rubber casting producing a slightly smaller contact area while Fuji film exhibited the smallest contact area. SPG produced an area very similar to the other techniques. Interestingly, they found the SPG was able to

predict contact contours of the other methods by examining certain proximity levels. This confirmed that higher contact pressures result in closer proximity.

Patellofemoral contact area magnitudes presented in the literature range from 150 to 600 mm^2 (Figure 2-8). Results have shown that contact area increases with increasing knee flexion, increases and then decreases or plateaus throughout knee flexion.

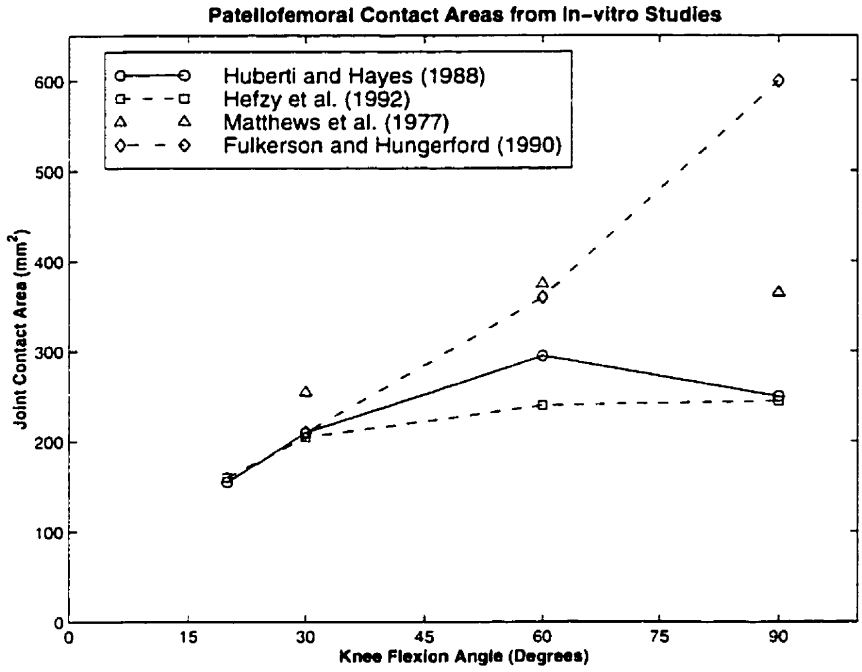

Figure 2-8 Patellofemoral contact area reported for in-vitro studies.

2.7 Summary

The patellofemoral joint consists of complex anatomy through which muscle forces and surface geometries must interact to function. The patella is designed to distribute compressive forces during increased knee flexion and to transfer these forces over the articulating surfaces. A good interaction will result in a large distribution of forces and lower stress in the joint. This means that the articulating surface geometries of the PF joint need to

be sufficiently similar to distribute load across a large area.

Fulkerson and Hungerford (1990) stated that abnormal surface geometry does not necessarily result in pain and that normal surface geometry does not always indicate absence of PF problems. As a result abnormal mechanics are sited to be a cause of instability and pain. However, abnormal tracking is not clearly defined.

Previous researchers have completed in-vitro studies of PF tracking. The quantification 3D patellar motions has been done using RSA, magnetic tracking devices and using an external device attached directly to the patella measuring motion with a protractor. These methods require data collection at discrete flexion angles (quasi-static). Using a motion analysis system allows continuous kinematic data collection. In combination with the MTS (Materials Testing System, Minneapolis, MN), the PF tracking can be measured throughout a continuous flexion angle.

Kinematic results of PF tracking presented in the literature have been variable. Most have indicated lateral patellar shift and lateral tilt with increasing knee joint flexion, however, medial shift and tilt have also been reported. Patellar rotation has been reported as either medial or lateral. Tibial rotations have been shown to influence patellar motion and could be one explanation for the varied results. However, many other factors such as loading condition and individual geometry differences could explain the variation as well.

With the exception of Hefzy et al. (1992), all studies have constrained the tibia in a motion jig. The experimental setups also required that the tibia and femur be transected just above and below the knee joint. The addition of the tibia and foot could have significant inertial affects on tibial rotation throughout knee joint flexion as well as adding weight. This creates a larger moment and compressive force on the patella, which could also significantly affect

its tracking pattern. In-vivo, the knee joint is also subjected to internal forces caused by the ground reaction force. This force could also affect the kinematics of the PF joint.

Therefore, this study will use the MTS and Motion Analysis System to measure dynamic PF tracking through the knee extension phase, allowing the tibia and foot to move freely. Loading through the calcaneous will also be introduced.

The interaction of the articulating surfaces are indicated by the kinematics. However, the effectiveness of this interaction in distributing load through the patella can only be investigated by obtaining the surface geometries of the PF joint. Past techniques used mechanical measurement methods to quantify the surface topography, which involved direct contact with the surface. Stereophotogrammetry allows the surfaces to be measured without contact but require expensive equipment. Recent advances in optical technology enabled the development of multi-station digital photogrammetry, which has improved accuracy and provided more readily available equipment.

Quantifying the surface requires mathematical representation of the surface points. The thin plate spline provides a single mathematical expression for the surface. Using this expression, contact areas can then be calculated and used to describe the functional internal mechanics of the PF joint.

3.0 Methodology

The investigation of surface geometry effects on patellofemoral kinematics involves two main methodological aspects; the quantification of joint kinematics and the determination of the surface geometries. This section will address the data collection and calculations required to relate joint kinematics to surface geometries.

3.1 Knee Joint Kinetic and Kinematic Quanification

3.1.1 Specimen Preparation

Six fresh frozen cadaveric limbs (mean age 71.7 +/- 8.2 years), removed just distal to the greater trochanter, were used in this study. In preparation for testing, all soft tissue was removed to just proximal of the femoral condyles, leaving the quadriceps tendon exposed. The quadriceps tendon was sutured to a nylon strap, that formed a loop to allow connection to the MTS actuator. The tendon tissue was subsequently covered with a saline-soaked gauze pad. Care was taken to ensure the remaining soft tissues of the joint and the joint capsule remained intact.

Motion measurement required the insertion of reflective markers attached to rigid bone mounted pins. The bone pins were affixed to the bone using screws. The screws were inserted into the bone and then the bone pins were screwed into the threaded centre of the bone screw. Screws were used so that the orientation and length of the marker(s) from the bone remained consistent if the screw were removed and replaced. Nine bone screws (Figure 3-1) were needed to hold an arrangement of twenty-one markers (The marker arrangement is described in detail in section 3.1.3). In the femur, two screws were inserted on the anterior shaft, aligned perpendicular to the long axis of the femur. One bone screw was inserted into the medial

condyle, perpendicular to the other two screws. Three small screws were placed into the patella in an 'L' shape configuration, where the apex was located at the centre of the patella, oriented distally and to the right. The tibia required two bone screws located on the tibial crest, oriented anteriorly and on the medial condyle perpendicular to the tibial crest and parallel to the femoral condyle screw.

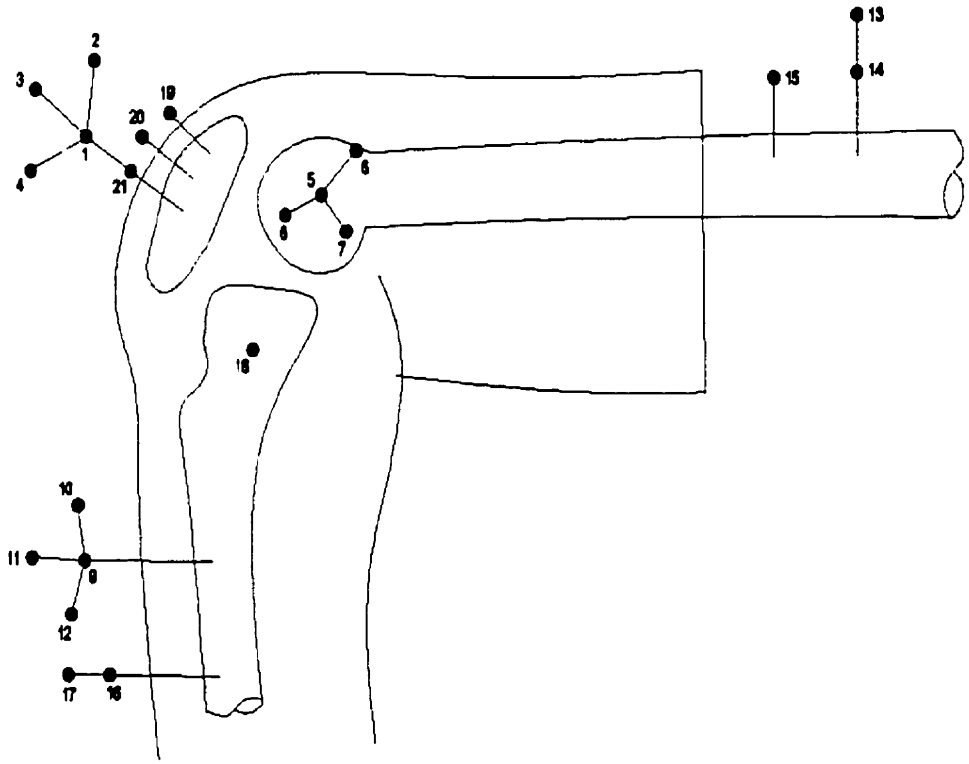

Figure 3-1 Locations of bone screws in the femur, patella and tibia.

Holes were drilled into the bone using a Makita 12V reversible drill. Three different drill bit sizes (26, 35 and 36) were used in order to accommodate variations in the size and density of the different bones. Typically, the tibia was extremely dense and required both drilling and tapping. The femoral shaft, like the tibia, was dense and hard, however, the femoral condyles were porous, and so drilling alone was sufficient. Smaller screws were used on the patellae

due to the small surface area and thickness of the patella. Drilling without tapping yielded a more rigid fixation of the screw to the patellar bone. The bone surface in the local vicinity (2-3 cm diameter) of the bone screws, of the patella and the femoral condyle was scraped and dried to promote the adhesiveness of the bone cement. Poly-Methyl-Methacrylyte bone cement was used on these areas to secure the position of the bone screws.

3.1.2 Experimental Setup

The basic components of the experimental setup included: dynamic extension, kinetic measurement (quadriceps tendon loading), kinematic measurements and external axial loading. Dynamic extension was achieved by rigidly clamping the femoral shaft to a table and loading the quadriceps tendon to produce extension of the knee joint. The limb was aligned such that the femoral crest was oriented posteriorly down leaving the tibia to hang unconstrained (about 90° flexion). A rod was inserted through the nylon strap loop sutured to the quadriceps tendon. This rod was attached to a separate rod and hook system that connected the MTS (Materials Testing System, Minneapolis, MN) actuator to the limb (Figure 3-2). This four-rod linkage system was designed to slide on two guide rods, whose contacting surfaces were coated with teflon to minimize friction during contact. The purpose of this system was to emulate, as close as possible, the line of action of the quadriceps, or more realistically the rectus femoris muscle, line-of-action.

In order to set the experimental parameters of the MTS testing protocol, the limb was moved through a range-of-motion, starting at approximately 90° (variation depended on the straightness of the femoral shaft and the loading condition) through full extension (0°). Full extension was determined visually as the point where no further movement of the tibia could

be observed and experimentally as the point in which the force of the MTS actuator increased more than 100N in a 1 second interval. The length of the displacement of the MTS actuator at terminal extension was recorded and implemented into the MTS controller program as the maximum displacement value for the experiment.

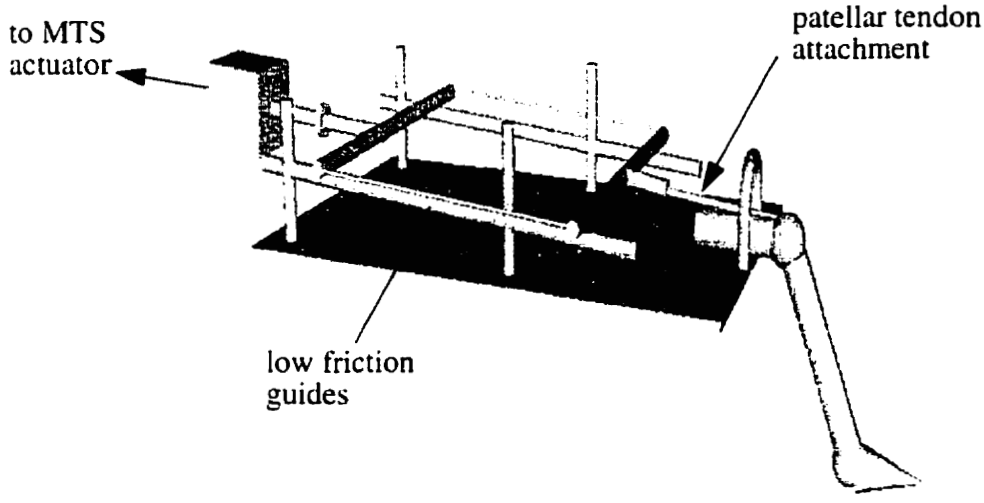

Figure 3-2 Experimental apparatus for kinematic testing protocol.

Kinetic loading was produced by the MTS actuator (1000N load cell) which retracted at a constant speed of 20 mm/s. The computer controlled the actuator for constant displacement and recording of applied force. After the initial attachment to the limb the quadriceps tendon was pulled taut with minimal force of less than 10N. This was set as the initial position and the force on the actuator was zeroed. At the completion of each trial, some creep of the tendon could be observed, indicated by a residual length when force had returned to zero. The actuator position was recorded and the position was then used as the next zero point. The final three data collections (right limbs 1737, 1748 and left limb 1748) were accidentally zeroed

to force rather than length. This causes the starting position to be identical for each trial, not compensating for creep. If the creep were significant, terminal extension would not be reached.

Dynamic patellar tracking was assessed under three load conditions: no external load, external load of 89N and external load of 222N. One static and five dynamic trials were recorded for each condition, following the dynamic loading protocol outlined above.

External loading was accomplished with a custom designed loading device. This loading device consisted of a 1/2" steel base plate (24" square) with two vertical members (adjustable height) supporting pulleys (4" dia.). The plate was secured under the load floor for stability. The pulleys were aligned visually with the estimated knee joint flexion axis. A polypropylene rope was positioned around each pulley and underneath the heel of the lower limb specimen, just proximal to the calcaneous. The location of this rope was further secured with a secondary attachment over the top of the foot. External loading was applied by attaching free weights to the rope, for a total loading of 89N or 222N (Figure 3-3).

Kinematic measurement involved the video motion capture of markers attached to the bone pins. Four Falcon Hi-Res (Motion Analysis Corp., Santa Rosa, CA) (480 vertical lines resolution) cameras, equipped with infra-red strobe lights, were used to record the 2D spatial position of the reflective markers. The cameras were placed in a semi-circular arrangement over a 130° angle with alternating heights of one and two meters (Figure 3-4). This arrangement optimizes the optical convergence angles producing more accurate 3D reconstructions (Woltring, 1990). Expert Vision Analysis (EVA, Motion Analysis Corp., Santa Rosa, CA) software was used to collect the dynamic trials at 60 Hz for 10 seconds. The field of view was calibrated using a 12 point calibration frame (250 x 380 x 356 mm) and a

three-point wand (0.5 m length).

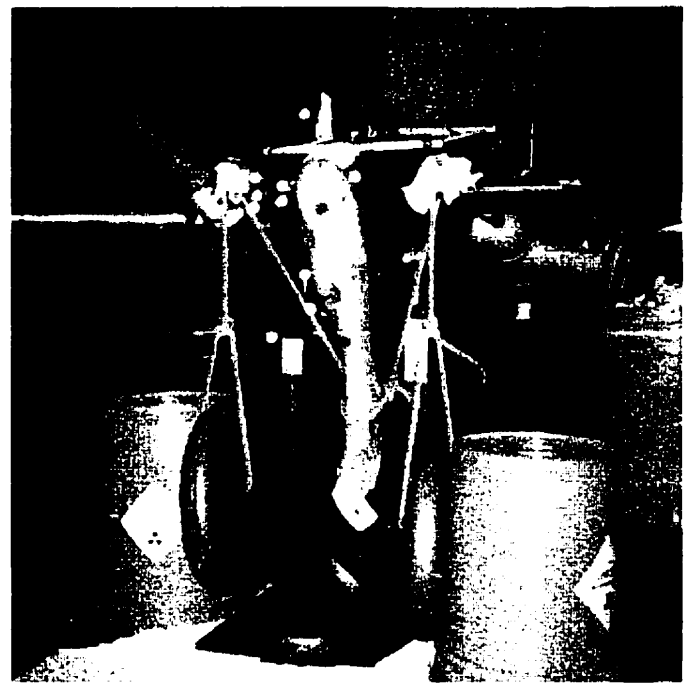

Figure 3-3 Loading apparatus

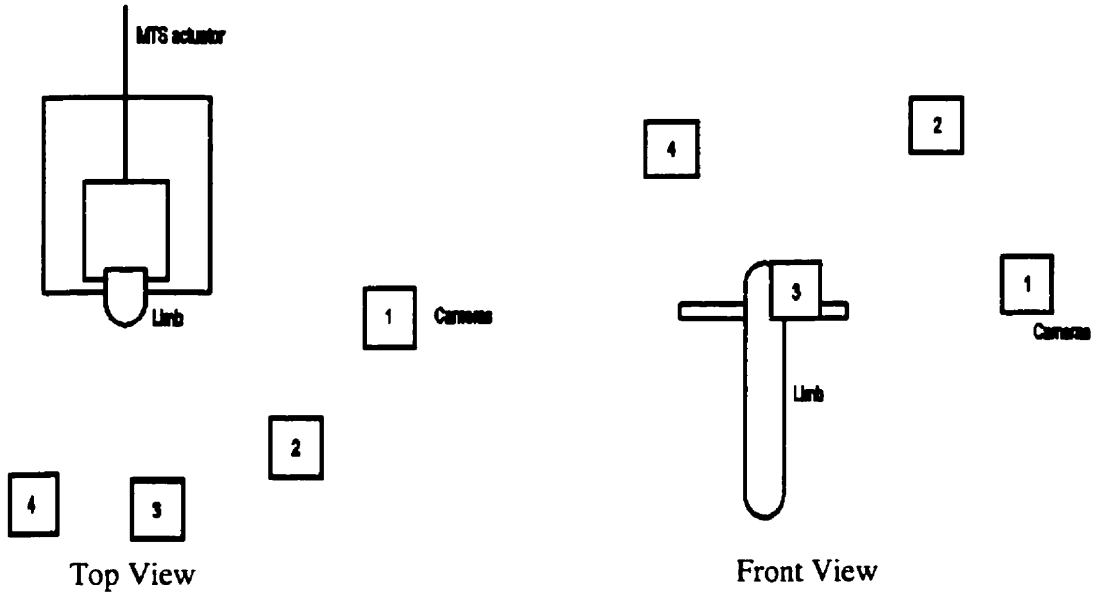

Figure 3-4 Motion analysis camera set-up.

All trials were tracked using EVA software for all frames of collected data. This produces the 3D coordinates of each marker which were further input into a MATLAB program to determine specific knee joint motions.

3.1.3 Quantification of Knee Joint Kinematics

Meaningful quantification of the kinematics, in this thesis, requires the use of several coordinate systems. A global or lab coordinate system (LCS) for the camera system is created with the cube calibration. All kinematic marker positions are recorded in this coordinate system. Relative segment motion could be calculated, using any combination of three markers per segment, in this coordinate system but it would have no clinical or anatomical meaning. Therefore, anatomical coordinate systems (ACS) were created using additional markers. Due to experimental limitations, e.g. skin impingement and marker merging, the anatomical markers could not remain during dynamic motion trials. Marker trees, used in dynamic motion trials, were constructed to minimize skin impingement, allow flexibility to optimize marker position for the specific camera configuration and to represent rigid body rotation and translation. The marker trees consisted of four markers, arranged on stiff metal wire similar to a tripod (one marker was in the centre, the rest on separate wires). A static trial was done to relate the 3D positions of the anatomical markers (which were subsequently removed during dynamic trials) to the marker tree 3D positions. Thus, through a series of coordinate transformations, the data measured in lab system coordinates could then be calculated in anatomical system coordinates.

The objective of this section is to describe the anatomical coordinate systems that were used to describe relative bone motion in a clinically relevant way. The work outlined in this

section has been previously published (Powers et al. 1998). A five step process was utilized:

1) Anatomical coordinate system determination for each bony segment (i.e. FCS for femur, PCS for patella and TCS for tibia).

2) Relationship between dynamic and static markers - Use the static trial to convert marker tree positions into their respective ACS

3) Dynamic motion determination - Calculation the rotation and translation between the LCS and ACS for each frame of data.

4) Relative segment motion determination - Multiplication of matrices to describe relative motion

5) Body segment motion description - Decomposition of the matrices in Step 4 to find angles of rotations about segment axes and translations along segment axes

ANATOMICAL COORDINATE SYSTEM DETERMINATION

The creation of segment coordinate systems and their relative movement were unique in this study. The segment coordinate systems were required to be anatomically meaningful, and independent of experimental setup and orientation of the limb in the lab coordinate system. For efficiency and accuracy, the measurements to define the ACS were obtained with the Motion Analysis System (MAS). Consequently, the coordinate systems were established using reflective markers attached to bone pins. This required using as few markers as possible, strategic placement to avoid impinging motion and to minimize marker merging in the various camera views. The development of these anatomical coordinate systems is described in detail in the following sections. Each coordinate system was defined by three directional vectors and an origin which can be expressed as a transformation matrix. The method of creating transformation matrices is explained in section 2.4, and will be used in this study to work between various coordinate systems.

FEMUR

The femoral coorinate system (FCS) was specified with the longitudinal axis (y) of the femur directed positive proximally, the superior/inferior axis (z) directed positive superiorly, and the medial/lateral axis (x) directed positively medial. For specification of the yz-plane, three markers were placed anteriorly/posteriorly along the long axis of the femur (Figure 3-5). The markers were rigidly attached to rods inserted in the bone. The distal rod had a single marker attached, while the proximal rod consisted of two markers placed one on top of the other. This double marker rod defined the orientation of the z axis. The origin was located at the intersection of the line connecting the medial and lateral aspects of the femoral condyles with the centre of the long axis of the bone, the yz plane.

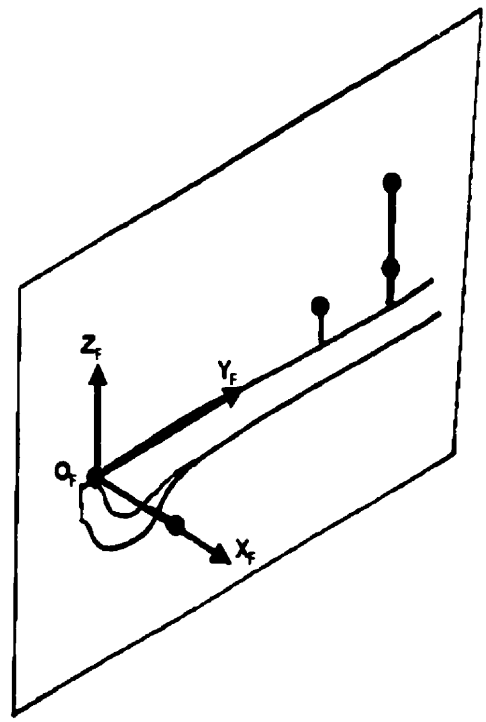

Figure 3-5 The femoral coordinate system.

TIBIA

The tibial coordinate system (TCS) was defined similarly to the FCS. The yz plane was specified with three markers implanted on the tibial crest (Figure 3-6). The x-axis was defined by a marker inserted in the medial tibial condyle. The origin of the tibial coordinate system was defined by the point of intersection of the x-axis with the yz plane. The z-axis was defined by the vector passing through the markers of the distal bone pin on the tibial crest. The vector cross product of the z and x-axes defines the y axis.

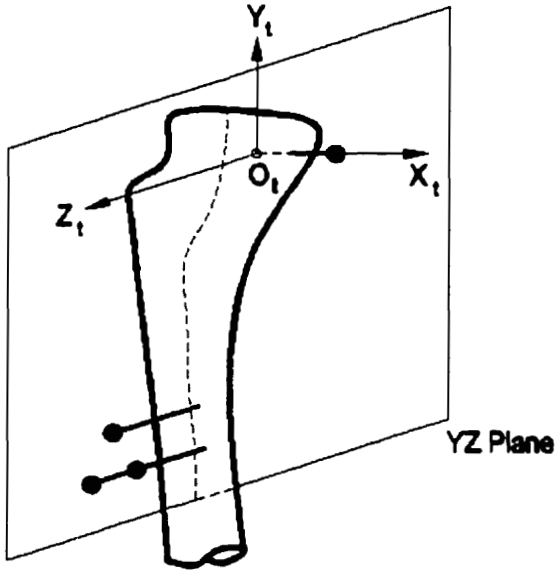

Figure 3-6 The tibia coordinate system.

PATELLA

The small size of the patella required a slightly modified method. Three markers were arranged on the surface of the patella to form a plane. This was considered the xy-plane. The normal of this plane was defined as the z-axis. The three markers in this plane were also arranged in an L shape, with the corner of the L in the centre of the patella. The two markers

lying anterior/posterior along the long axis were used to determine the y-axis. The y-axis was then calculated as the vector cross product of the z and x axes. The origin was found by translating the central marker along the z-axis into the centre of the patella by a measured distance O_p (Figure 3-7).

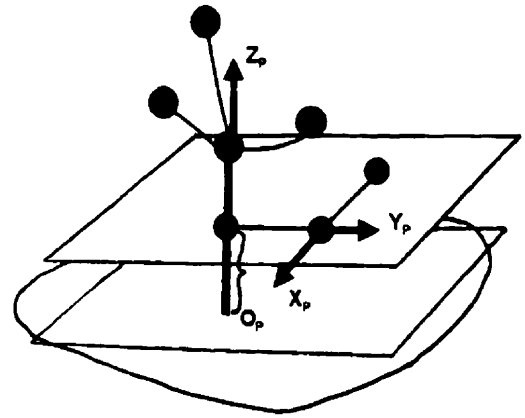

Figure 3-7 The patella coordinate system.

RELATIONSHIP BETWEEN DYNAMIC AND STATIC MARKERS

The unit vectors describing the axes of the FCS were arranged as columns in a [3x3] rotation matrix. The origin of the FCS was placed in the fourth column and [0 0 0 1] filled in the fourth row, creating a [4x4] transformation matrix $[{}^{L}T_{F}]$. A similar procedure was applied for the patella and tibia, yielding matrices $[{}^{L}T_{P}]$ and $[{}^{L}T_{T}]$ respectively. The marker tree coordinates attached to each segment could then be described in the respective anatomical coordinate systems by:

$$[M_F] = ([{}^{L}T_{F}]^{-1} \cdot [M_{LF}]) \quad 3.1$$

$$[M_P] = ([{}^{L}T_{P}]^{-1} \cdot [M_{LP}]) \quad 3.2$$

$$[M_T] = ([{}^{L}T_T]^{-1} \cdot [M_{LT}]) \quad 3.3$$

where M_F, M_P and M_T are the marker position coordinates in the femur, patella and tibia coordinate systems respectively. M_{LF}, M_{LP} and M_{LT} are the marker position coordinates in the lab coordinate system for the femur, patella and tibia respectively.

DYNAMIC MOTION DETERMINATION

The resulting marker positions described in their respective ACS and the marker positions described in the LCS for each video frame were then input into the algorithm presented in Söderkvist and Wedin (1993) implemented in a MATLAB algorithm. This resulted in a transformation between the LCS and ACS for each frame of data. For example,

$$[{}^{L}T_F]_i = soder(M_{F_0}, M_{F_i}) \quad 3.4$$

$$[{}^{L}T_P]_i = soder(M_{P_0}, M_{P_i}) \quad 3.5$$

$$[{}^{L}T_T]_i = soder(M_{T_0}, M_{T_i}) \quad 3.6$$

where i = frame number and

soder is the algorithm described in Söderkvist and Wedin (1993).

RELATIVE SEGMENT MOTION DETERMINATION

Relative motion between segments can be described as the motion of one segment described in the coordinates of another anatomical coordinate system. The relative motion of the patella with respect to the femur and of the tibia with respect to the femur can be calculated by multiplying the transformation matrices together, i.e.

$[{}^{F}T_P] = [{}^{L}T_F]^{-1} \cdot [{}^{L}T_P]$ for patella motion relative to femur and

$[{}^{F}T_{T}] = [{}^{L}T_{F}]^{-1} \cdot [{}^{L}T_{T}]$ for the tibia motion relative to femur.

BODY SEGMENT MOTION DESCRIPTION

The transformation matrix can be broken down into three rotations, $[R_{\alpha}]$ rotation about the x-axis, $[R_{\beta}]$ rotation about the y-axis and $[R_{\gamma}]$ rotation about the z-axis, and three translations along its axes [H_x, H_y, H_z]. The rotations are sequence dependent i.e. $[R_{\alpha}] \cdot [R_{\beta}] \cdot [R_{\gamma}] \neq [R_{\alpha}] \cdot [R_{\gamma}] \cdot [R_{\beta}]$. This study incorporated the order of rotation proposed by Cole et al. (1993). The first rotation is about the flexion/extension axis (x), the second rotation about the ab/adduction axis (z), and the final rotation about the internal/external axis (y). Therefore, patella flexion (α), tilt (γ), rotation (β) and shift (H_x) can be determined from the matrix $[{}^{F}T_{P}]$. Tibial flexion (also termed knee joint flexion, α), ab/adduction (γ) and rotation (β) can be determined from the matrix $[{}^{F}T_{T}]$. The careful selection of the axes and rotation sequence in this study produces the same joint coordinate system proposed by Grood and Suntay (1983).

3.1.4 Kinematic Data Analysis

The kinematic data were described as relative motions with respect to the femur. Variables of interest included: patellar flexion, tilt, rotation, shift and tibial ab/adduction and rotation. All kinematic data were smoothed using a low-pass filter set at 3 Hz with a resampling frequency of 20 Hz. These variables were all plotted as a function of knee joint flexion angle (flexion of tibia relative to femur) for analysis. In the description of motion of the patella and tibia in this study, all left limb results were multiplied by (-1) for graphical comparison with

right limbs.

3.1.5 Kinetic Data Analysis

The MTS actuator was used to produce an extension motion of the knee joint. In addition, the amount of force required to extend the limb was recorded. This can be referred to as the extensor mechanism force (EM force). The EM force was collected at 100 Hz, for a 10 second duration. The MTS and Motion Analysis System were connected electronically to allow synchronization of the kinematic data and the force data. A hand-held trigger was used to send a voltage drop to both machines to achieve the synchronization. EM force is presented as a function of time.

3.1.6 Sensitivity to Alignment Analysis

The accuracy of the kinematic results depends not only on the video accuracy but on experimental factors as well. This study examined the alignment of the limb in the experimental apparatus and its effects on the calculated kinematic parameters. Two limbs were used to study alignment (L1621 and L1702). Limb L1621 was not included in the regular kinematics because there were no load comparisons completed on this limb. To examine the effects of alignment, the MTS actuator was oriented 15° medially and 15° laterally with respect to the femoral longitudinal axis and the limb was extended through 90° ROM following the protocol outline (section 3.1.2). The data were tracked and calculated as described in section 3.1.2 and section 3.1.3. Differences between the neutral and altered alignments were tested for statistical significance at 15°, 30°, 45°, 60° and 75° using a one-way analysis of variance. Significance was further tested using pair-wise Bonferroni tests.

The repeatability of the marker positions was also examined. Six static trials were

completed, where the static markers were removed, replaced, switched, and the free-hanging limb was perturbed and allowed to settle again. The mean marker coordinates were calculated over all 60 frames of each trial. Means and standard deviations were calculated between all 6 trials, for each marker coordinate to determine the variability.

3.1.7 Statistical Analysis

All statistics for this study were calculated using Excel (Microsoft Office'97, Microsoft Corp., Redmond, WA) software. A two-way analysis of variance was used to test for interaction between loading conditions. The slope of the curve between 30° and 75° of knee joint flexion was chosen as the most representative factor to test the shape of the curves. This was considered reasonable only because most of the curves followed an increasing or decreasing progression as a function of flexion angle in this range. Had wavering or more complicated curves been presented this method would not be valid.

If significant interactions were found, pairwise tests, using the Scheffé method (Lapin, 1990), were subsequently performed. This method allowed for multiple contrasts, to determine confidence intervals. A significance factor of α=0.05 was chosen for all tests. The null hypothesis was $\mu_1=\mu_2$, i.e. the mean (over five trials) of each condition were equal.

Single factor ANOVAs were performed on limb L1702, at 15°, 30°, 45°, 60° and 75° of flexion, to test for significant interaction in kinematic variables due to a change in the alignment of the EM pull. In variables where significant interactions were found, pairs were tested using the Bonferroni method (Lapin, 1990). This test uses a student -t distribution to test for significant differences. A significance factor of α=0.05 was used and the null hypothesis tested was that the means of the trials were equal.

3.2 Quantification of Articular Cartilage Surface Geometry

The components involved in quanitifying the articular cartilage surface geometry include: specimen preparation, multi-station digital photogrammetry, image digitization, 3D image reconstruction, surface representation and curvature description and contact area quantification. The procedures employed were based on those described by Ronsky et al. (1999) and Boyd (1997). A brief overview of these procedures, and description of unique aspects employed in this study are presented in this section.

3.2.1 Specimen Preparation

For cartilage surface imaging, the knee was disarticulated, taking care not to disturb the surface or the reflective markers. The cartilage surface was immediately covered with saline-soaked gauze to maintain hydration levels. The femur was attached to a wooden block with wood screws, and then rigidly mounted on a tripod. For use with multi-station digital photogrammetry, a ring with eight control posts of varying heights was carefully oriented around the trochlea and secured using three screws. These posts defined the ring coordinate system during image reconstruction. The patella was fixed in a similar manner to a control post ring and frame and subsequently mounted on a tripod. All experiments were conducted at room temperature (about 18°C).

3.2.2 Multi-Station Digital Photogrammetry

Digital images were recorded using two DCS 420 Kodak cameras (Eastman Kodak Company, Rochester, NY) with CCD sensor resolution of 1524 x 1012 pixels. Camera one was calibrated for a small field-of-view (210 x 140 mm), incorporating only the articulating surface and ring. Camera two was calibrated for a larger field-of-view (200 x 300 mm),

incorporating the kinematic markers as well as the articulating surface and ring. The calibration required the use of two different calibration frames. Camera 1 was calibrated using a 32-point calibration frame 100 mm in diameter with three different post heights (15, 34 and 54 mm) distributed and arranged in concentric circles (Figure 3-8). The base and post stems were painted black with white tops, for enhanced contrast to facilitate improved edge detection.

Camera two was calibrated with a 12-point rectangular calibration frame (125 x 80 x 135 mm) (Figure 3-9). The control points on this frame consisted of spherical reflective markers of similar size (10 mm diameter) as those used in the kinematic data collection.

The 3D spatial positions of the marker centroids for all control points on the calibration frames were measured with the Coordinate Measuring Machine (CMM, Bright 1200 Series, Mitutoyo, Japan) to an accuracy of ± 1 μm.

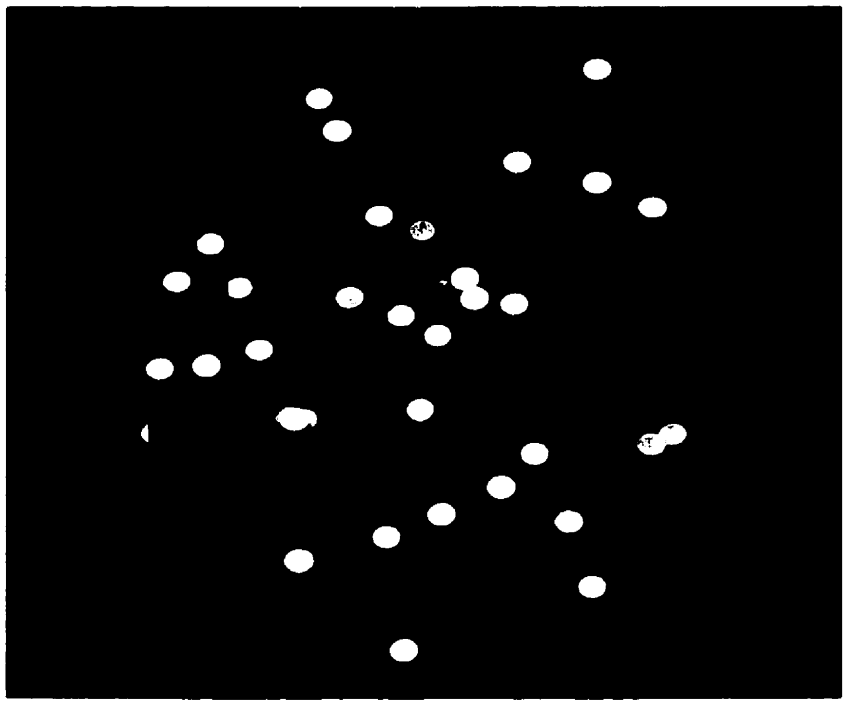

Figure 3-8 Surface calibration frame.

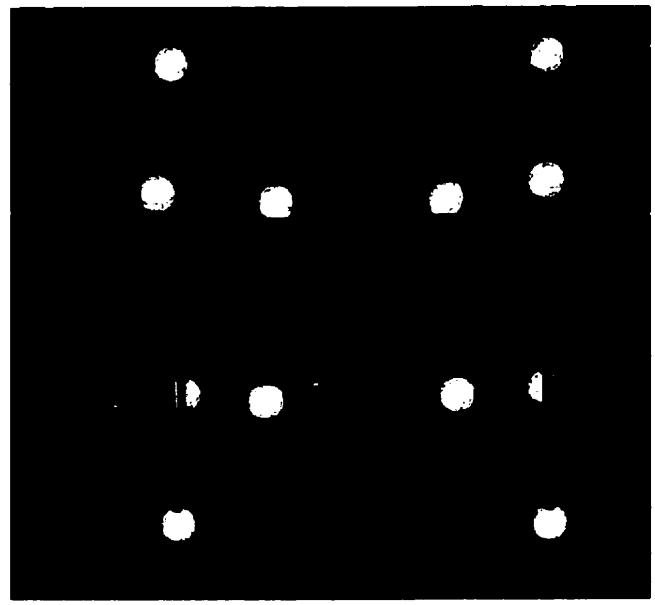

Figure 3-9 Kinematic calibration frame

Calibration of each camera was necessary for calculating the internal parameters and lens distortions. Sixteen images were taken for each calibration. The optical axis of the camera was set at a 45° angle to the calibration frame and a bright flood light was shone directly above the calibration frame for improved contrast between the post tops and the background and for the elimination of shadows caused by the room lighting. The calibration frames were rotated 45° clockwise for each image (8 different positions) and the camera was rotated 90° clockwise about its optical axis for the final eight photographs. This provided a 90° convergence angle for the image reconstruction.

To record the surface topography of the articular cartilage and subchondral bone of the patella and femur, a slide projector was positioned perpendicular to the joint surface. A grid

was projected onto the joint surface to provide identifiable reference points in each image for later grid reconstruction. The sharpness, contrast and spacing of the grid is important for accurate, repeatable points in the digitization process. Trial photographs of a series of slides were taken and enlarged (more than 200%) to determine which provided the sharpest grid lines. Once the optimal grid size and shutter speed were determined, the camera was placed at six different locations around the specimen (Figure 3-10). Camera locations were chosen for optimal convergence angles. The shutter speed was set to a 1.5 - 2.0 second exposure time. The entire image acquisition process took about 30 minutes to complete.

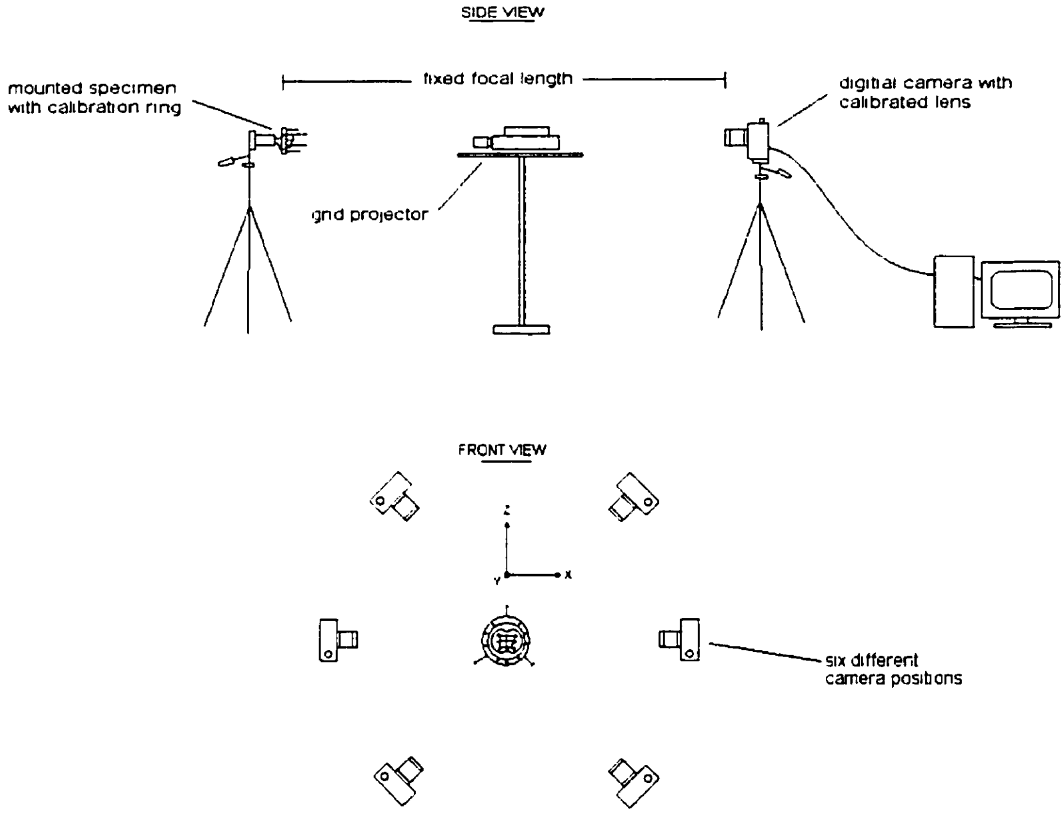

Figure 3-10 Multi-station digital photogrammetry experimental setup.

Images were acquired remotely using Adobe Photoshop 5.0 (Adobe Systems Inc., San Jose, CA) and an IBM compatible PC (Pentium II, 400 MHz processor, 64 MB RAM).

Images were converted to 8-bit greyscale and saved as raw format (This is the format that is compatible with the digitizing programs described in section 3.2.3). Six images were obtained for each cartilage surface including the projected grid and control-post ring.

The orientation and location of the joint surface relative to the kinematic markers was measured with Camera 2. Six images of the control posts, ring and kinematic markers were obtained using the same camera orientation as used in the joint surface measurements with Camera 1.

For imaging of the subchondral bone surfaces, the kinematic markers were carefully removed, avoiding contact with the control post ring. Articular cartilage and all other soft tissue were dissolved by immersing the bone and control ring in a 5.25% solution of sodium hypo-chloride (regular household bleach) for a period of 8-12 hours. The bone surfaces were then imaged using the same procedure outlined above.

3.2.3 Joint Surface Digitization

The acquired images required precise digitization of a) the 2D centres of control post tops on the ring and b) the 2D grid intersections. This was accomplished using MATLAB (v.4.2, Mathworks Inc., Natick, MA) programs written by Boyd (1997); Digitizer.m (a) and Grider.m (b), respectively.

Control Post Digitization

For 2D centre calculation, the sharp contrast feature of the white control post tops and the black background, enabled the use of edge detection algorithms. Sub-pixel accuracy for the edge point is provided by the edge detection algorithm. The edge detection algorithm (Digitizer.m) requires an area specified by the user as input. The centre of gravity is

calculated based on a weighting of pixels in the prescribed area, according to grey-scale intensities. The area of the control post top is then divided into four regions and a one-dimensional edge detector algorithm is applied to each region (Boyd, 1997). The interim results of the edge detection are displayed and the user may optimize the fit by manually removing outlier points. These optimized edges are fit to an analytical model of an ellipse based on a least-squares fit algorithm. The centre of the ellipse was then recorded as the 2D position of the post. The 2D positions of the spherical markers on the calibration frame for Camera 2 and the kinematic markers were also digitized in this way.

Grid Intersection Digitization

The grid intersection points on the joint surface were used for 3D surface reconstruction. The first stage of this process required identification of the 2D coordinates of these grid intersections in all six images. The algorithm for 2D grid intersection coordinate determination (Grider.m) was based on user defined seed points, input between grid intersections, for each horizontal and vertical line. The program then took +/- 10 pixels to either side of the seed point, in a perpendicular direction to the seed points to map the pixel intensity across the line. The pixel of the lowest intensity was specified as the centre of the line. The coordinates of each centre point of the line were saved and then fit to a third-order cubic spline. For areas of high curvature, additional seed points at more frequent intervals provided a better spline fit. This process was completed for each horizontal and vertical line. Line intersections were then calculated and superimposed on the original image. The user could then optimize these intersection points through manual removal or addition of intersection points. All intersection points were then numbered consistently and

systematically for all images using the three darkened grids as a coordinate system orientation (Figure 3-11). These 2D grid intersection points for each image were then input into the bundle adjustment algorithm.

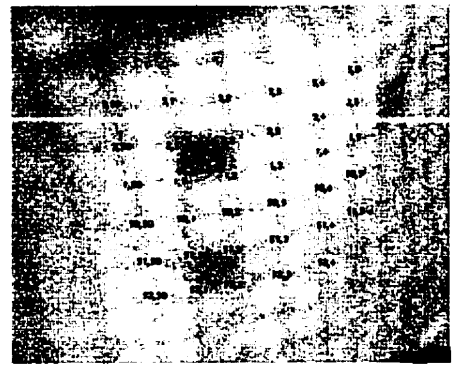

Figure 3-11 Grid intersection numbering system

3.2.4 Three-Dimensional Reconstruction

The reconstruction of multiple 2D images into a 3D image was accomplished using a finite element bundle adjustment method (Lichti, 1996). A program written by D. Lichti (Geomatics Department, University of Calgary, 1998) was used for this process. This was a two-step process involving camera calibration and image point reconstruction. Camera calibration solved for the principal distance and focus which are required for image point reconstruction.

Step 1: Camera calibration was achieved using a self-calibrating bundle adjustment performed on the highly redundant 16-image network photographed as described in section 3.2.2. The 2D post centre (for Camera 1) or spherical centre (for Camera 2) positions of the calibration frame (from the digitizing process) and their respective 3D known positions (measured with the CMM) were the only inputs. The self-calibrating bundle adjustment

solved for the exterior camera positions as well as the interior parameters of the camera simultaneously.

Step 2: 3D reconstruction of surface points and of the kinematic marker centres were solved. Inputs included the interior camera orientations from Step 1 and the 2D post centre and grid intersection points from the digitization process. The 2D post centre positions provided the control points for the image bundle adjustments. The 2D grid intersections were added as the unknown tie points for which the bundle adjustment would solve.

3.3 Mathematical Model of the Human Knee Joint

The relationship between knee joint kinematics throughout the range of motion and the corresponding patellofemoral joint contact patterns were investigated using a 3D mathematical model. This knee joint contact model required the combination of the kinematic data with the original surface data points from the bundle adjustment. However, as these data sets were obtained in different coordinate systems, coordinate transformations were required to determine the relative positions of the joint surfaces from the kinematic data (Figure 3-12). The 3D surface data, provided by the bundle adjustment and thin plate spline (described in section 3.3.1), was in the ring coordinate system (RCS). The kinematic data could be output in either the lab coordinate system (LCS) or the segment coordinate systems (SCS). The femur coordinate system (FCS) was chosen for the mathematical model, because it was meaningful and the femur did not move with respect to this coordinate system.

The kinematic markers remained rigidly fixed in both the kinematic data collection and the surface data collection procedures. The marker tree data from the dynamic trials were measured in the lab coordinate system (LCS). The transformation matrix between the femur

RCS and the LCS $[{}^{L}T_{Fring}]$ and the patella RCS and the LCS, $[{}^{L}T_{Pring}]$ were calculated at each frame of kinematic data using the algorithm described in Söderkvist and Wedin (1993). This algorithm was also used to find the transformation matrix between the femur FCS and the LCS, $[{}^{F}T_{L}]$, and likewise for the patella, $[{}^{P}T_{L}]$.

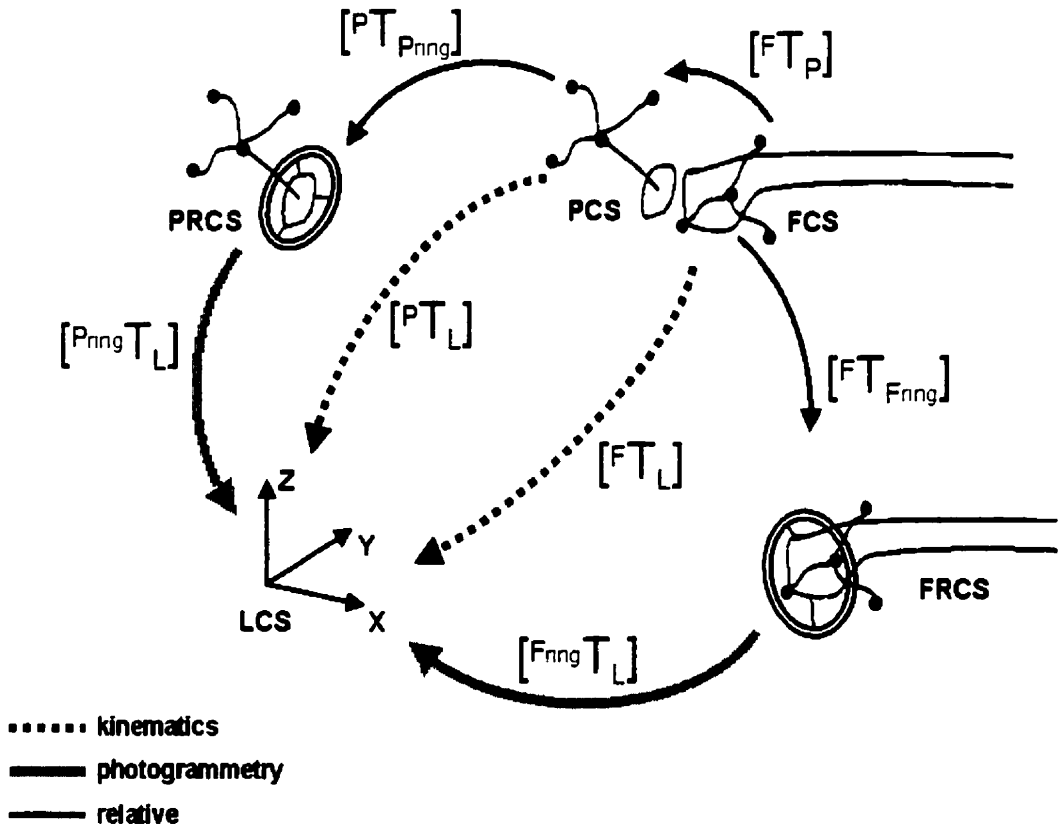

Figure 3-12 Schematic of coordinate system transformations.

Using matrix multiplication, the transformation matrices to convert surface grid point data (RCS) into the FCS, is outlined in equations 3.7 to 3.10.

$$[{}^{P}T_{Pring}] = ([{}^{P}T_{L}] \cdot [{}^{L}T_{Pring}]) \quad 3.7$$

$$[{}^{F}T_{P}] = ([{}^{F}T_{L}] \cdot [{}^{P}T_{L}]^{-1}) \quad 3.8$$

$$[{}^{F}T_{Pring}] = ([{}^{F}T_{P}] \cdot [{}^{P}T_{Pring}]) \quad 3.9$$

$$[{}^{F}T_{Fring}] = ([{}^{F}T_{L}] \cdot [{}^{L}T_{Fring}]) \quad 3.10$$

One further manipulation to the data was done at this point to ensure the most accurate surface representation possible. Because the thin plate spline is sensitive to curvature in the z (depth) direction, the surface data was manually rotated about the x-axis until the femoral trochlea was located as much as possible in the x-y plane.

3.3.1 Joint Surface Representation

The description of surface in a single mathematical expression can be accomplished by fitting the data to a thin plate spline. A thin plate spline algorithm implemented by Boyd (1997) was used for this step. The program, written in MATLAB, required the original surface data points of either one or two surfaces and the resampling grid spacing. The calculations in this program are presented below. More detail can be found in Boyd et al. (1999).

Any point on the surface, S(x,y), can be described as a function of x and y:

$$S(x, y) = [F][C]^{T} \quad 3.11$$

where:

$$[F] = \left[f_1\ f_2\ f_3\ \ldots\ f_n\ 1\ x\ y\right] \text{ and } f_i \text{ is the translate of the bi-variate function,} \quad 3.12$$

$$[C]^{T} = \left[c_1\ c_2\ c_3\ \ldots\ c_n\ c_{n+1}\ c_{n+2}\ c_{n+3}\right] \text{ and } c_i \text{ are the constants for the bi-variate function,} \quad 3.13$$

and x and y is any point in the 2D surface.

The first n terms of [F] and [C] correspond to the interpolating projector Q and the last three terms correspond to the polynomial projector P. The translates for bi-variate function of x and y are f_i and are calculated as follows:

$$f_i(x, y) = r_i^2 \log(r_i) \tag{3.14}$$

where:

i = the experimental data points and

$r_i^2 = (x - x_i)^2 + (y - y_i)^2$ is the Euclidean distance between 2 data points. (3.15)

The contents [C] are the only unknowns and are solved using the following matrix multiplication.

$$\begin{bmatrix} [A] & [B] \\ [B]^T & [0] \end{bmatrix} [C] = [Z] \tag{3.16}$$

where:

$$[A] = \begin{bmatrix} a_{1,1} & a_{1,2} & \cdots & a_{1,n} \\ a_{2,1} & & & \\ & & & \\ a_{n,1} & \cdots & \cdots & a_{n,n} \end{bmatrix} \Rightarrow \left\{ \begin{array}{c} a_{i,j} = f_i(x_j, y_j) \\ a_{i=j} = 0 \end{array} \right\} \text{ i,j = 1 to n data points,} \tag{3.17}$$

$$[B]^T = \begin{bmatrix} 1 & 1 & 1 & \cdots & 1 \\ x_1 & x_2 & x_3 & \cdots & x_n \\ y_1 & y_2 & y_3 & \cdots & y_n \end{bmatrix}, \text{ [0] is a 3x3 zero matrix,} \tag{3.18}$$

$$[Z] = \begin{bmatrix} z_1 & z_2 & z_3 & \cdots & z_n & 0 & 0 & 0 \end{bmatrix}^T \text{ and } x_i, y_i \text{ and } z_i \text{ are the experimental data points.} \tag{3.19}$$

Therefore, rearranging equation 3.16.

$$\begin{bmatrix} C \end{bmatrix} = \begin{bmatrix} \begin{bmatrix} A \end{bmatrix} & \begin{bmatrix} B \end{bmatrix}^T \\ \begin{bmatrix} B \end{bmatrix} & \begin{bmatrix} 0 \end{bmatrix} \end{bmatrix}^{-1} \begin{bmatrix} Z \end{bmatrix} \qquad 3.20$$

3.3.2 Contact Area and Cartilage Thickness Measurement

Contact between articulating surfaces can measured as the calculated distance between the surfaces. The distance between two surfaces is measured along the surface normal $\bar{n}$, projected from a resampled point on the origin surface to its intersection with the destination surface. For this study the origin surface was always the femur and the destination surface, the patella. Proximity calculations are outlined below.

The parameterized equations of the surface normal are:

$$x_l = n_x t + x_o \qquad 3.21$$

$$y_l = n_y t + y_o \qquad 3.22$$

$$z_l = n_z t + z_o \qquad 3.23$$

where:

(x_o, y_o, z_o) is a point on the origin surface and

(x_l, y_l, z_l) is a point a distance t along the line.

The intersection of the line with the destination surface (S_d) occurs at a height z_l at (x_l,y_l).

$$S_d(x_l, y_l) - z_l = 0 \qquad 3.24$$

or substituting equations 3.21 - 3.23

$$S_d(n_x t + x_o, n_y t + n_y) - (n_z t + z_o) = 0 \qquad 3.25$$

The only unknown is t which can be solved for through fixed point iteration. This requires

the rearrangement of equation 3.25.

$$t' = t - \frac{S_d(t) - (n_z t + z_o)}{\frac{d}{dt}(S_d(t) - (n_z t + z_o))} \qquad 3.26$$

where:

$$\frac{dS_d}{dt} = \left(\frac{\partial S_d}{\partial x}\right)\left(\frac{\partial x}{\partial t}\right) + \left(\frac{\partial S_d}{\partial y}\right)\left(\frac{\partial y}{\partial t}\right)$$

When $\bar{n}$ is normalized, the thickness t, is calculated in the same units as the surface points (mm). Cartilage thickness was quantified using this method and was tested on one limb in this study.

Contact was defined by the positive proximity or overlap of the articular surfaces (>0) because all surface data was collected on undeformed cartilage. The total contact area was calculated using a numerical method which sums the estimated area of each grid within the contact region. The centroid of the contact area was calculated as the mean (x,y,z) position of all grid intersection points on the origin surface (femur) with positive proximity. These positions are in the x, y and z coordinate directions of the femur anatomical coordinate system and are reported in mm.

The contact area was calculated at 30°, 45°, 60°, 75° and 90° knee joint flexion angles, for each trial. The means and standard deviations of the total contact area and of the centroid location, were calculated and plotted against flexion angle.

3.3.3 Articular Sulcus Angle Measurement

Traditionally, clinical evaluation of a patellofemoral problem involves acquiring a 2D x-ray measurement of the sulcus angle. The x-ray is taken at various knee flexion angles (30°-

60°) to evaluate the difference throughout flexion. A similar measurement can be made using the mathematical model presented earlier, with a method developed by B. Kralovic (1999).

A 2D slice was selected at the location of the centroid of the contact area. The slice was oriented parallel to the surface normal at this point. The contour of the femoral condyles and the retropatellar surface were then plotted on a graph. The abscissa was selected as the medial/lateral femoral axis (plotted in mm) and the ordinate axis was selected as the depth along the surface normal in mm. A computer algorithm was then written to automatically locate the most superior points on both femoral condyles and the most inferior point in the trochlear groove using local minimum and maximum finding technique. The lowest point on the retropatellar surface was also found and plotted. The three points on the femur were used to calculate the articular sulcus angle.

4.0 Results

3D kinematics of the patella and tibia movement relative to the femur were investigated in this study. Because of large inter-limb and inter-study variability presented in the literature, surface geometries were examined to better understand the role geometry may play in the resulting patellar tracking patterns. The results will be presented in two main sections: kinematics and surface geometry.

4.1 Knee Joint Kinematics and Kinetics

Six cadaveric lower limbs were used in the kinematic analysis part of this study. The specimen demographics are listed in Table 2.

Table 2 : Specimen Demographics

Specimen	Limb	Gender	Age
1702	left	Male	57
1632	left	Female	75
1737*	left	Female	70
1737*	right	Female	70
1748**	left	Male	79
1747**	right	Male	79

*, ** denote matched pairs

The kinematics for this study were calculated under three different conditions: no load, loaded with 89N and loaded with 222N of force. Five trials were collected for each condition. The variability between trials was very small (Figure 4-1). In fact the variability between the trials was so small that significant differences due to loading or alignment could be found with only a 1-3° difference in curves.

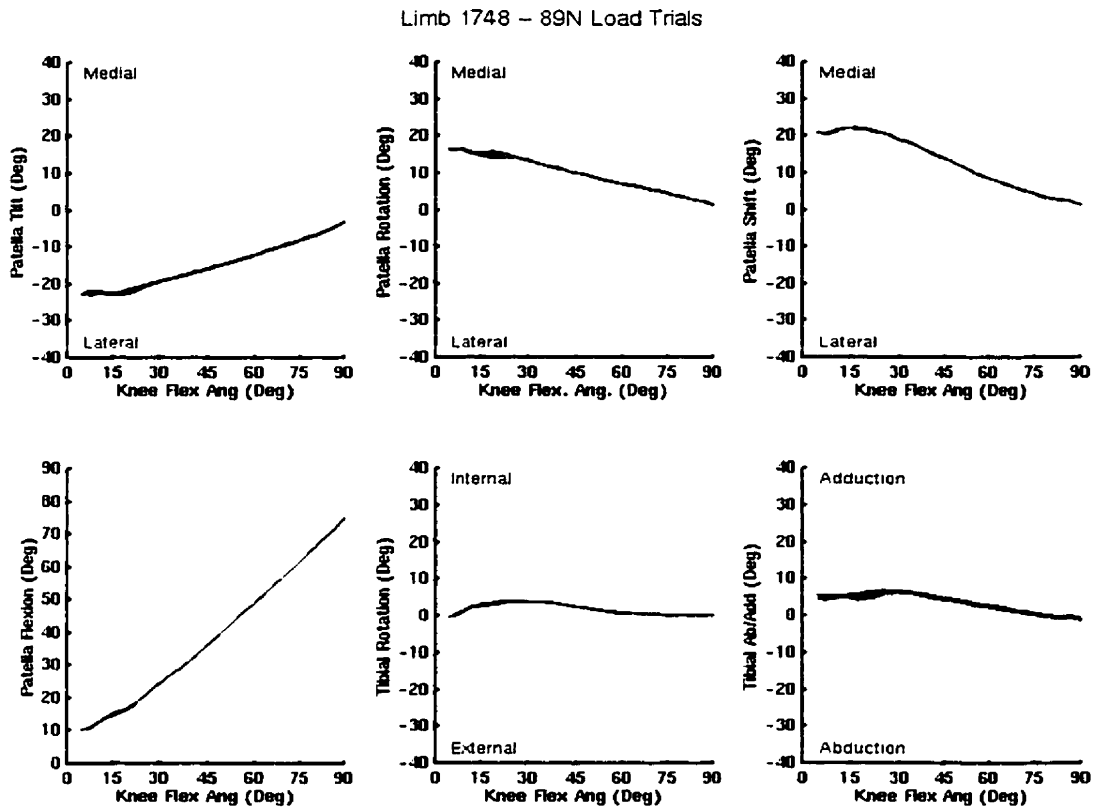

Figure 4-1 Repeatability of 5 trials: limb L1748

In the following sections a representative trial for every specimen and for each variable is plotted against the knee joint flexion angle, from 0° (full extension) to 90° flexion.

4.1.1 Kinematics of Patellofemoral Joint - No Load

PATELLA FLEXION

The rotation of the patella about the medial/lateral axis of the femur is classified as patellar flexion. The patella flexion angle consistently increased with increasing knee joint angle (Figure 4-2). Patella flexion lagged knee joint flexion throughout the range of motion (ROM), typically by 10-20°.

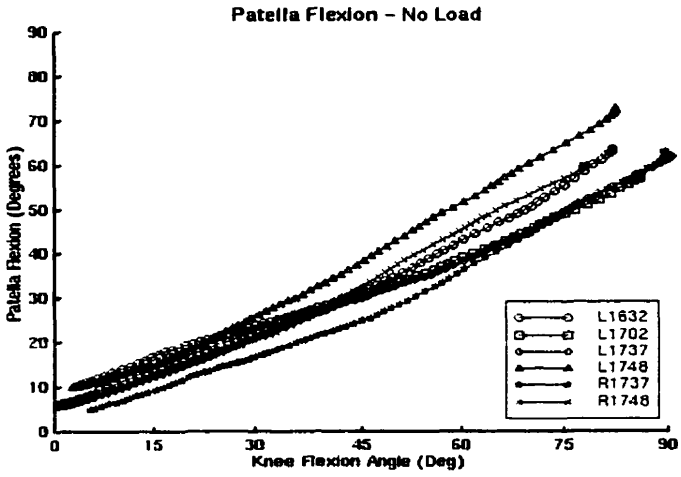

Figure 4-2 Patella flexion vs. knee joint flexion angle: Patella flexion increases with increasing knee flexion.

PATELLA TILT

Patella tilt is the rotation of the patella about its longitudinal axis. The patella tilt curves were variable, with several characteristic features (Figure 4-3). Overall the ROM for this variable was 5-10°. These results indicated the utilization of very different strategies in the first 20° of flexion. Three limbs began to tilt medially about 5° in the first 20° of flexion. Limb L1737 and R1737 were neutral in the first 15°, tilted medially (5-7°) between 15° and 30° knee joint flexion. Limb L1748 tilted laterally (5°) for the first 20° of flexion. From 30° to 90° two different trends were observed for patella tilt. Three limbs (R1748, L1702, L1737) showed a steady lateral tilt of 5° as the knee flexed while two other limbs (L1748, R1737) showed a medial tilt of about 6°. Limb L1632 tilted laterally about 3° between 20° and 40° of flexion and then tilted medially until 90° of flexion. All limbs demonstrated an inflection point between 10° and 20° knee joint flexion.

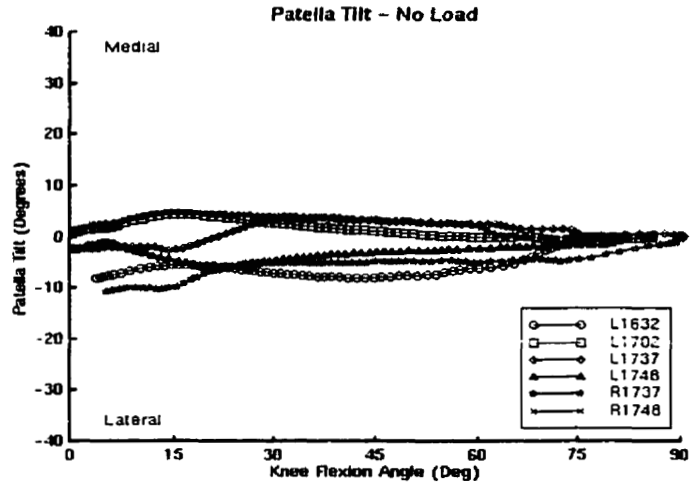

Figure 4-3 Patella tilt vs. knee joint flexion: Patella tilt was unstable in the first 20° of flexion. As knee flexion increased the patella tilted either medially or laterally about 5° depending on the limb.

PATELLA ROTATION

Patellar rotation is the rotation of the patella about the floating axis of the JCS where the rotation of the apex (distal end) of the patella towards the medial condyle is termed medial rotation.

Patella rotation showed a consistent trend among all six limbs (Figure 4-4). All limbs rotated laterally with increased knee joint flexion. Three limbs (R1737, L1632 and L1702) demonstrated a steeper slope and a larger range of patella rotation (17-20°) than the other three limbs (5-9°).

PATELLA SHIFT

The translation of the patella along the femoral medial/lateral axis is termed patella shift. In the first 20° of flexion, large variability was observed in patella shift, with most limbs demonstrating an excursion of ~2-5 mm medially, while limb L1737 shifted laterally 2 mm (Figure 4-5). All limbs exhibited a lateral shift of the patella with increased knee joint flexion.

Limb L1702 was the only limb that exhibited a slightly different pattern, shifting medially slightly (2 mm) between 20° and 35° flexion before shifting laterally again. Limbs R1748 and L1748 shifted a total of 10 mm laterally while limbs L1702 and L1737 shifted about 14 mm. Limb 1632 and R1737 shifted a very large amount (20mm and 30 mm respectively).

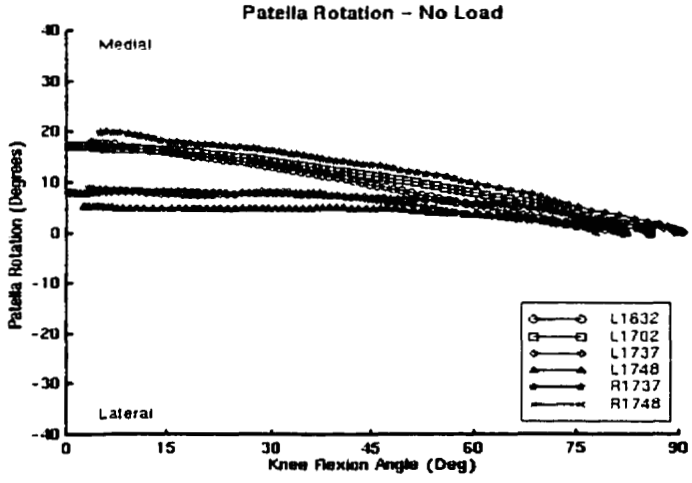

Figure 4-4 Patella rotation vs. knee joint flexion: The patella rotates laterally with increasing flexion for all limbs.

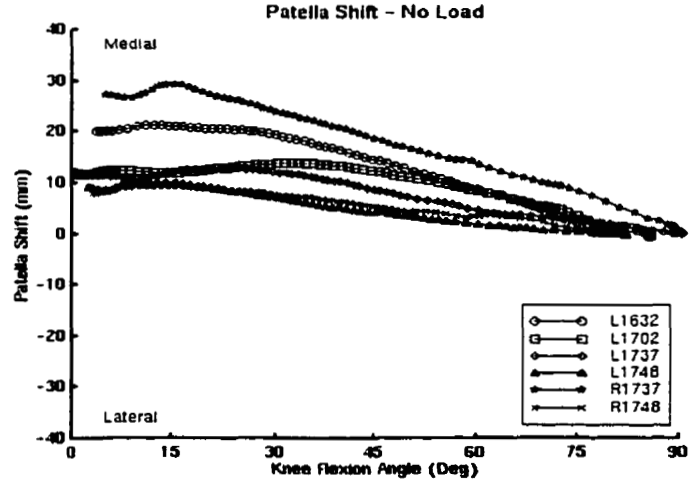

Figure 4-5 Patella shift vs. knee joint flexion: All limbs shift laterally as knee flexion increases. Limbs L1632 and R1737 exhibit an abnormally large lateral shift.

TIBIAL ROTATION

Tibial rotation is defined as the internal/external rotation of the tibia about its longitudinal axis. Five of the six limbs exhibited a similar trend (Figure 4-6). All five internally rotated (5-10°) in the first 30° of flexion and then steadily rotated externally as knee joint flexion increased to 90°. The external rotation from 30° of knee flexion until 90° of knee flexion ranged from 3° (L1702) to 20° (L1737). Limb L1748 externally rotated throughout knee flexion, over a range of 7°.

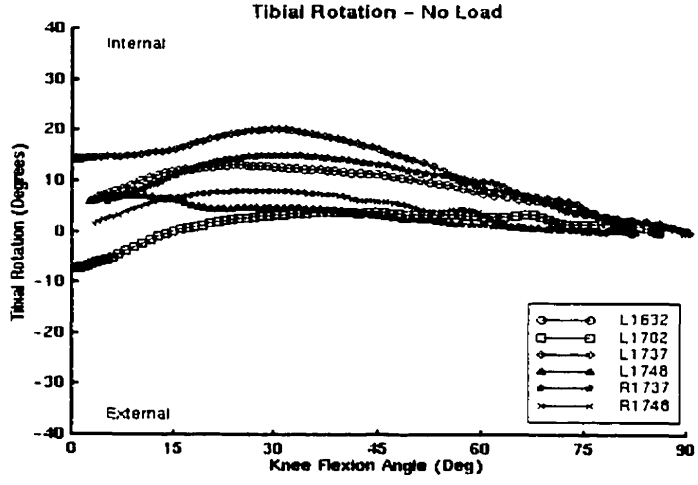

Figure 4-6 Tibial rotation vs. knee joint flexion: Five of the six limbs show tibial internal rotation in the first 30° of knee flexion, followed by tibial external rotation.

TIBIAL AB/ADDUCTION

Ab/Adduction of the tibia occurs about the floating axis of the JCS. Tibial ab/adduction exhibited more inter-limb variability than the other variables (Figure 4-7). All limbs exhibited fluctuations in the final stages of knee flexion (50 - 90°). Four limbs (L1632, R1737, L1737 and L1702) demonstrated adduction, ranging from 3° (R1748) to 23° (L1632), through 0° until about 50° of knee joint flexion. Limb L1702 and L1737 then abducted

through a range of 5° as the knee joint angle increased from 50° to 90°. Limb L1748 remained neutral for the first 30° of knee flexion, then abducted. Limb R1748 showed very little ab/ adduction movement (<3° total) throughout knee joint flexion.

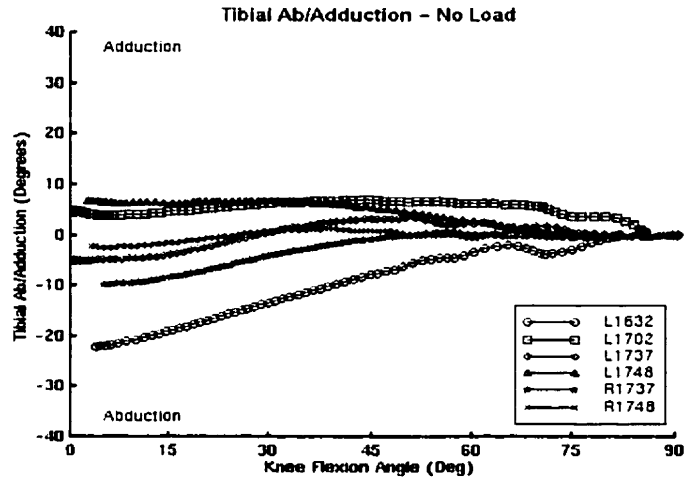

Figure 4-7 Tibial ab/adduction vs. knee joint flexion: In general most limbs demonstrated tibial adduction with increasing knee joint flexion. The tibia shows instability in the last 40° of knee flexion due to experimental setup.

4.1.2 Kinematics of Patellofemoral Joint - Loaded

To study the effects of loading on the patellofemoral joint kinematics, an axial compressive load was introduced through the calcaneous. Two loads were applied: 89N and 222N. Each limb responded to these loads differently (Powers, 1999). Therefore, the results will be presented individually, concluding with an overall summary. In general, as the load increased, the pattern of the individual curves, plotted against knee joint flexion, remained very similar, exhibiting some offset in response to loading.

Limb L1737

Patella flexion was the least affected variable during loading. All five other parameters were statistically significantly (α=0.05) different when load was applied. There was an

offset, about 2° for 89N and 4° for 222N, of the patella incurred due to loading which was consistent throughout the ROM (Figure 4-8). Patella tilt was 1-2° more lateral, the rotation about 2° more lateral and the shift 3° more medial, with an 89N load than in the no load condition. The tibia was also internally rotated 5° and adducted about 3° more in 89N load than in the no load condition. Throughout extension the patella tilt offset remained constant for 89N, but increased approximately 10° more laterally when loaded with 222N. Patella shift increased medially by about 5° for each loading condition around 30° of flexion. Tibial external rotation was greater by about 5° consistently throughout flexion for each load condition. Tibial ab/adduction exhibited two different strategies for the different loading conditions. For 89N load, the tibia remained more adducted, with the offset decreasing throughout extension while it abducted as much as 8° more for the 222N load condition.

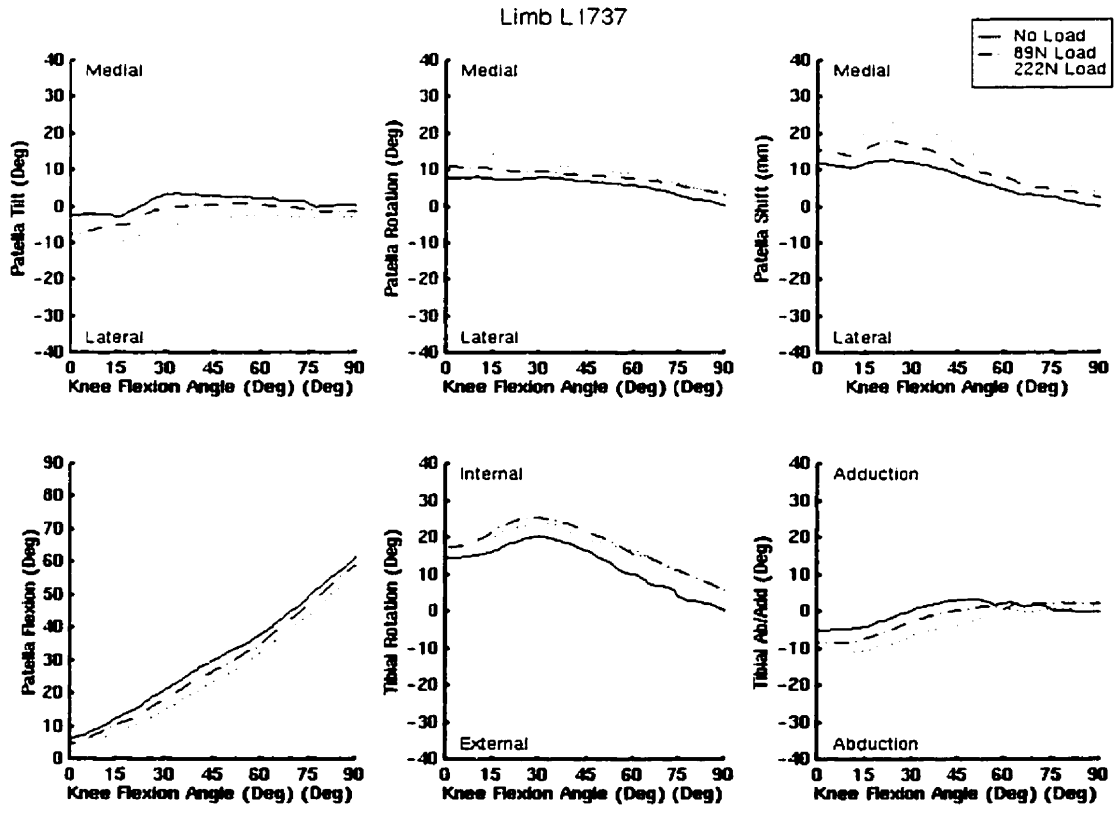

Figure 4-8 Limb L1737 loading effects on patella and tibial variables.

LIMB L1702

Only two variables, patella rotation and tibial ab/adduction, were significantly affected by loading for this limb. Patella rotation, tilt, shift and tibial internal/external rotation exhibited a small offset (1° lateral rotation, 1° medial tilt, 3mm medial shift and 1° internal rotation) due to the 89N load but returned back to the unloaded values when the 222N load was applied (Figure 4-9). The tibia abducted (2° at 90° flexion, increasing to about 10° full extension) for both loading conditions. Patella flexion was not influenced by loading for this limb.

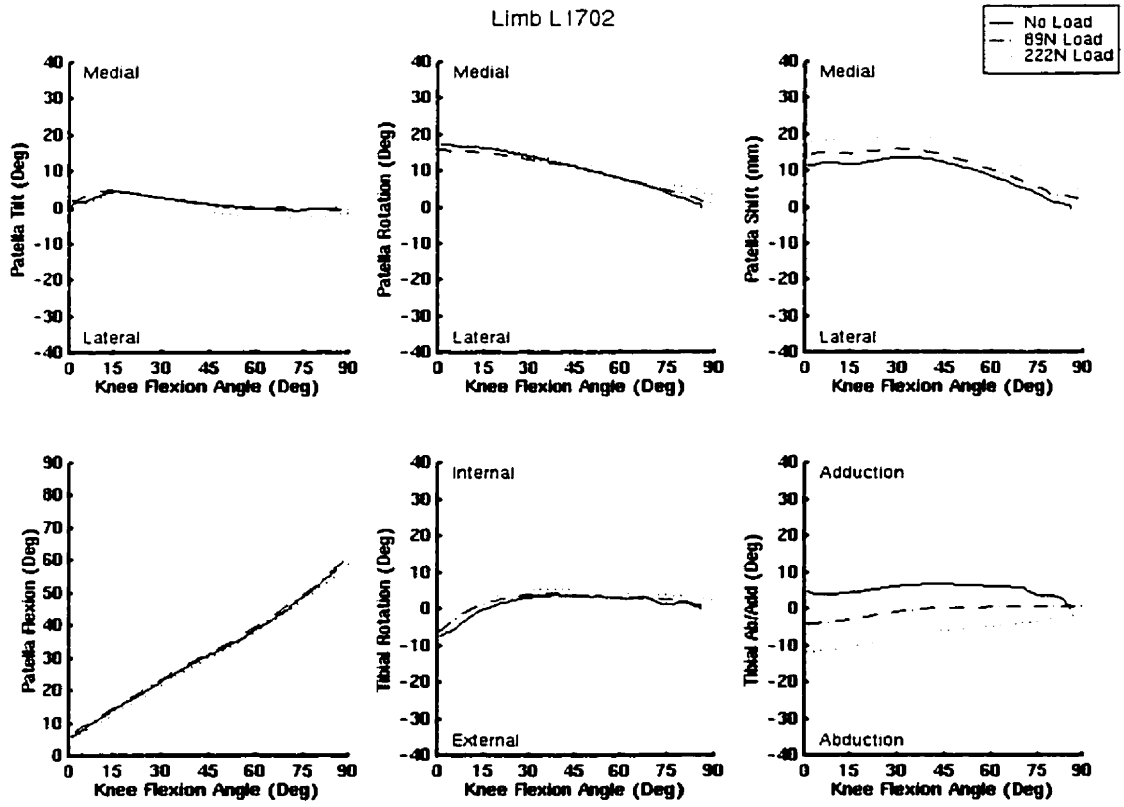

Figure 4-9 Limb L1702 loading effects on patella and tibial variables.

LIMB R1737

Loading resulted in an increased lag of patella flexion (~3°), relative to knee flexion

(Figure 4-10). Increasing the load from 89N to 222N, resulted in an increased lag of patella flexion of ~6°. Generally, loading resulted in an offset in the magnitude of the variables with the slopes of the curves not differing statistically significantly for each loading condition. In patellar tilt this offset was only about 2° lateral, patellar rotation showed a 2°-5° medial offset while shift had a 3-5 mm medial offset throughout knee flexion. Tibial internal rotation increased by 5° and 10° more with 89N and 222N loads, respectively. Tibial ab/adduction was the only variable which was statistically significant between the no-load and loaded conditions. Little offset (<1°) occurred at 90° knee flexion. Throughout extension more abduction occurred with loading ending with an increase of 5° (89N load) and 13° (222N load) abduction at full extension.

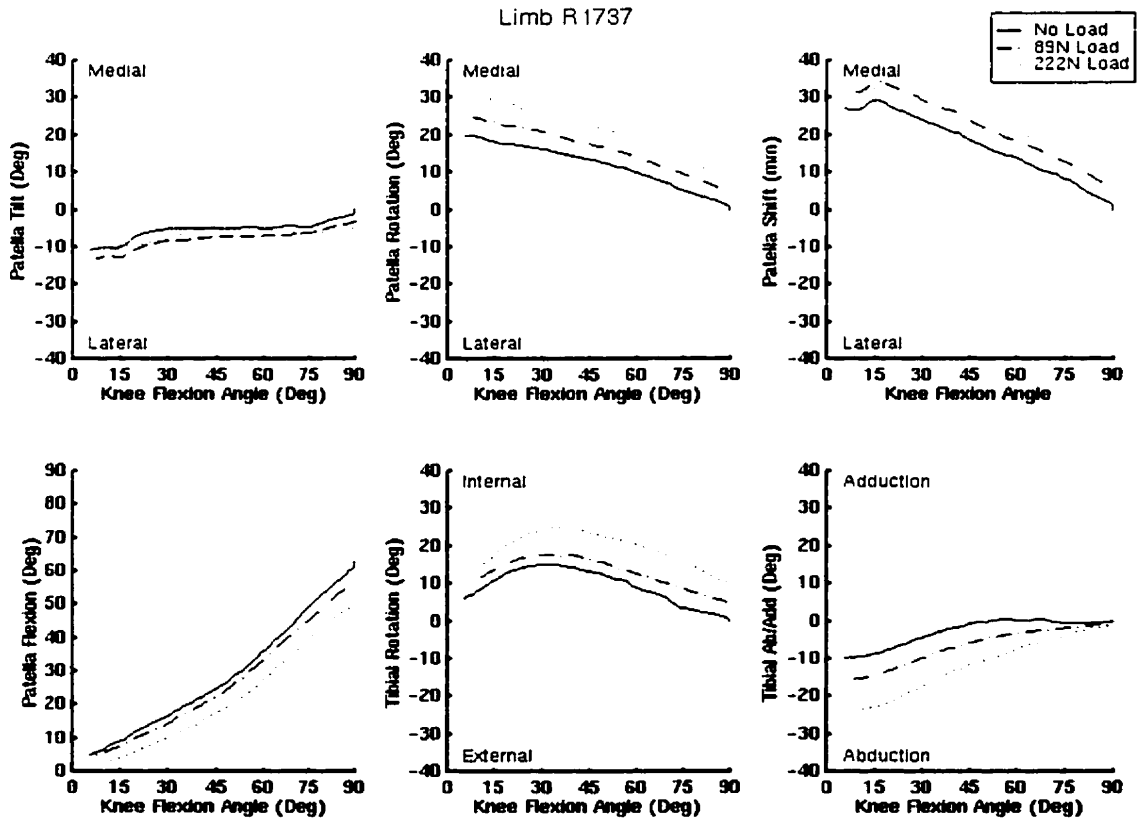

Figure 4-10 Limb R1737 loading effects on patella and tibial variables.

LIMB R1748

Patella flexion remained unaffected by loading (Figure 4-11). Statistically significant slope changes were seen for patellar rotation with the 89N load. Statistically significant slope changes were also observed for tibial ab/adduction and rotation for the 89N and 222N loading conditions respectively. The patella tilted slightly more medial at 90° flexion and rotated more medially (~2°). Loading caused 15° more abduction at 89N yet only 8° more abduction at 222N, throughout ROM.

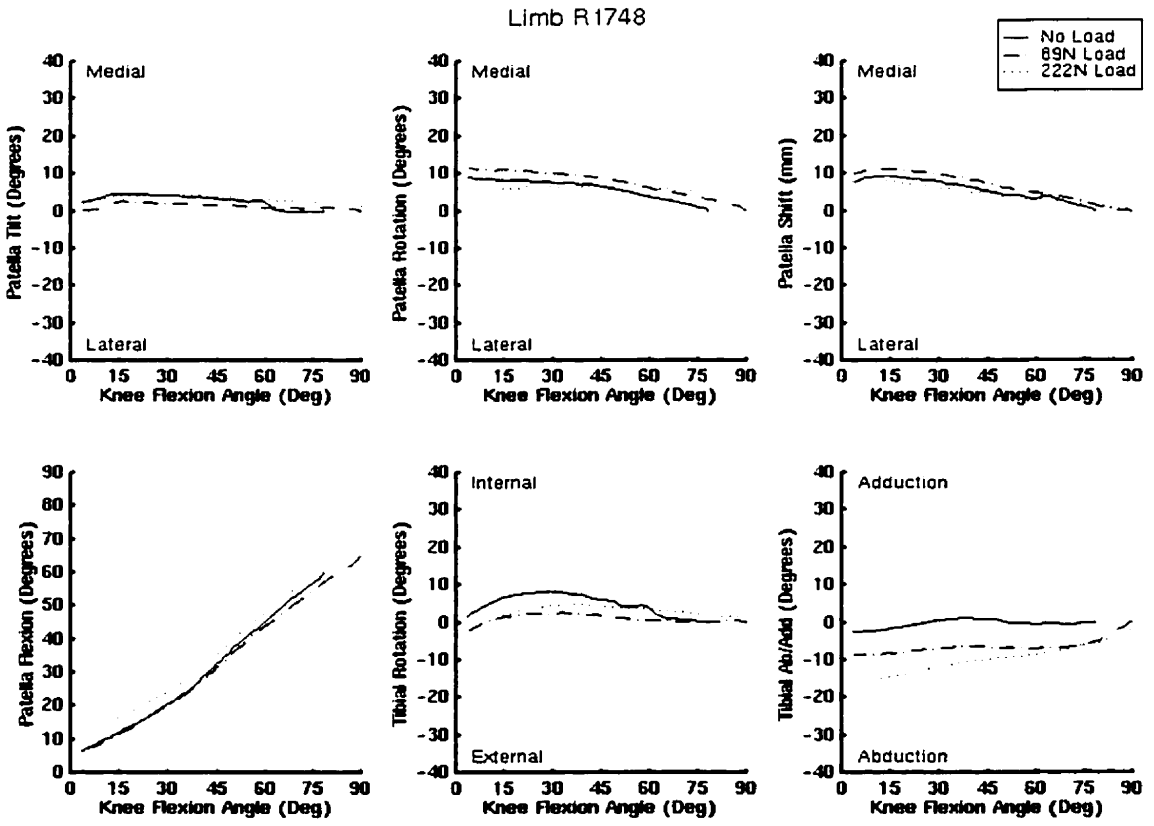

Figure 4-11 Limb R1748 loading effects on patella and tibial variables.

LIMB L1748

The effects of loading on patella flexion were extremely similar for both the 89N and

222N loading conditions (Figure 4-12). Patella flexion was observed to lag only slightly more (~2°) with loading. Patella rotation, tilt and shift were all statistically significantly affected with loading. Patellar tilt, originally ranging only 5° laterally throughout extension, increased to a 20° lateral range with load, with a 5°-7° offset at 90° flexion. Patella rotation increased from 5° medial rotation to 15° medial rotation throughout extension when loaded. Patella shift also increased from a 10 mm medial shift to a 20 mm medial shift when loaded. Tibial rotation showed only an influence due to loading (both conditions) between 0 and 30° knee joint flexion. Tibial ab/adduction was not affected at 89N load but was offset slightly (1-2°) at the 222N load.

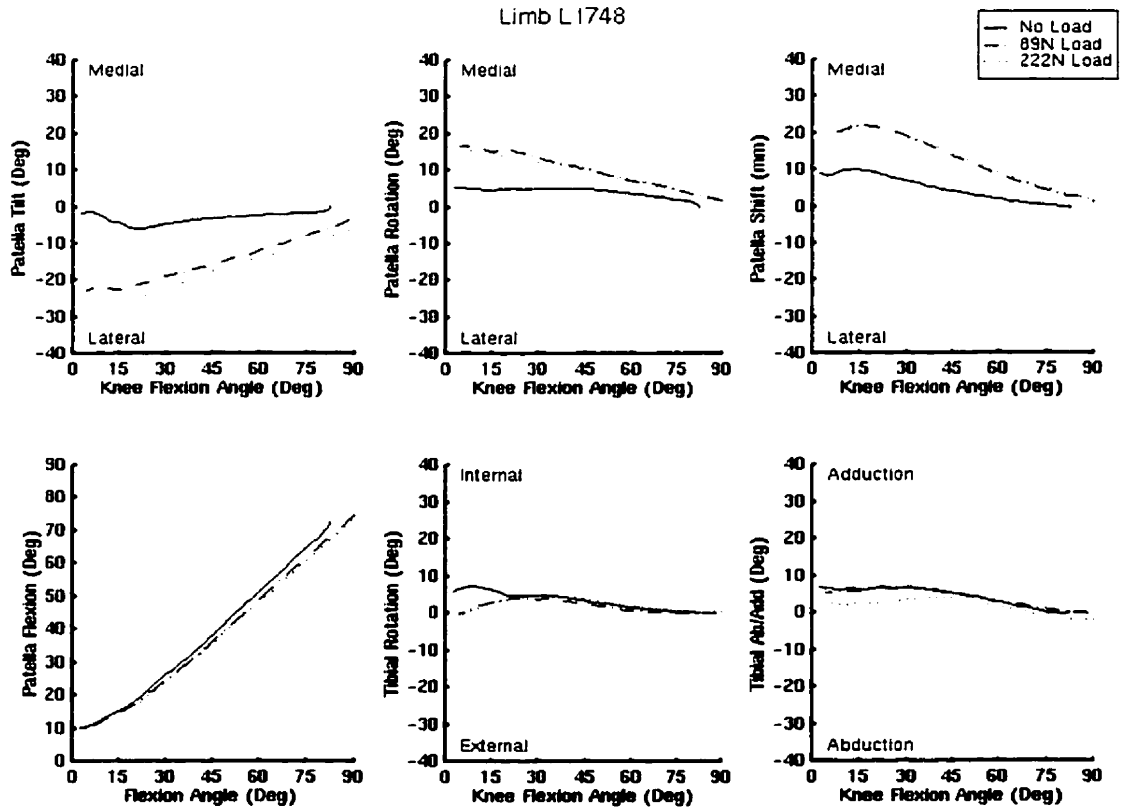

Figure 4-12 Limb L1748 loading effects on patella and tibial variables.

LIMB L1632

Due to technical difficulties with the loading jig, the 222N loading condition could not be tested with this limb. Offsets due to loading were observed (see Figure 4-13), but no statistically significant differences in slope were found. Patellar tilt remained 2° more lateral throughout extension in the loaded condition. Patellar rotation remained only slightly medial (no greater than 1°) when loaded. Patellar shift was not obviously different with loading. Tibial rotation showed a similar affect due to loading as the patellar variables, being offset only slightly. The oscillations during the initial extension phase (90° to 60°) of tibial ab/ adduction were eliminated when loading was introduced. A 27° range of abduction occurred with loading compared to the 22° range in the unloaded condition.

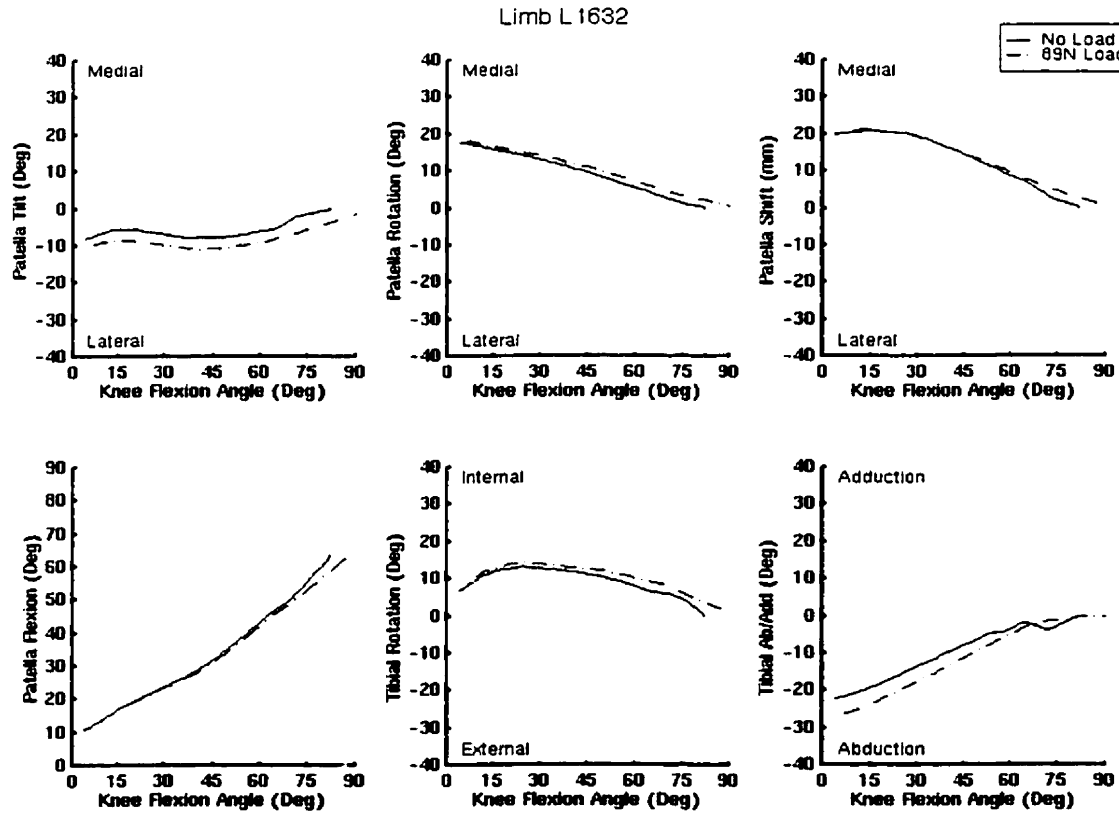

Figure 4-13 Limb L1632 loading effects on patella and tibial variables.

OVERALL TRENDS

This section presents an ensemble of the kinematic data with all the limbs to investigate general trend effects from loading. Patella flexion curves remained very similar between all limbs for the no-load and 89N-load conditions (Figure 4-14). At 222N, R1748 and L1748 demonstrated a steeper slope than the rest of the limbs. L1748 was distinctly different from the rest of the limbs in both the 89N and 222N loading conditions demonstrating a lag of only 10% compared to 20% for the other limbs.

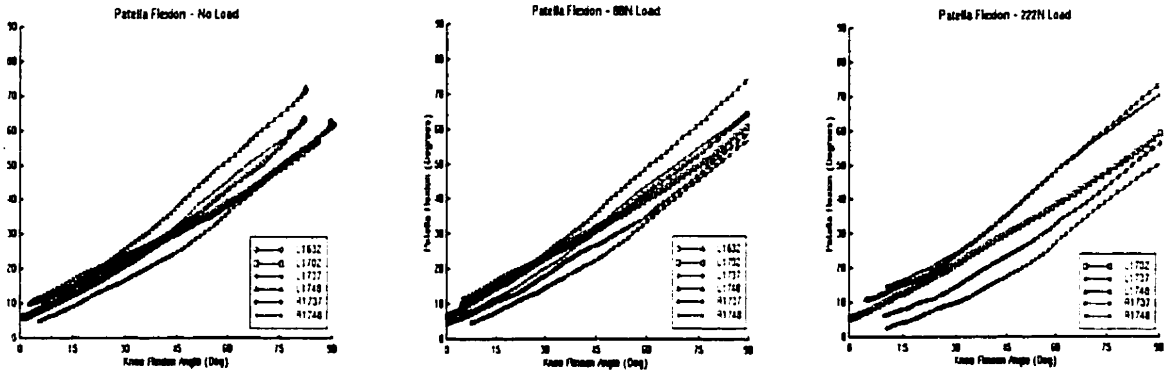

Figure 4-14 The influence of loading on patellar flexion for all limbs.

Patella tilt showed considerable changes due to loading. The inflection seen in the no-load condition became less noticeable (reduced from ~5° to 0° in some limbs) in the loaded conditions (Figure 4-15). Limb L1632 still followed a considerably different trend for the 89N load, tilting medially in the first 20° of flexion, then laterally between 20 and 50° and then tilting medially again until 90°. Limb L1748 shows the most distinctive change due to loading. The patella tilted medially ~24° throughout extension. In general, most limbs exhibited an increased range of magnitude of tilt with loading and the wavering tilt seen in

the initial 15° of knee flexion is diminished.

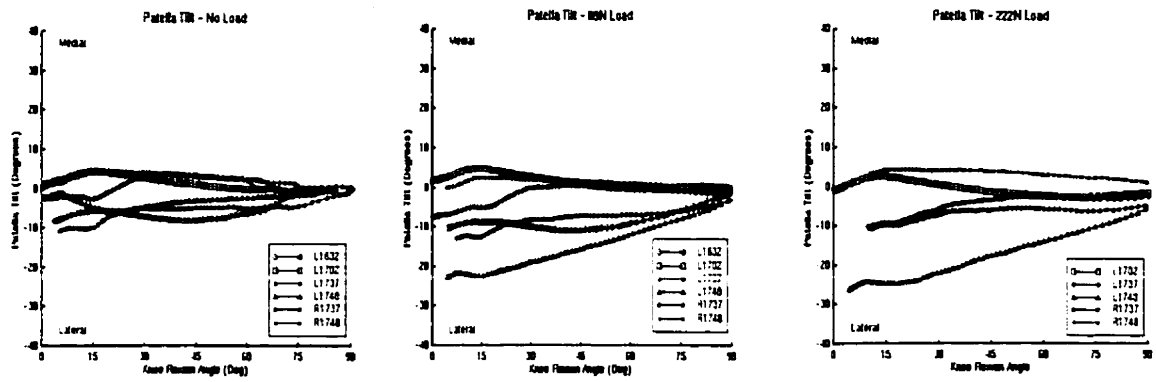

Figure 4-15 The influence of loading on patellar tilt for all limbs.

The no-load condition for patella rotation showed two distinctly different trends. L1748, L1737 and R1748 displayed roughly 8° lateral rotation, whereas R1737, L1702, L1632, displayed roughly 18° lateral rotation (Figure 4-16). At the 89N-load, R1737 was the only outlier with R1748 showing similar trends with L1632, L1748 and L1702 only in the last 40° of flexion (from 70 to 100°). At the 222N-load condition both R1748 and R1737 were distinct outliers showing much less and much greater lateral rotation respectively, than the other limbs.

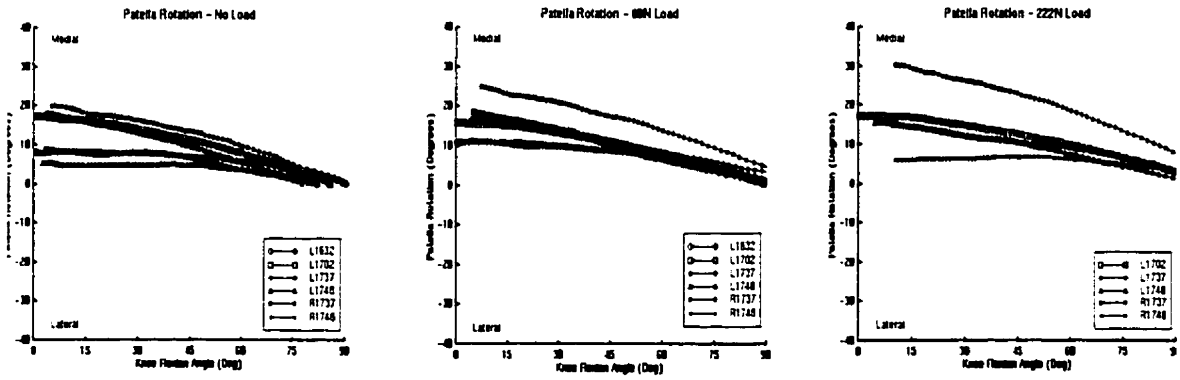

Figure 4-16 The influence of loading on patella rotation for all limbs.

The overall trend for patella shift was relatively uniform across limbs with the exception of R1737 (Figure 4-17). The lateral patella shift for this limb was large (as much as 2x the shift of others) throughout all loading conditions. Limbs L1702, L1737 and L1748 increased in lateral shift (~5°) when loaded. For both loading conditions R1748 shifted noticeably less (about half) than the rest.

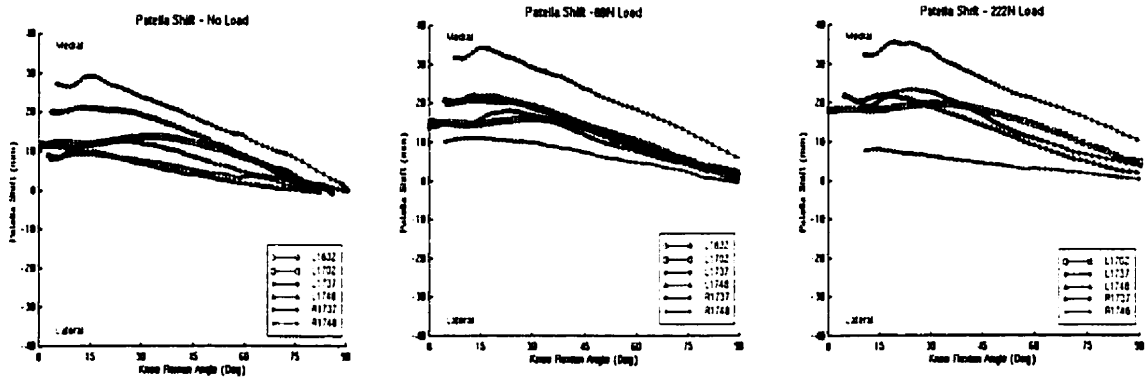

Figure 4-17 The influence of loading on patella shift for all limbs.

Tibial rotation showed a general curve shape in the no-load condition with only one outlier: L1748 (Figure 4-18). When the load was introduced (both 89N and 222N) two distinct patterns emerged: R1737, L1737 and L1632 continued to have a larger external rotation from 30°-90° than the other 3 limbs. The remaining limbs conformed to an internal rotation of 5° in the first 30° of flexion, then maintained this rotation from 30° to 100° of flexion.

Tibial ab/adduction curves became more linear with the application of load (Figure 4-19). L1632 demonstrated a larger abduction in both the no-load and 89N-load conditions. L1748 was the only limb that retained an adduction throughout all load conditions.

Table 3 summarizes the statistically significant differences due to loading for each limbs.

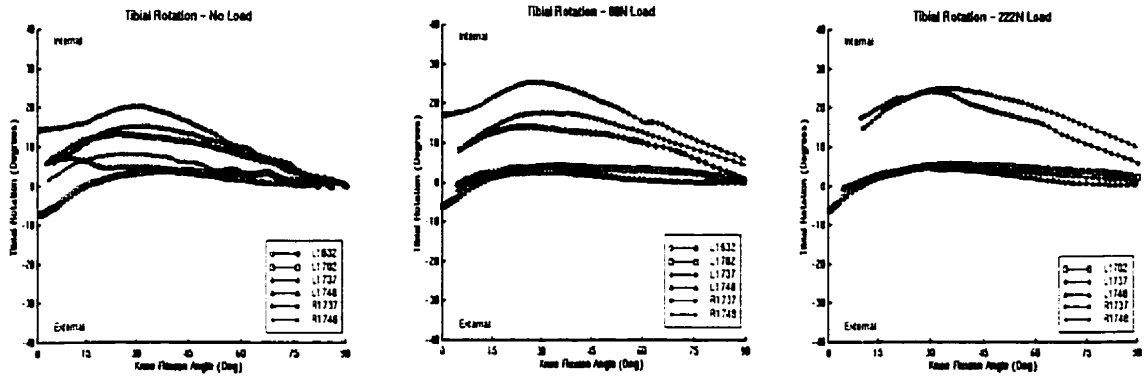

Figure 4-18 The influence of loading on tibial rotation for all limbs.

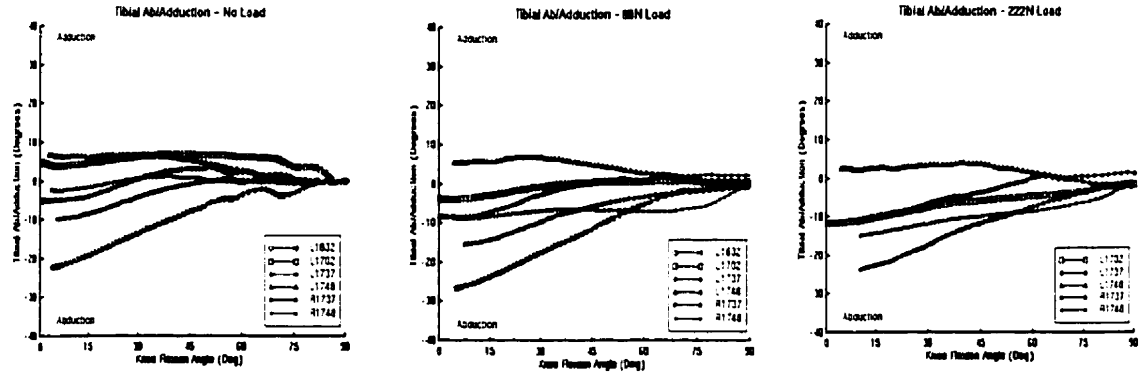

Figure 4-19 The influence of loading on tibial ab/adduction for all limbs.

Table 3 : Statistically Significant Differences between Loading Conditions

		L1702	L1737	L1748	R1737	R1748
Patella	Flexion			■ ▲	▲	
	Tilt		■ ▲ ●	■ ▲	■ ●	■ ▲
	Rotation	■ ▲	■ ▲ ●	■ ▲ ●	▲ ●	▲ ●
	Shift		■ ▲ ●	■ ▲	▲	■ ▲ ●
Tibial	Ab/Ad	■ ▲ ●	■ ▲ ●	▲ ●	■ ▲ ●	■ ▲ ●
	Rotation		■ ▲		■ ▲	■ ▲

■ 0 & 89 N Load ▲ 0 & 222 N Load ● 89 N & 222 N Load

4.1.3 Sensitivity of Kinematics to Limb Alignment

The effect of a 15° change in the quadriceps line-of-action on the patellar and tibial motions was tested on 2 limbs: L1702 and L1621. L1702 was used in the analysis of kinematics presented previously whereas L1621 was omitted due to the absence of loading data. The results of L1702 will be presented here. The results for L1621 demonstrated very abnormal patella flexion (only 4° change in flexion throughout the extension movement), a very large patellar rotation (35°) and shift (40°). As this does not appear to be representative of normal tracking characteristics, analysis of the effects of quadriceps alignment on these variables is questionable and therefore will not be presented.

The single factor ANOVAs performed at 15°, 30°, 45°, 60° and 75° for each variable across the three alignment conditions (neutral, 14° medial and 14° lateral), indicated significant interaction. Further testing using the Bonferroni method resulted in significant differences between the neutral condition and the medial and lateral alignment configurations at all angles for all variables with only 2 exceptions; the medial alignment for tibial ab/ adduction at 30° knee joint flexion and the lateral alignment for tibial rotation at 75° knee joint flexion. This means that the variability between conditions was significantly greater than the variability between the 5 trials completed in each condition at the α=0.05 confidence interval. The effect of alignment changes on the patellar and tibial motions is plotted in Figure 4-20 for one representative trial in each alignment configuration.

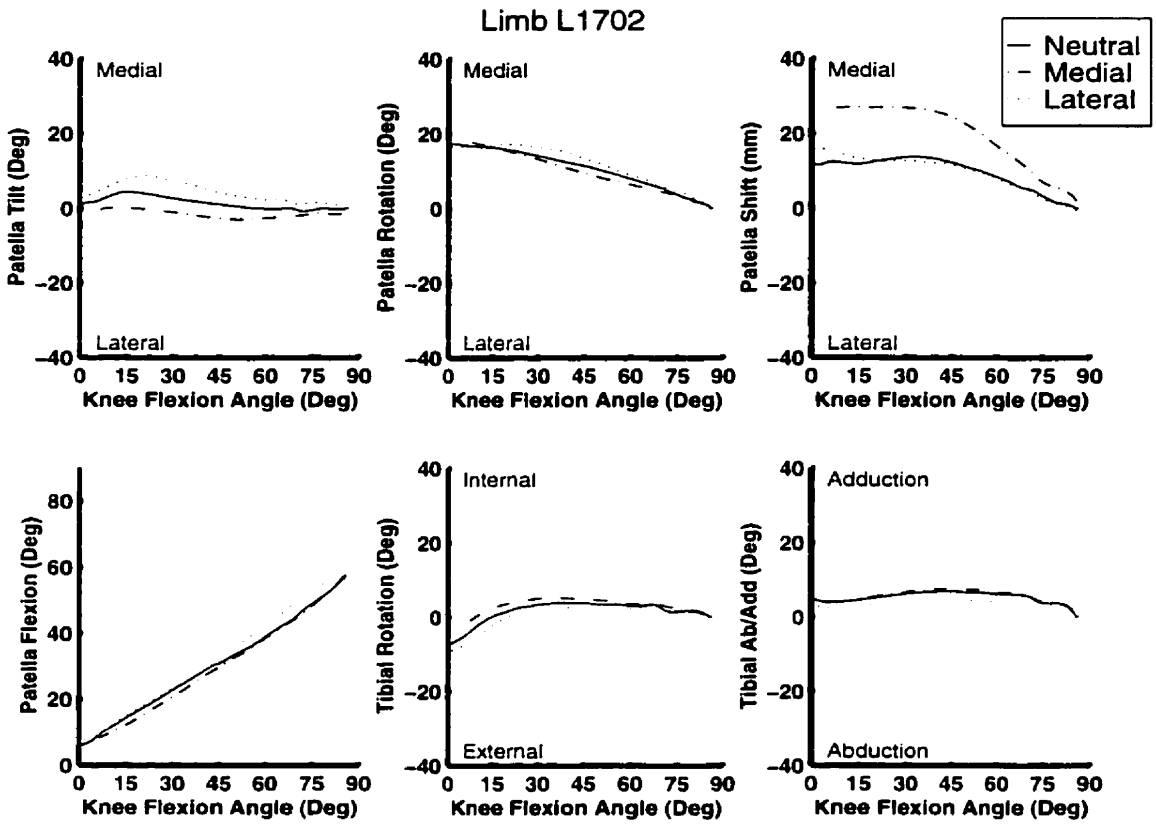

Figure 4-20 Sensitivity of kinematic variables to limb alignment for limb L1702.

Patella shift showed the most sensitivity to alignment particularly in the medial direction. Patella tilt demonstrated sensitivity to alignment in both the medial and lateral directions. Patella tilt, rotation, flexion and tibial rotation and abduction were most effected by an altered lateral alignment. Medial alignment effects patella shift and tilt and tibial rotation. Sensitivity to medial alignment is important in evaluating the differences between rotation about the mechanical axis of the femur (reported to be a more functional measure) and the anatomical axis, which is roughly 6° lateral.

4.1.4 Marker Repeatability

The markers demonstrated superb repeatability in all configurations tested. The maximum standard deviation of all the 3D coordinate positions of all the markers was 1.9 mm. Standard deviations above 1mm occurred only on two markers, the y-value of the proximal femur marker (1.15 mm) and the x-value of medial patella marker (1.91 mm). All other marker coordinates remained below a 0.4 mm standard deviation.

4.1.5 Accuracy of Kinematics

The accuracy of the kinematic measurements depends directly upon the cube and wand calibration for the MAS. The camera calibration used a 12-control-point cube and aimed for a goodness-of-fit value around 0.3 (±0.05) pixels. Up to three control points were eliminated per camera to obtain this value. A wand calibration was performed to increase the accuracy throughout the entire field of view. The best estimate of the accuracy of the entire system was found by reviewing the mean residual of a tracked trial. This was a measurement of how closely the projected rays of each camera intersect to create a 3D point. The mean residual of the kinematics trials in this study were between 0.25 and 0.30 mm.

4.1.6 Extensor Mechanism Force

The force of the MTS actuator (and thus the quadriceps tendon) required to pull the limb from 90° flexion into full extension was recorded. Creep, defined as the amount of length left after the force had returned to zero, was also noted. Force required to extend the limb throughout the ROM was not of key interest in this study. Consequently, no in depth analysis of force variables was conducted. However, the general trends are presented here.

In general, during the first phase of motion (approximately 90-60° flexion), force

increased steadily with noticeable oscillations. By 60° the force levelled off before rising sharply in the final 20° before full extension (see Figure 4-21). The maximum force required by the actuator to extend the knee was limb dependent. L1702 required the most force, 800 N, but was also a larger and heavier limb than the others. R1737 required about 230N of force, R1748 about 240 N, L1748 about 300N, L1632 about 300N and L1737 required about 600 N of force to extend the leg.

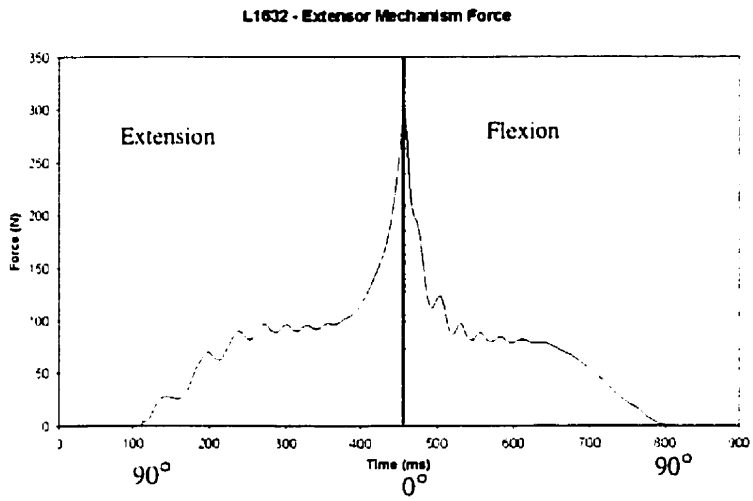

Figure 4-21 Extensor Mechanism Force vs. Time

Loading introduced a higher force level throughout the extension motion. Two different types of curves were observed. The first type resembled the shape of the unloaded condition curve with a higher force (maximums ranging from 360 N to 850 N) (Figure 4-22a). The second type demonstrated a large force required to move the limb, followed by a reduced force through the middle phase of extension, again rising sharply just before full extension (Figure 4-22b).

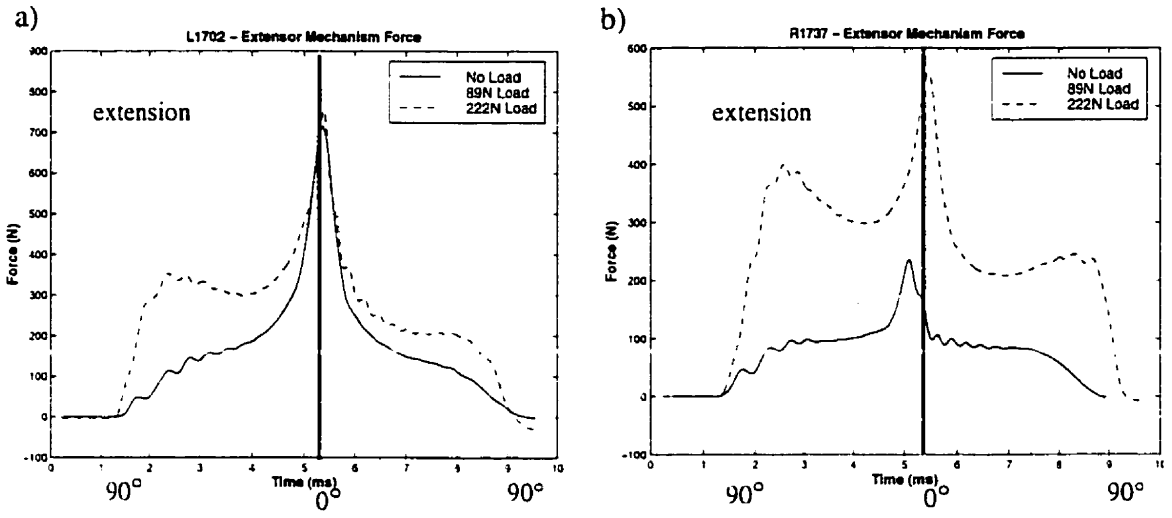

Figure 4-22 Effects of Loading on Extensor Mechanism Force

4.2 Articular Cartilage Surface Geometry

Five limbs were used in this section. L1737 was omitted because one of the drill holes had punctured the posterior side of the patella. The effect of this on the cartilage surface was unknown and therefore the images were not processed further.

The accuracy of the bundle adjustment was directly influenced by the 2D digitizing process of each image. Large differences were observed in digitized values for grid intersections between an inexperienced user and an experienced user. An experienced user was required to obtain convergence, particularly for the femur grid intersection points. Table 4 lists the number of grid intersection points used to obtain the 3D surface points and the reconstruction error (in μm) in the x, y and z directions of the ring coordinate system (RCS) where z corresponds roughly to the cartilage depth.

Table 4 - Bundle Adjustment Results for Cartilage Surfaces

Limb	Patella Cartilage Surface				Femur Cartilage Surface			
	# pts	x(μm)	y(μm)	z(μm)	# pts	x(μm)	y(μm)	z(μm)
L1702	141	59	60	80	334	59	57	90
L1748	239	36	34	64	457	54	76	107
R1748	224	32	23	48	293	51	63	102
L1632	198	50	49	83	222	51	59	82
R1737	150	56	50	82	365	39	48	93

4.2.1 Surface Reconstruction

The reconstructed 3D array of points from the bundle adjustment were input into a thin plate spline program implemented by S.K. Boyd (1997). The data were resampled in a 1.5 mm grid spacing. This grid density allowed reasonable calculation times (about 2 min. on a Silicon Graphics Indigo^2 computer). Ideally, the grid density would be small enough that other calculations, i.e. contact area, would be unaltered by further reduction in grid spacing. Unfortunately, because of the size of the knee joint surfaces, smaller grid spacing (<1mm) required a large computational time (30-100 minutes per surface) and. This also made it difficult to properly view the reconstructed surface. The effect of the grid spacing on the contact area for limb L1632 (trial1, no-load condition, flexion angle 60°) is presented in Table 5. These results suggest that a choice of a 1.5 mm grid spacing, the contact area results are overestimated by roughly 20 mm^2 or 3%.

Table 5 : Effect of Grid Spacing on Contact Area

Grid Spacing(mm)	Contact Area (mm^2)
2.0	630.2
1.5	619.2
1.0	604.2
0.5	594.1
0.4	606.4
0.3	600.9

In Figure 4-23, the original data points are plotted on the reconstructed thin plate spline surface. The thin plate spline represents the original data well, with no obvious smoothing or interpolation errors.

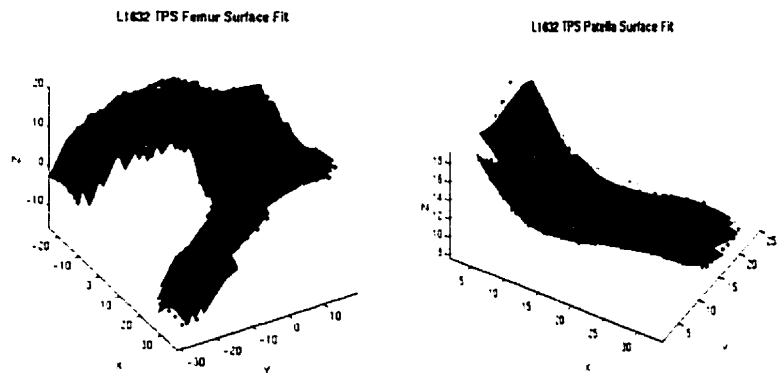

Figure 4-23 Original Data Points Plotted on the Reconstructed Surface.

4.2.2 Mathematical Model

Construction of a mathematical model of the knee joint requires the combination of kinematic data and the corresponding TPS surfaces of the patella and femur. Triad markers

from the kinematic data collection provided the common reference frame in both the kinematic data and the photogrammetric data. These markers, covered in reflective tape, were not spherical within the field of view of the photogrammetric camera. Thus, the elliptical fit algorithm in the digitizing process resulted in rms values of about 1 (The rms value reported by the program is the standard deviation of the radii used to fit the ellipse. A best fit is rms=0 pixels). Additionally, the patella markers, in order to satisfy constraints of the kinematic data collection and the photogrammetric mounting frame, were located approximately 10 cm behind the patella for the image collection. This is in the least accurate measurement direction of the camera, the depth of the field. The reconstructed kinematic marker accuracies are presented in Table 6. Note that the z direction is the depth of the field and therefore the least accurate measurement.

Table 6 - Bundle Adjustment Accuracies for Kinematic Markers

Limb	Patella Markers			Femur Markers		
	x(μm)	y(μm)	z(μm)	x(μm)	y(μm)	z(μm)
L1702	95	91	158	49	48	80
L1748	131	98	275	57	66	86
R1748	150	97	217	50	45	61
L1632	110	102	195	58	60	101
R1737	111	88	186	63	61	87

Original surface data was measured in the RCS. Transformation matrices between the RCS and SCS for each point in time were found using the method presented by Söderkvist and Wedin (1993). The rms values from the marker positions in RCS and SCS were used as a check for accuracy between the kinematic data collection and the photogrammetry data. A

large rms (> 1) indicated inconsistent numbering of markers (between kinematic data and photogrammetry data) or relative marker movement between the data collections. The rms values for all five limbs ranged from 0.05 to 0.38 with one outlier at 0.62.

Two problems were encountered while reorienting the surfaces. Limb L1748 was missing two static patella markers in the static trial for 222N load. The markers were created virtually by using the transformation matrix (found using the Söderkvist and Wedin (1993) method on marker trees) between the 89N and the 222N-load conditions (rms=0.05). The validity was tested by applying the transformation to a known marker and comparing it to the actual coordinates. The difference was [-0.6050, -0.0143, 0.2579]mm.

The second problem involved limb R1748. The no-load condition did not have the same marker configuration as the photogrammetry. This was probably due to bumping of the triad when the loading jig was placed around the limb. Consequently, construction of the joint model was not possible for this specimen.

One set of bone surfaces were digitized to test the error introduced through the surface reorientation procedure. If bone-bone or bone-cartilage surfaces were to overlap, larger contact areas would be reported erroneously. Limb R1737 was used for this test. No bone-bone or bone-cartilage overlapping occurred, thus indicating that the error was no larger than the cartilage thickness. The thickness of the patella cartilage ranged from 1 to 5mm and the femur cartilage thickness ranged from 1 to 2mm (see Figure 4-24).

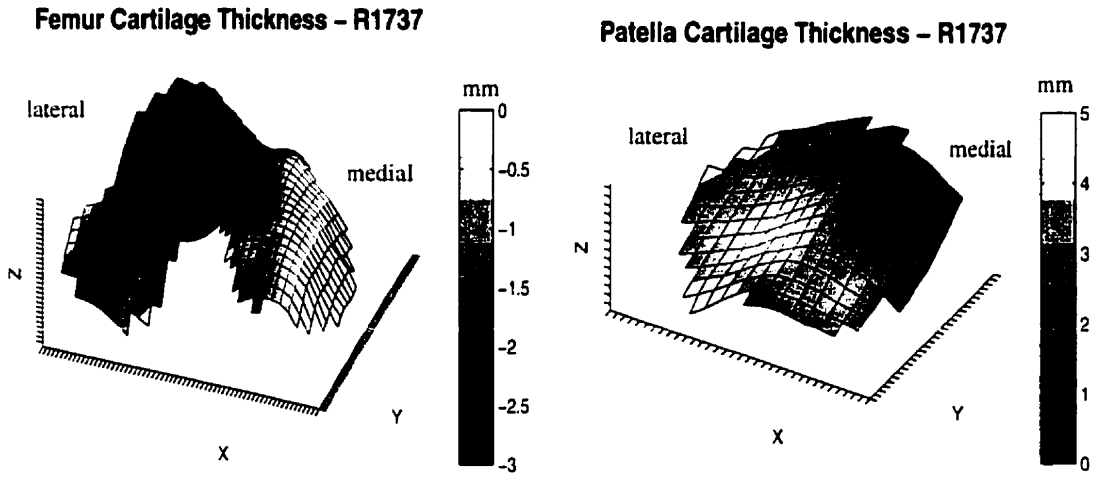

Figure 4-24 Thickness contours of the patella and femur - limb R1737

4.2.3 Contact Areas

Contact area is an indicator of the functional mechanics of the PF joint. A large contact area would lead to lower stresses in the joint. In addition, the movement pattern of the contact area over the cartilage surface may be associated with cartilage wear and degeneration. Ronsky (1994) suggested that a reduction in the migration of the contact area was seen in the ACL deficient knee. Therefore, the centroid of the contact area is presented here to illustrate the movement of the contact area over the surface.

Contact area was defined as the area of cartilage overlap between the patella and femur. Therefore a proximity greater than zero was labelled as contact as it is indicative of cartilage overlap.

As shown in Table 5, the contact areas calculated in this study are highly dependent on the resampled grid spacing. Therefore the values presented here are over approximations of the

true contact area (Figure 4-25).

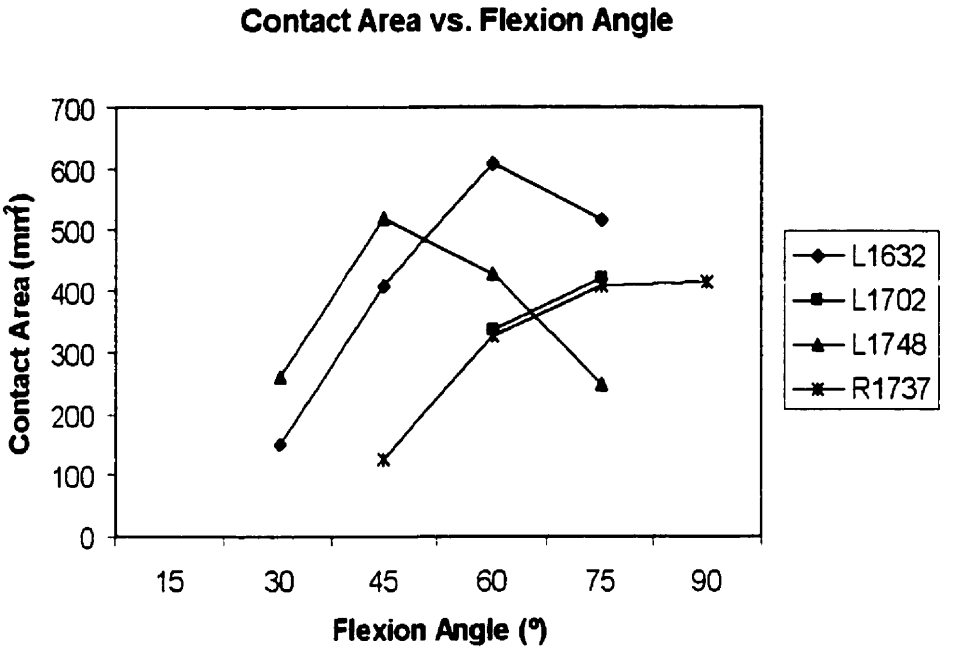

Figure 4-25 Contact area vs. Knee joint flexion for four limbs.

Contact area increased with increasing knee flexion between 30° and 60° and decreased between 60° and 75° flexion. The centroid of the contact area for limb L1632 moves distally along the femoral trochlea with increasing flexion angle and proximally along the patella (Figure 4-26a). At the 89N load level, the contact area at 75° and 90° knee joint flexion decreased. The centroid of contact is located mainly on the lateral condyle.

For limb L1702, contact was first measured at 45° of knee joint flexion. The centroid of the contact area for the no-load condition was located centrally in the trochlea at 45° and 60° knee joint flexion and the moved laterally at 75° of flexion. Contact area increased between 45° and 60° flexion. At the 222N load level, no contact occurred at 45° flexion and the location of the centroid of the contact area shifts laterally.

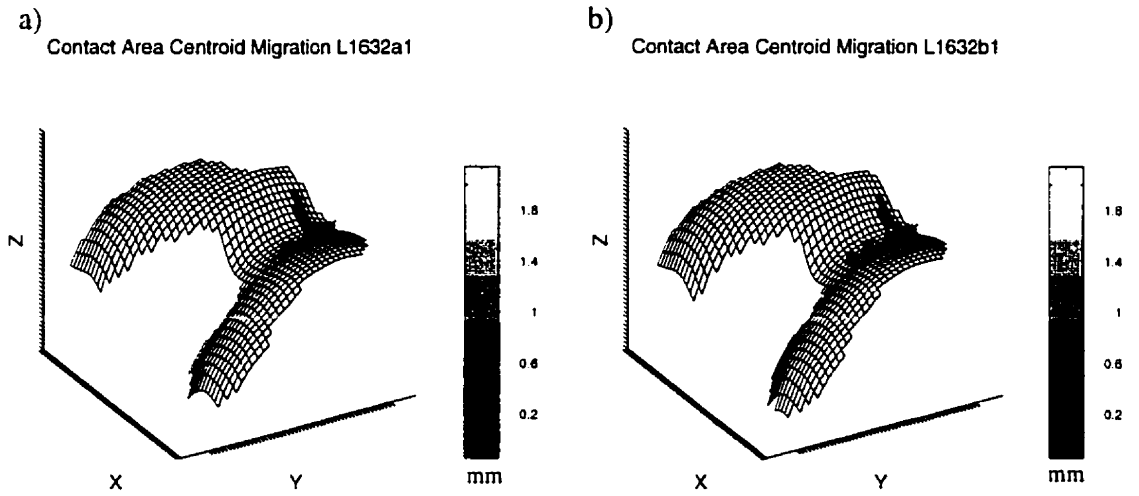

Figure 4-26 Location of Centroid of Contact Area for L1632 a) No Load, b) 89N Load.

For limb R1737 contact occurred on the lateral condyle and progressed distally through the trochlear groove with increasing knee joint flexion. Contact area increased throughout knee flexion.

Limb L1748 also demonstrated laterally located contact areas. However, contact area increased between 30° and 45° flexion and then decreased with further knee flexion.

Of the five limbs tested, L1748 and R1737 had very little or no contact at 75 and 90° of flexion in the loaded conditions. A series of rigorous tests revealed that only the EM force, measured by the MTS, differed from the other limbs. The EM force for the limbs with very little contact correspond with the EM force in graph Figure 4-22 b.

4.2.4 Articular Surface Sulcus Angle

Sulcus angle is a clinical measure used to describe the femoral groove geometry. 2D slices removed from the 3D surface illustrated not only geometry but the cartilage contact and patella orientation (Figure 4-27). The articular sulcus angle measured remained relatively

constant throughout knee joint flexion (varying a maximum of 9°).

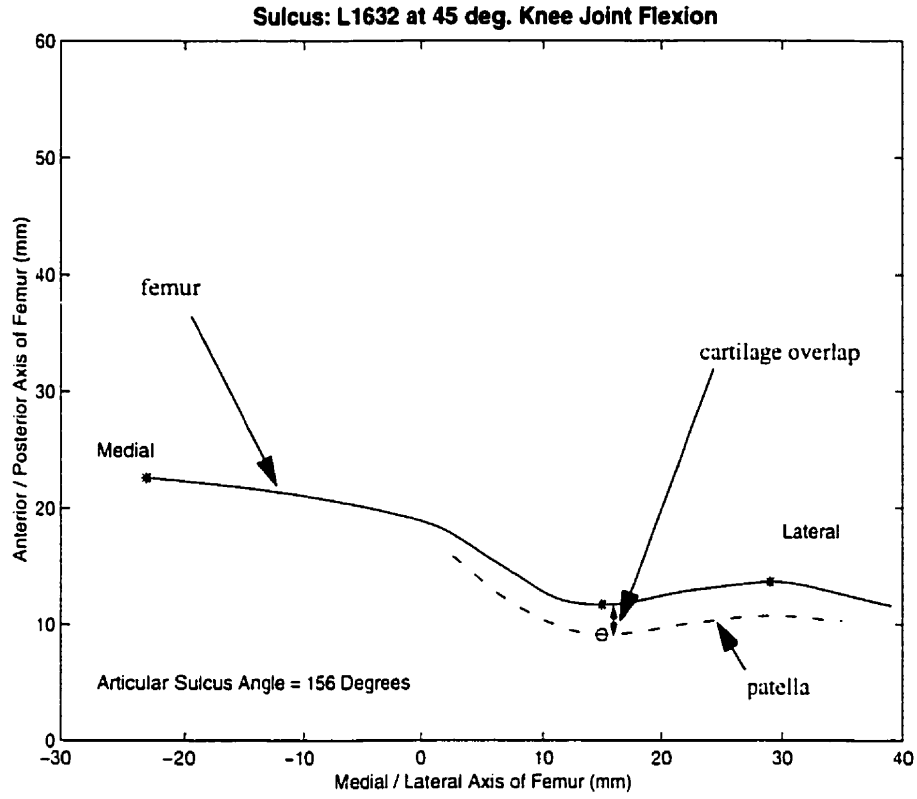

Figure 4-27 Determination of the 2D articular surface sulcus angle.The solid line is the contour of the femur cartilage surface and the dotted line is the contour of the articular cartilage surface of the patella.

The 2D slice provides a good view of the movement and overlap of the patella and femur. Other clinical measures such as congruence angle, used to indicate patella centralization, and tilt angle, used to indicate tilt compression syndrome, are not quantified here because these measures are based on bony surfaces, while cartilage surface geometry was the primary focus

of this study.

Table 7 : Articular Sulcus Angle Results

Flexion Angle	30°	45°	60°	75°	90°
L1632	153	156	157	150	
L1702		157	160		
R1737		163	158	156	155
L1748	153	144	141	145	

4.3 Integrated Kinematic and Cartilage Surface Geometry

This section will outline the combined results from the kinematics and cartilage surface geometries for each limb.

LIMB L1702

One notable feature of this limb was that the patella sat very high in the trochlea with respect to the knee flexion angle. Therefore the measurable contact area centroid moved very little throughout the range of motion. The curvature map (Figure 4-28 f) showed a very symmetrical trochlea and condyle geometry. The trochlea was flat with very little curvature, whereas the patella also had a very flat medial facet. The kinematics of the patella showed consistent trends in all conditions, with a relatively small range for patella tilt. Patella rotation was the only variable to significantly change due to loading. The sulcus angle demonstrated that in the no-load condition, the patella rode on the flat medial facet. When load was introduced, the patella rode on the more rounded (convex) lateral facet. (Figure 4-28)

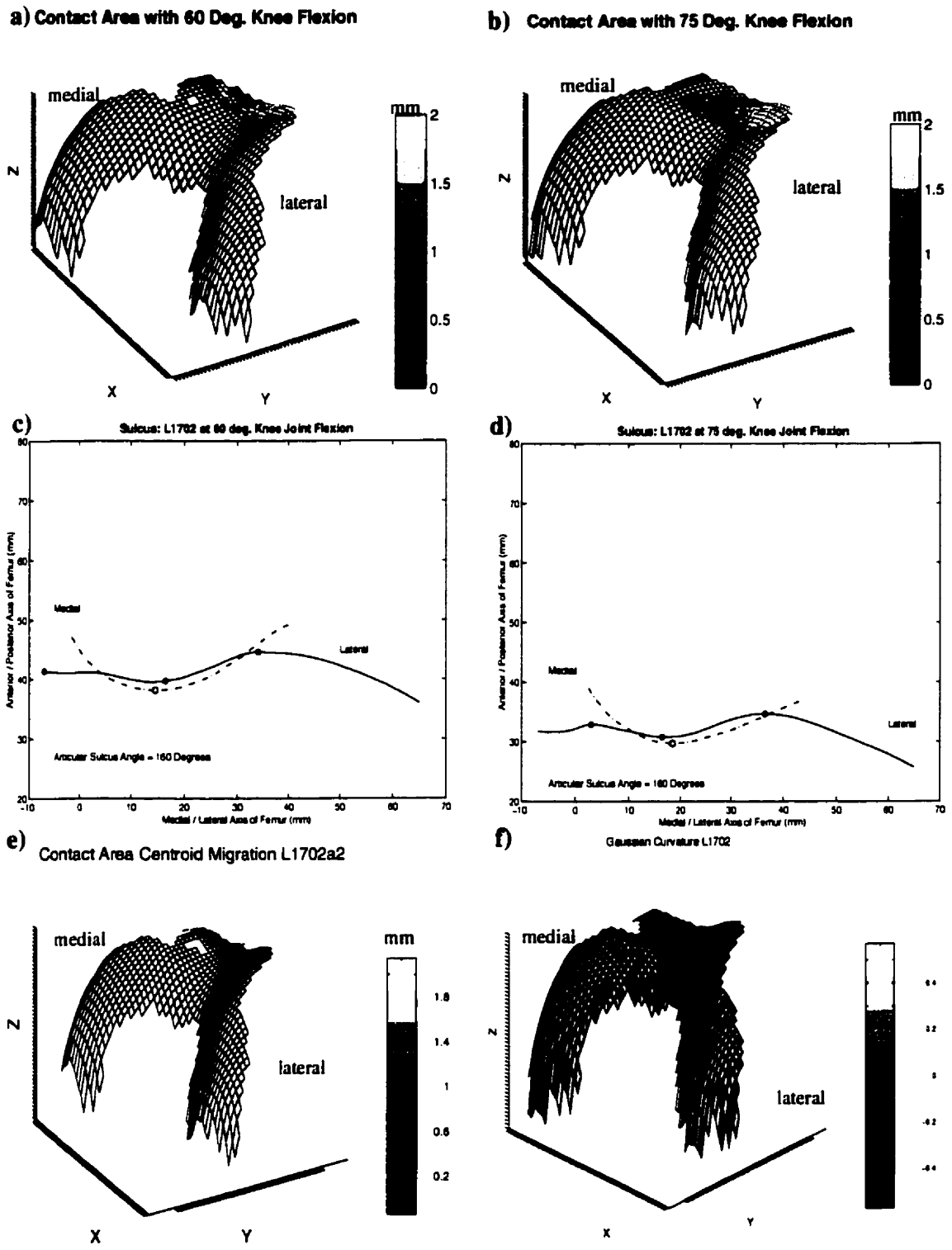

Figure 4-28 Limb 1702 a) Contact area at 60° and b) at 75° c) articular sulcus angle at 60° and d) at 75° e) centroid of contact migration f) Gaussian curvature

LIMB L1632

The centroid of the contact area in limb L1632, remained very centrally located in the trochlea and progressed throughout flexion (Figure 4-29). The medial femoral condyle was steeper (more curved) than the lateral condyle. The patella had a concave lateral facet and convex medial facet. The sulcus angle data indicated that the patella rode centrally in the trochlea, contacting with both facets of the patella. The kinematics showed relatively small patellar tilt and no significant effects due to loading. There was also very little kinematic variation between trials. The ovoid (white) area, which indicates a flatter area, in the trochlea (seen on the curvature map) corresponded to an osteoarthritic location. The contact area for this limb decreased between 60° and 75°. This corresponded to a medial patellar tilt of 5° and similar lateral shift and rotation of 5° and 4°, respectively.

LIMB R1737

The centroid of contact for limb R1737 was located on the lateral side of the trochlea (Figure 4-30). The curvature map showed a high lateral femoral condyle with a considerably smaller medial condyle. The patella had no obvious ridges with a concave distal end of the lateral facet. The most notable kinematic variable was the very large lateral shift (30 mm) which was accompanied by about 20° of patellar rotation. The 2D slices indicated that at higher flexion angles of 75° and 90°, the medial femoral condyle was higher than the lateral condyle. This forced the patella to shift laterally. At 45° flexion, there was almost no medial condyle and the patella shifted medially. This condyle elevation shift was also directly responsible for the patella rotation.

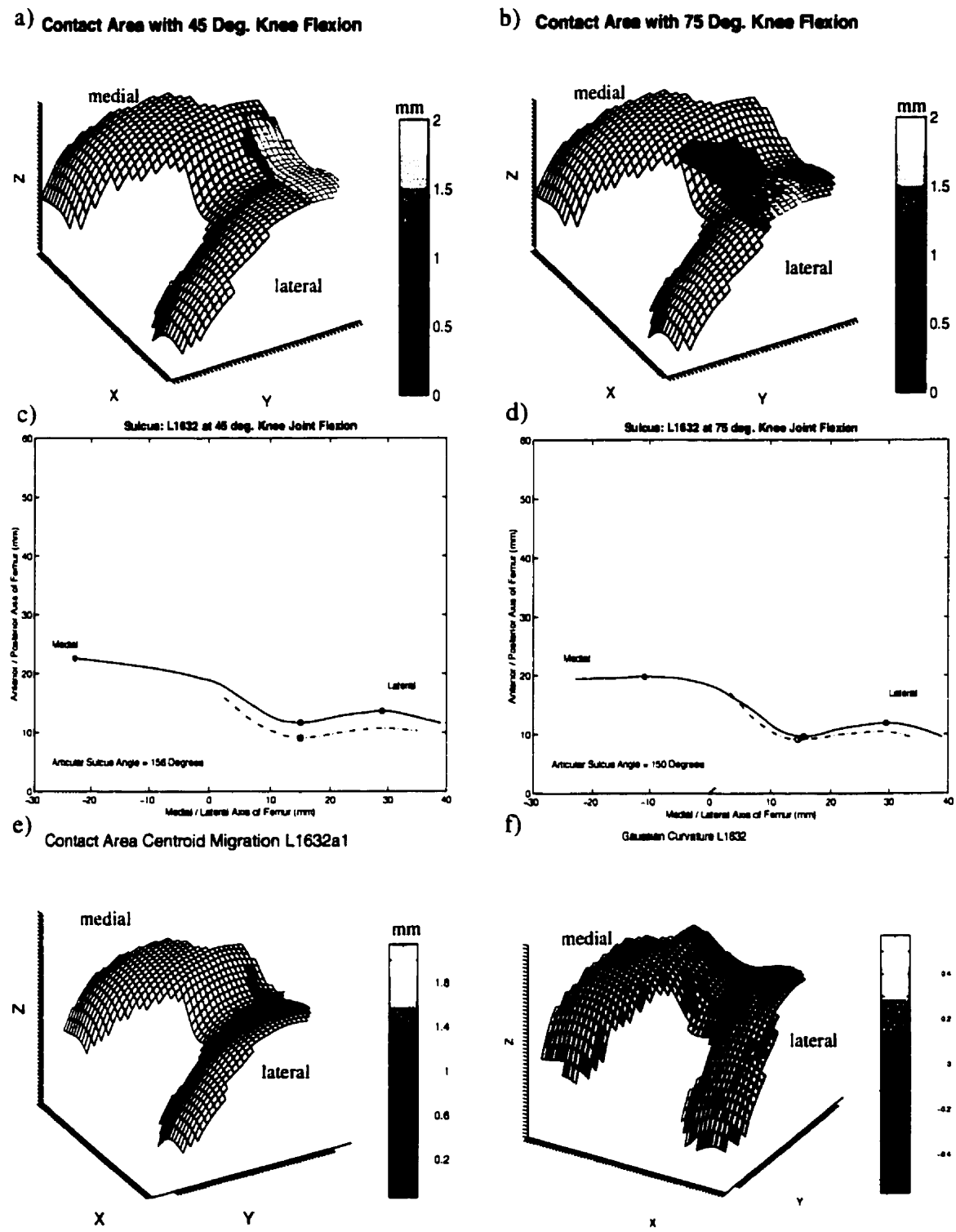

Figure 4-29 Limb L1632: a) Contact area at 45° and b) at 75° c) articular sulcus angle at 45° and d) at 75° e) centroid of contact migration f) Gaussian curvature

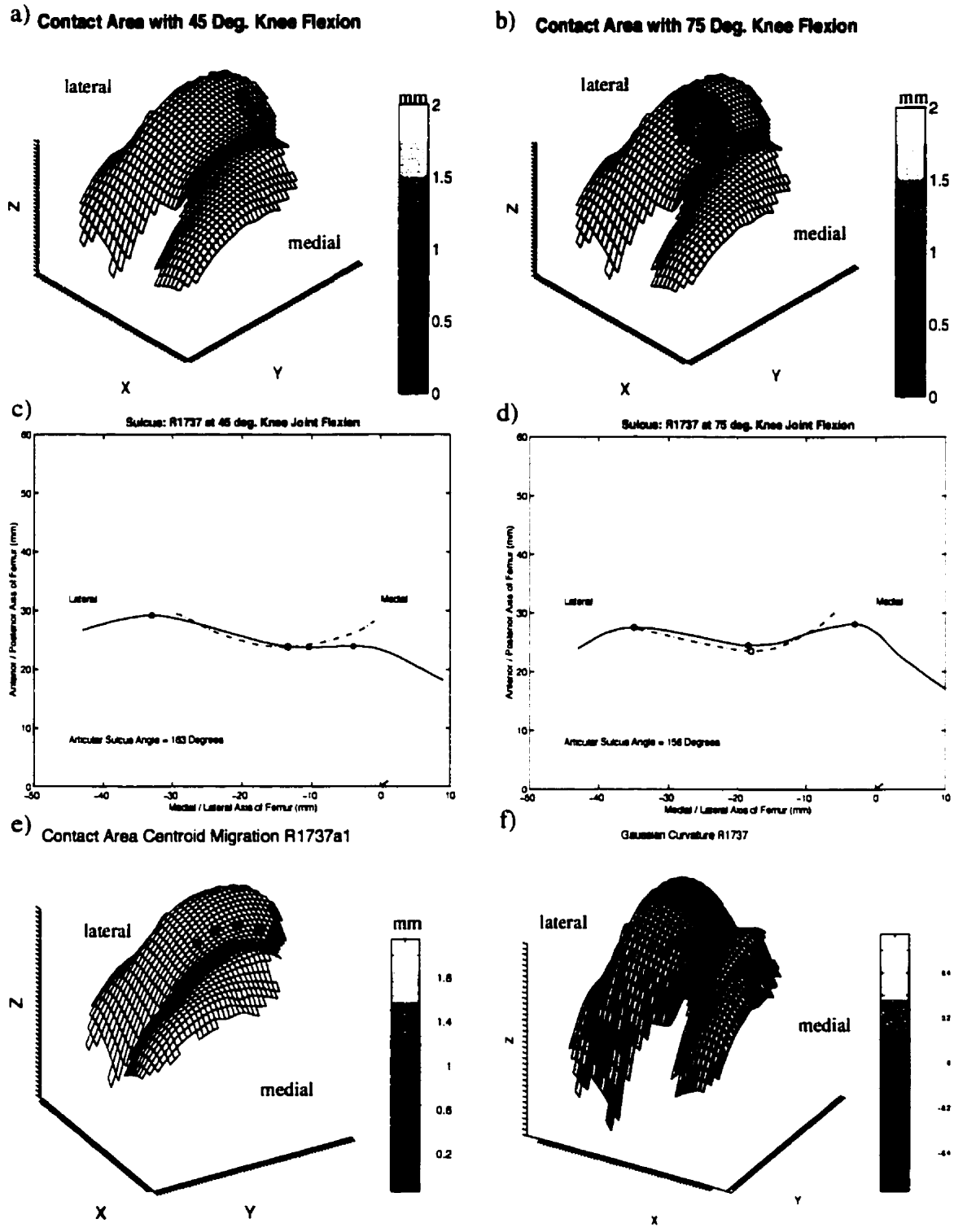

Figure 4-30 Limb R1737: a) Contact area at 45° and b) at 75° c) Articular Sulcus Angle at 45° and d) at 75° e) Centroid of contact migration f) Gaussian Curvature

The contact area increased with increased knee flexion. This limb showed a medial tilt with a large lateral shift and lateral rotation. At 45° the patella showed a rounded contour whereas at 75° a more prominent lateral facet existed (Figure 4-30 c, d). Relating these findings to the patellar geometry indicated the patella shifted and rotated to produce a larger contact area, compensating for the medial patellar tilt. The smoothly curved patellar cartilage surface allowed this abnormal tracking to occur with minimal consequence on the PF contact area.

LIMB L1748

The centroid of the contact area for limb L1748 was also located laterally on the femur (Figure 4-31). The curvature maps indicated the trochlea was shallow and only slightly curved. The patella had a steep, concave lateral facet with a considerably smaller medial facet. The patella showed an opposite tilt pattern as well and the lowest patella shift and rotation compared to the rest of the limbs. It also demonstrated an atypical tibial rotation and abduction. When loaded the patellar tilt was extremely medial, 23° (89N load) and 25° (222N load). The contact area decreased between 45° and 75° knee joint flexion which corresponded to a medial patellar tilt and very small patellar shift and rotation. The articular sulcus angle plots (Figure 4-31 c, d) indicated that the medial tilt between 45° and 75° knee joint flexion forced the patella onto the small medial facet which resulted in lower contact areas.

LIMB R1748

No contact information could be calculated for this limb because the markers were bumped. The curvature maps showed a trochlea of fairly constant curvature throughout giving rise to ovoid condyles. The lateral facet of the patella was concave (sellar curvature),

with the medial/lateral ridge indicated by ovoid curvatures. The kinematics showed the ab/adduction of the tibia did not directly alter the patella's movement. The patella also demonstrated relatively little rotation and tilt.

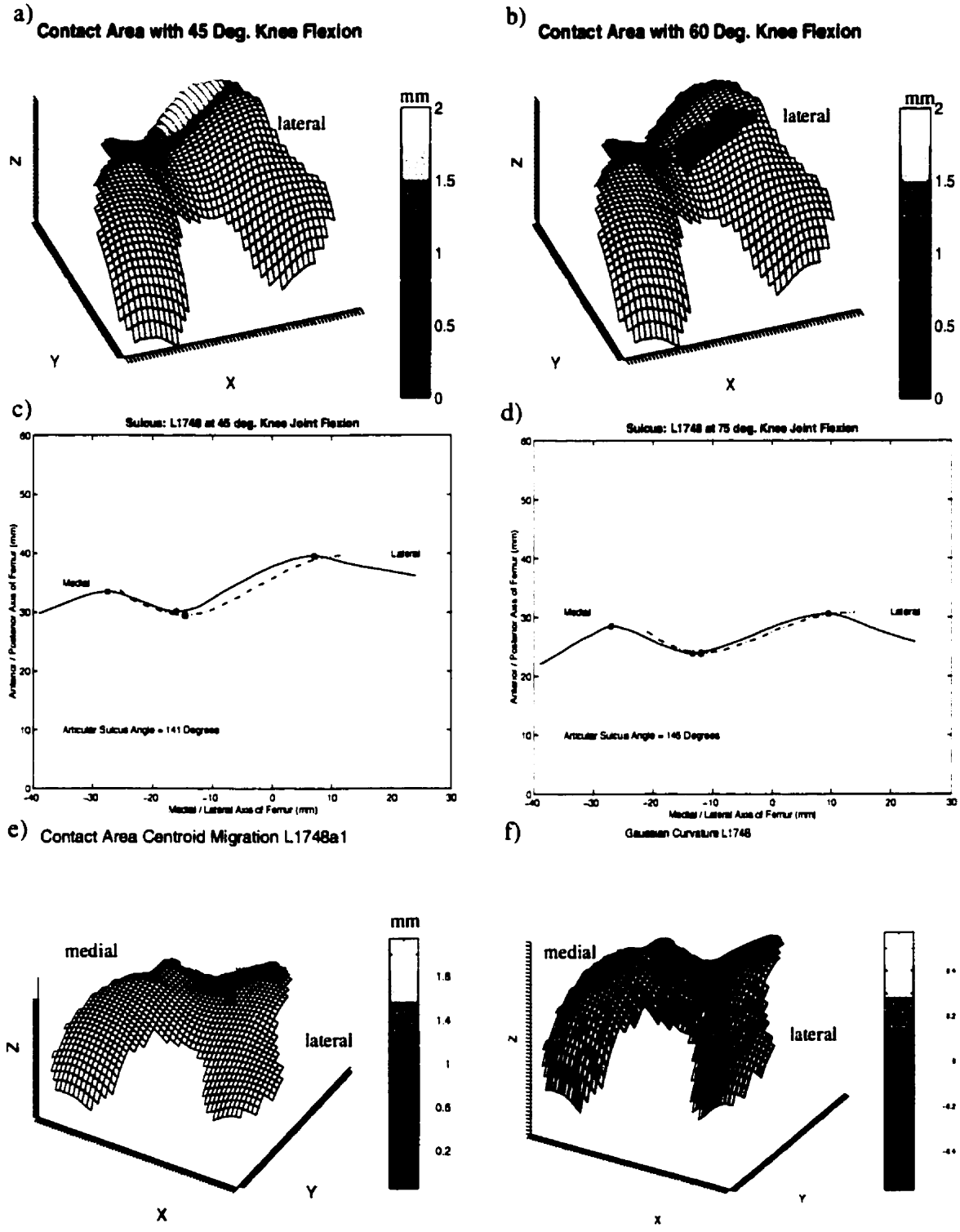

Figure 4-31 Limb L1748:a) Contact area at 45° and b) at 75° c) articular sulcus angle at 45° and d) at 75° e) centroid of contact migration f) Gaussian curvature

5.0 Discussion

Although patellofemoral joint kinematics have been extensively studied, the literature provides large variability of results (see Table 1). The objective of this study was to combine 3D PF joint kinematics with surface geometry measurement of the articulating surfaces. The interaction of the two may help to explain the variability in PF tracking reported in the literature. This study presents a dynamic extension model for measuring 3D PF joint kinematics in anatomically meaningful coordinate systems. An accurate 3D surface data acquisition method was adopted from S.K. Boyd (1997) and successfully implemented. This is the first time this method has been applied to human patellofemoral joints. A mathematical model, incorporating the kinematics and surface geometries, was constructed and used to obtain curvature characteristics, contact areas and sulcus angles.

The following sections will relate kinematic and contact area results from this study to those reported in the literature and to the hypothesis stated in the introduction. Sources of error and areas of improvement are also discussed. Finally, key findings of this study are presented and their clincial implications discussed.

5.1 Patellofemoral Kinematics

Six limbs were used in the kinematic analysis section of this study. An array of reflective markers attached to bone pins were used to record the motion. A unique system of static markers were strategically placed to form anatomically meaningful coordinate systems. The kinematic variables were calculated using the joint coordinate system presented in van Kampen and Huiskes (1990). Dynamic knee extension was accomplished using the MTS.

Several studies have investigated the PF joint kinematics in a cadaver model, e.g. Reider

et al. (1981), van Kampen and Huiskes (1990), Nagamine et al. (1995) and Hefzy et al. (1992). Each of these studies used different experimental setups and all were done quasi-statically. These four studies will be used in evaluating the validity of the results from this study.

Patellar flexion was found to lag knee flexion by 15°-30° in this study. This is in agreement with the literature. Patella flexion was the only variable that was consistent through all studies and was the least affected by tibial rotations and external loading.

Patellar rotation was consistent across all limbs in this study, rotating laterally with increasing knee flexion. Van Kampen and Huiskes (1990) reported that tibial rotation influenced patellar rotation, especially in the later stages of knee flexion (75° to 150°). In this study, the tibia rotated internally in the first 30° of knee flexion, then rotated externally until 90° of flexion. Therefore, the results from the initial 30° of flexion will be compared to the internally rotated tibia curves and the rest will be compared with the externally rotated graphs in the literature. Van Kampen and Huiskes (1990) found that all four of their limbs showed lateral patellar rotation with tibial internal rotation in the first 30° of knee flexion. Two of the limbs demonstrated lateral rotation between 30° and 90° of flexion. Hefzy et al. (1992) also reported lateral rotation with internal tibial rotation in the first 30° of flexion and with external tibial rotation between 30 and 90° rotation. Therefore, the consistent lateral rotation of the patellae in this study compared well to the literature.

Patella tilt has been described in other studies as wavering; tilting medially in the first 30° of flexion, then tilting laterally. Van Kampen and Huiskes (1990) reported that one of the four limbs demonstrated a medial patellar tilt in the first 30° of flexion which remained the same throughout the rest of flexion. The two abnormal knees reported in Nagamine et al.

(1995), also demonstrated this trend. Four of six limbs in this study tilt medially then laterally. One limb in this study (R1737) is similar to the abnormal knees presented in literature, tilting medially in the first 30° of flexion and remaining tilted throughout the rest of flexion. Finally, one limb (L1748) in this study behaved exactly opposite to the rest, tilting laterally in the first 20° of flexion, then tilting back medially until 90° of flexion.

Patella shift progressed consistently laterally with increasing flexion in this study. This is in agreement with the 'normal', or majority of knees reported in the literature. The range of shift was between 8 mm and 15 mm for most limbs, with one having 20 mm and the last having 30 mm shift. Shifts of up to 21 mm (Reider at al. 1981) have been reported in the literature. The large 30 mm shift in one limb of this study can be explained by the unusual geometry of the femoral condyles. At low flexion angles (less than 45°), the medial condyle showed a very low profile (hypoplasia, as defined by Fulkerson and Hungerford, 1990) allowing the patella to shift medially, while at higher flexion angles (75°-90°) the medial condyle was much higher than the lateral condyle, forcing the patella to shift laterally.

All limbs in this study followed a natural tibial internal rotation for the first 30° of flexion, then external rotation through the remainder of flexion to 90°. This is in agreement with two of the limbs presented in van Kampen and Huiskes (1990). They also showed that internal tibial rotation was linked to adduction of the knee throughout flexion. Four out of six limbs in this study also adducted with increasing knee flexion.

Van Kampen and Huiskes (1990) suggest that ab/adduction of the tibia influences patellar rotation. This study supports this suggestion. As the tibia abducts, the patella is pulled into a more medial rotation. This can be explained by examining the angle produced by abduction. As the tibial tubercle is forced more laterally, the patella is forced to rotate medially to realign

the quadriceps tendon with the patella tendon (Figure 5-1).

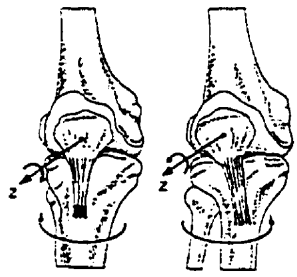

Figure 5-1 Influence of tibia rotations on patellar rotation. Adapted from van Kampen and Huiskes (1990).

Van Kampen and Huiskes (1990) have also suggested that patellar shift and tilt are coupled. This study does not support this statement in that a medial shift was accompanied with a lateral tilt. However, patellar rotation and shift appear to have similar trends and magnitudes which would indicate that they are coupled. Results of this study suggest that all three patellar variables (tilt, shift and rotation) reacted similarly, i.e. if an offset is visible in one, a similar offset is noticeable in the other two.

In conclusion, tibial rotation and ab/adduction seem to be important predictors of PF kinematics with regards to the direction of patellar shift, tilt and rotation. However, ranges of patellar tilt, rotation and shift would be very difficult to estimate using only tibial movements. The results of this study also indicate a direct correlation between patellar shift and tilt. To fully describe the patellar tilt that could occur however, would necessitate the inclusion of the specific patellar and femoral geometries.

5.1.1 Dynamic Motion

A major strength of this study, along with Barnes (1998), is that it is the first to introduce

a dynamic, continuous data collection with repeated trials. The kinematic results from this study compared well with the quasi-static measurements presented in the literature (e.g. van Kampen and Huiskes, 1990, Hefzy et al. 1992). One of the major differences in using a dynamic motion is the visibility of the 'screw-home' mechanism of the tibia. The 'screw-home mechanism' is the external rotation of the tibia as the knee approaches full extension. Blankevoort et al. (1988) did not find this in unloaded knees (tested 4 limbs) and suggested that it was not a passive characteristic of the knee but rather a result of the active stabilization produced by the muscles. The 'screw-home' mechanism was evident in this study during the last 20° of extension. However, the nature of the screw-home mechanism would appear to be directly related to the geometry of the tibiofemoral joint. This could explain why Blankevoort et al. (1988) observed the screw-home mechanism in loaded knees, when the tibiofemoral joint would be more compressed.

5.2 Effects of Loading on Patellofemoral Kinematics

Loading the knee joint produced variable effects on the specific kinematic patterns. The method of loading done in this study produced unexpected results. The attachment of the rope to the heel of the limb, forced an internal rotation and abduction of the tibia at 90°. It also forced the limb further into flexion. Three of the five limbs had little or no contact once loading was introduced. For limb R1737 and L1748, small contact areas were found for flexion angles up to 60° but no contact was found at 75 and 90° flexion. Several factors were investigated to explain this phenomena. The only factor that could be correlated with these limbs was their similar effects induced by loading on the EM force curve. In these limbs, the force increased (to similar levels as peak force in the no-load condition) sharply to overcome

the load at the initial phase of the test (90° flexion). After this the EM force then decreased until reaching terminal extension. It is hypothesized that the application of the load produced compression force between the tibial plateau and femoral condyles. At the start of the test the load resisted movement creating a large EM force. As the limb moved into extension, the pulley-weight system actually helped the motion of the tibia, due to the moment arm created. If the tibia was forced into extension slightly faster than the rate of length change of the MTS actuator, the patella tendon would become lax and reduce the compressive force on the patella. Thus a reduction of the EM force is seen. In this case, the patella could glide smoothly over the surface of the femur without causing any cartilage deformation. Physiologically this does not happen. The hamstring muscle group would resist the extension torques produced by this mechanism.

The torque created by the pulley-weight system, depended on the moment arm between the weights and the centre of mass of the tibia and foot. The pulleys were lined up with the knee joint centre defined as the centre of the femoral condyles. If this alignment were actually in front of the knee joint centre, the centre of mass of the tibia/foot would be behind the rotation centre of the pulley system. This requires the creation of a large torque to create movement, much the same way as trying to open a heavy door towards you when you are standing parallel to it. As the limb comes through 90-60°, the minimum force required to produce the torque occurs i.e. you are standing perpendicular to the door. The momentum created to overcome the initial movement would now carry the limb through the next phase of extension.

In light of this however, loading is important in attempting to relate PF kinematics to physiologic loading conditions. Loading conditions did produce statistically significant

differences in the kinematic variables measured. The results of two limbs give a good first approximation to weight bearing conditions that occur during locomotion. For other limbs where the geometries were more sensitive to alignment of the loading apparatus, an improved loading setup is recommended. The addition of a force on the hamstrings would help in guiding the limb and resist the knee extension which is actually assisted with the current loading mechanism. Care must be taken to ensure the pulleys are in line with the joint centre and that the quadriceps line-of-action was accurate. In-vivo studies could be completed to measure the kinematics of a squatting motion and then replicated in-vitro. This would involve a slightly different setup. The limb could be aligned vertically with the femur attached with spring loaded rod to a pin in a vertically moving slider. The foot could be held in place on the floor. This would induce a ground reaction force through the foot. The load would be introduced through the femur, as it is in-vivo, using the spring loaded rod. In this setup the hamstring and quadriceps muscles would have to be included.

5.3 Sources of Error

The accuracy of the kinematic measurement with Motion Analysis and EVA was 0.28 mm (mean residual of a tracked trial). This is the largest source of error in this study. The size of the field-of-view, camera positions, the calibration procedure, and the visibility of the markers can all affect the accuracy of the data. The field of view in this study was selected such that it was sufficiently large to capture the extension motion in the centre of the camera lenses. This decreases the amount of error due to lens distortion. The calibration cube was measured with the CMM machine on two separate occasions. The results were not substantially different to alter the 3D marker spacial coordinates calculated by EVA. The

camera positions were optimized by trial and error, using the cube calibration goodness-of-fit values as the indicator of accuracy. The markers on the bone pins were covered with reflective tape which became dull when in contact with moisture (e.g. water, biological tissue). This loss of reflectivity made it difficult for the camera and software to locate the marker. Therefore small errors in the calculation of the centroid of the marker can result.

Another source of error in kinematic values was the alignment of the segment coordinate axes. These axes are a direct result of the skill involved in placing the bone screws and pins. Upon visual inspection the markers used for anatomical axis alignments appeared acceptable. A skewed placement of any marker will directly influence the direction of the coordinate axes. For example, a slight angular offset of the anterior/posterior plane through the femoral shaft would cause an angular offset in the flexion/extension axes. This would have direct effects on the patellar shift and flexion values. The significance of a small angular offset could be tested mathematically by incorporating an error in the marker coordinates that form that plane. A comparison with the true results would then indicate the amount of error that would propagate through the calculations. The accuracy of these calculated axes compared to true functional axes is difficult to determine. There is no current standard for describing anatomical coordinate systems.

5.4 Multi-Station Digital Photogrammetry

This technique for joint surface topology measurement was first presented by Boyd (1997) for use on the cat PF joint. The accuracy reported in that study was 25.4 μm, in the least favourable direction, for a cylinder. This was a large improvement on the accuracy reported by Ateshian et al. (1991) as 90 μm. The improved accuracy was largely due to the increase

in the number of images used in the reconstruction (six in Boyd, 1997 compared to two in Ateshian, 1991) and the highly redundant calibration procedure. Accuracy on cartilage surfaces was reported as 15.7 μm, whereas this study obtained only at best 82 μm and at worst 107 μm, in the least favourable direction. There are several reasons for this error. The projected grids became distorted on the cartilage surface especially in areas of high curvature. Some of the images became blurry upon zooming. This could be due to the long exposure time used making it easy for a slight vibration to affect the camera during the exposure. The digitization process was also made difficult by the above mentioned problems. Because of the curvature of the femur (only one patella was difficult to digitize), some computer generated intersection points were not on the actual grid line intersection. This resulted in large areas of manual digitizing. All of these factors could be improved if the grid image were contrasted more with the surface. This could be accomplished through different lighting and grid projection. The slides used for the grids could be glass mounted which would reduce the distortion of the photo due to heat from the projector. A red or blue grid could give greater contrast, as could an opaque background. Lastly, a digitally produced slide would improve the grid line definition as the slides used in this study were based on photographs of a computer printed grid.

Additional improvements could be obtained with the use of a strobe projector with a power pack. Additional light sources in combination with a black felt or velvet background would also improve the contrasts of the posts as well as allowing for a shorter exposure time.

5.5 Patellofemoral Joint Surface Geometries

The surface geometries of all the limbs in this study were unique. Quantification of the

surface mathematically, allowed the calculation of several variables including curvatures, sulcus angles and contact areas. The combination of all these factors resulted in the ability to relate dynamic 3D PF tracking kinematics with known anatomy of the articulating surfaces.

5.5.1 Patellofemoral Joint Contact Area

Contact area is an indicator of the functional mechanics of the PF joint. The interaction of the articulating surfaces may give clues for the progression of cartilage degeneration, i.e. whether small contact area is a factor or if contact area migration is a factor or both. Many researchers have quantified patellofemoral contact in humans, e.g. Seedhom et al. (1977), Fujikawa et al. (1983), Huberti and Hayes (1984), Hefzy et al. (1992). To the best of this author's knowledge, this is the first time that human PF contact area has been reported using the photogrammetric (either stereo or multi-station) technique.

Hefzy et al. (1992) used a set-up very similar to the current study. Surface points were obtained by digitizing a grid, using a stylus pointer, on the surface and fitting it to a mathematical model. The contact areas calculated in this study are much larger (200 - 300 mm^2) than those reported by Hefzy et al. (1992). On the contrary, contact areas presented by Fulkerson and Hungerford (1990), compare well with the magnitudes presented in this study (ranging from 200 - 600 mm^2).

Grid spacing chosen for the resampling of the TPS and for the calculation of the contact area was shown to directly influence the contact area (Table 5). Therefore the results presented in this study are overestimates to the true contact. However, a grid spacing of 1.5 mm (used in this study) should only overestimate results by approximately 20 mm^2 or 3%. A faster computer would eliminate the problem of larger than ideal grid spacing in future

studies.

No contact area was found for flexion angles below 30° for all limbs in this study and two limbs (R1737 and L1702) did not have contact at 30°. Possible explanations for this lack of contact include: limits of the captured surface data and normal PF biomechanics where the patella has not seated in the trochlear groove at low flexion angles. The upper limit of the trochlear groove was not always captured on the images. For the images that had a good view of this area, the grid was distorted and difficult to distinguish. This would produce surface points very prone to error and therefore were not used. Other researchers have reported that the patella is not in contact at such low flexion angles which is consistent with the findings in this study.

At 30° of flexion, there was still very little contact found for the same reasons stated above. At 45°, 60°, 75° and 90° of knee flexion, the proximal/distal location of the contact resembles that of Hefzy et al. (1992). Limb L1702 of this study demonstrated a more proximal contact area at all flexion angles, than the rest of the limbs. One reason for this could be that the patellar tendon was unusually long in this particular specimen.

The literature reports inconsistent contact area results for flexion angles between 60°-90°. Aglietti et al. (1975), Seedhom and Tsubuku (1977) and Hefzy et al. (1992) reported that contact areas increase with increasing flexion. Hille et al. (1985), Ahmed et al. (1983). and Huberti and Hayes (1984) reported the contact area remains constant between 60° and 90° flexion whereas Matthews et al. (1977) reported a decrease in contact area in this flexion range. The results of this study have shown increases (L1632, L1702 and R1737) and a decrease (L1748). Explanations for these results involve the complex interaction between the specific PF geometries and kinematics. A large medial tilt (L1748) in combination with a

small medial patellar facet and very small patellar rotation and shift, resulted in smaller contact areas. Increases in PF contact were the result of the patella tilting, shifting and rotating in order to utilize larger patellar facets.

The centroid of contact was also calculated in this study. This has not been reported in literature previously. It is a good variable to quantitatively describe the movement of the patella throughout knee flexion. In this study, differences could be seen between limbs using the centroid of contact measure, that would not be as noticeable with contact area measures. No connection between the location of the centroid of contact and kinematics could be found. This suggests that lateral or central centroid location of overall contact is not a predictor of altered kinematics. Perhaps the progression of this centroid location on the femur could be useful in determining wear problems. L1702 had relatively small centroid progression compared to the other limbs. Although no degeneration was found in this joint, the donor was considerably younger than the others (57 years).

These results support the hypothesis that PF kinematics are directly related to geometry of the articulating surfaces. Further study will be required with a larger sample size to fully characterize the relations between PF kinematics and joint surface geometries.

5.5.2 Articular Surface Sulcus Angle

Clinical evaluation of AKP has addressed the relation between PF geometry and abnormally functioning knees. Patellar and femoral geometries have been classified to describe the abnormal function or kinematics. This study attempted to correlate geometries and kinematics using similar tools for classification that clinicians use.

The measurement for the articular surface sulcus angle in this study is an approximation

of the traditional sulcus angle. Clinically, the sulcus angle is determined from a radiograph. The 'sulcus' angle in this study was measured on the cartilage surface of the femur. The cartilage thickness in the trochlea is thicker than the cartilage on the condyles, as was demonstrated in limb R1737 in this study. This would give a slightly larger angle measurement than that calculated on bone.

The articular sulcus angles reported in this study are about 10 °larger than the normal sulcus (140° ±5) reported by Fulkerson and Hungerford (1990). This is partly due to the cartilage surface as explained above, but also due to the fact that a mathematical algorithm was used to calculated the angle. X-rays involved projecting a beam onto a film which is a certain distance away, creating a distortion. This distortion creates an error in the measurement. Farahmand et al. (1998) reported sulcus angles of 150° that remained consistent throughout knee joint flexion. Although not explicitly stated, these measurements were completed with the articular cartilage intact and closely match those reported here.

As well, the algorithm used to choose the points which are used to calculate the angle, are chosen as maximums and minimums across the surface. Slight alterations in alignment of the flexion/extension axis of the femur result in a skewed surface which can create other minimums. For example, if the centre of the sulcus angle measurement is always the centre of the trochlea, when the femur is tilted in the coronal plane, the minimum found by the algorithm is no longer the centre of the trochlea. Improvements could be made to this algorithm to search for the local minimum of the curve, which would be the inflection point. This should estimate the centre of the trochlea better. An interactive tool could also be developed to hand pick the point. This creates subjectivity to the measurement but would closely match the technique used by clinicians.

The relation between this measurement and contact areas is of interest. Limb L1748 was the only limb that demonstrated a decrease in contact area between 45° and 75° of knee joint flexion. It was also the only limb to show an increased sulcus angle (5°) in the same range of flexion. The other three limbs demonstrated either a decreased or constant sulcus angle between 45° and 75° knee joint flexion and increased contact areas. This is an interesting trend but it is unlikely that using this measurement alone would be indicative of joint function. An adaptation of the Merchant's congruence angle (the angular difference between the bisector of the sulcus angle and a line drawn from the centre of the trochlea through the apex of the patella), would be useful for measure. Currently it is used clinically as an indicator of patellar centralization and subluxation. It is measured on the bony surfaces but an extension of the technique to include articulating surfaces could be a very useful clinical tool.

Results from this study indicate the importance of knowing the articulation characteristics at specific flexion angles. The articular sulcus angle slice shows very distinctly how the shape of the patella and femoral condyles changes throughout flexion. Therefore, classifications based on the entire surface of the patella and femur are not good indicators of function. Perhaps this could explain the variable outcomes observed after surgical intervention.

5.6 Physiolocial Significance

The PF joint function in-vivo, is influenced by many factors that could not be addressed in this study. The directions of pull of the vastus medialis and vastus lateralis were not incorporated in this model. However, the alignment tests, where the force through the quadriceps tendon was moved 15° lateral and medial, was a way of testing the sensitivity of

the kinematics to this. These results in general, did not show large differences due to alignment (patellar tilt and shift were most affected), indicating that the omission of loading each individual tendon was reasonable. This result may explain why physiotherapy attempts to alter the strength of certain muscles may not create significant effects on the PF kinematics. However, in-vitro studies can not address the effects of alternating neuromuscular recruitment and co-ordination of the quadriceps muscles on PF kinematics. For example, during a regular gait cycle the quadriceps muscles work to flex and extend the knee as well as to induce some tibial ab/adduction and internal/external rotation. Previous studies as well as this study have indicated the tibial rotation and ab/adduction influence PF kinematics. The alignment of the knee with respect to the ground reaction force vector could also produce alterations to the PF kinematics. This study attempted to use dynamic, external loading in order to best replicate such situations. The tibia was free to rotate and 'respond' to the pull of the quadriceps tendon. In light of these limitations, it is believed that the data presented here reflects the basic functioning of the patella in-vivo.

5.7 Summary

The experimental protocol used in this study incorporated several new techniques for quantifying 3D PF joint motion including a unique development of anatomical coordinate systems, dynamic leg extension and continuous data collection. This is the first study to incorporate specific geometry into the description of human patellofemoral tracking. It is also the first to report human PF joint contact areas using an optical (no cartilage surface contact with probe or other substance) surface quantification method.

The kinematic results of this study reflect the variability previously reported in the

literature. This suggests that classification of abnormal knees on the basis of kinematics alone is difficult because of the variability in 'normal'. In general the patella demonstrated a wavering tilt, lateral shift and lateral rotation in combination with tibial adduction and an internal tibial rotation in the first 30 °of knee flexion and external rotation for 30°-90° knee flexion. Loading induced an increased medial patellar tilt, increased lateral patellar rotation and increased lateral patellar shift and induced internal tibial rotation and tibial abduction.

Joint contact area was shown to increase with increased knee joint flexion in 3 limbs and decreased between 45° and 75° flexion for one limb. This limb demonstrated a medial tilt through this range of motion which forced the patella to contact on a small medial condyle. The other 3 limbs seemed to 'optimize' their tracking to produce an increased contact area. Finally an adaptation of the clinical sulcus angle was introduced which used the centroid of contact and the surface normal at that point to define a 2D slice. This method provided new insights in joint congruence. Joint congruence changes throughout knee flexion angle. The 2D articular sulcus views demonstrate the cartilage articulation where the contact is occuring in contrast to an x-ray which does not have this capability.

In conclusion, this study illustrates the complex relationship of patellofemoral kinematics with articular surface geometries and contact areas. This is an important first step in understanding the intricate mechanical influences on patellofemoral kinematics. A larger study, incorporating more specimens needs to be completed to fully characterize this relationship and extrapolate the findings to clinical use. Of course obtaining in-vivo data would be ideal. Currently, MRI and fluoroscopy are being used to quantify joint surfaces and showing promising results. However, quantification of patellofemoral kinematics during gait and other functional activities do not have a viable, non-invasive alternative.

The results from the contact areas measured versus flexion angle suggest that the kinematics and individual geometry work together to determine contact. This finding could be extrapolated to suggest that total knee replacement should always include a cap on the patella which would be designed to 'fit' the geometry of the femoral implant trochlear groove. Leaving an original patella surface intact could lead to abnormal contact, unless the patella is able to alter patellar kinematics through muscular activity adequately. Additionally, these altered kinematics may result in pain arising from the soft tissues.

The clinical implications of the study indicate that abnormal geometry does not necessarily relate to abnormal kinematics. If abnormal kinematics are not compensated by retro-patellar surface geometry, abnormal contact area will occur. Abnormal contact could lead to abnormal stresses on the articular surfaces which may predispose the joint to degeneration. A long-range study that included clinical disorders associated with AKP would be beneficial in characterizing this problem.

In summary, through rigorous experimental quantification of combined PF joint kinematics and cartilage surface geometries, we have gained new insights into the complex interactions which lead to contact mechanics. This provides a foundation for further studies to understand the role of various injuries and pathologies on contact mechanics. From a clinical perspective, this study reinforces the statement made by Fulkerson and Hungerford (1990) that abnormal geometry does not necessarily present with PF problems and normal geometry does not always insure absence of disease.

References

Abdel-Aziz, Y. and Karara, H.M. (1971) Direct linear transformation from comparator coordinates in object space coordinates in close-range photogrammetry. Papers from the American Society of Photogrammetry Symposium on Close-Range Photogrammetry, Urbana, Illinois. 433, 1-18.

Aglietti, P., Insall, J.N., Walker, P.S., Trent, P. (1975) A new patella prosthesis. Clinical Orthopedic and Related Research, 107: 175-187.

Ahmed, A.M. and Burke, D.L. (1983) In-vitro measurement of static pressure distribution in synovial joint - Part II: retropatellar surface. Journal of Biomechanical Engineering, 105:226-236..

Ateshian, G.A., Kwak, S.D., Soslowsky, L.J., Mow, V.C. (1994) A stereophotogrammetric method for determining in situ contact in diarthrodial joints, and a comparison with other methods. Journal of Biomechanics 27, 111-124.

Ateshian, G.A. (1993) A B-spline least-squares surface-fitting method for articular surfaces of diarthrodial joints. Journal of Biomechanical Engineering 115, 366-373.

Ateshian, G.A., Rowenwasser, M.P., Mow, V.C. (1992) Curvature characteristics and congruence of the thumb carpometacarpal joint: differences between female and male joints. Journal of Biomechanics 25, 591-607.

Ateshian, G.A., Soslowsky, L.J., Mow, V.C. (1991) Quantitation of articular surface topography and cartilage thickness in knee joints using stereophotogrammetry. Journal of Biomechanics 24, 761-776.

Atkinson, K.B. (Ed.) (1996) *Close Range Photogrammetry and Machine Vision.* Whittles Publishing, Scotland, UK.

Banks, S.A., Otis, J.C., Backus, S.I., Laskin, R.S., Campbell, D.A., Lenhoff, M.A., Furman, G.L., Haas, S. Knee Arthroplasty Mechanics during Gait using Simulaneous Fluoroscopy and Motion Analysis. Proceedings of the International Society of Biomechanics XVIIth Congress, Calgary, AB, Aug 8-13, 378.

Barnes, K.P. (1998) Quantification of Alterations in Patellofemoral Joint Mechanics Following Anteromedialization of the Tibial Tubercle in a Cadaveric Model of Patellar Instability, M.Sc. Thesis, Calgary, University of Calgary.

Blankevoort, L., Huiskes, R., Lange, A. de (1988) The envelope of passive knee joint motion. Journal of Biomechanics 21, 705-720.

Blankevoort, L., Kuiper, J.H., Huiskes, R., Grootenboer, H.J. (1991) Articular contact in a three-dimensional model of the knee. Journal of Biomechanics 24, 1019-1031.

Boyd, S.K. (1997) A 3D In-Situ Model for Patellofemoral Joint Contact Analysis in the

Normal and Anterior Cruciate Ligament Deficient Knee, M.Sc. Thesis, Calgary, University of Calgary.

Boyd, S.K., Ronsky, J.L. (Submitted Dec. 1998) Normal and ACL-deficient in-situ measurement of patellofemoral joint contact. Journal of Applied Biomechanics.

Boyd, S.K., Ronsky, J.L., Lichti, R.D., Salkauskus, K., Chapman, M.A. (In press) Joint surface modelling with thin-plate splines. Journal of Biomechanical Engineering.
Cohen, Z.A., McCarthy, D.M., Ateshian, G.A., Kwak, S.D., Peterfry, C.G., Alderson, P., Grelsamer, R.P., Henry, J.H. and Mow, V.C. (1997) In vivo and in vitro knee joint cartilage topography, thickness, and contact areas from MRI. Transcripts in Orthopedic Research Society 22(2), 625.

Bray, R.C. and Roth, J.H. (1987) Clinical Evaluation of Anterior Knee Pain. Diagnosis, October: 69-96.

Cole, G.K., Nigg, B.M., Ronsky, J.L., Yeadon, M.R. (1993) Application of the joint coordinate system to three-dimensional joint attitude and movement representation: a standardization proposal. Journal of Biomechanical Engineering 115, 344-349.

Eckstein, F., Gavazzeni, A., Sittek, H., Haubner, M., Lösch, A., Milz, S., Englmeier, K.H., Schulte, E., Putz, R., Reiser, M. (1996) Determination of knee joint cartilage thickness using three-dimensional magnetic resonance chondro-crassometry. Magnetic Resonance in Medicine 36, 256-265.

Erkman, M.J. and Walker, P.S. (1974) A study of knee geometry applied to the design of condylar prostheses. Biomedical Engineering 9, 14-17.

Farahmand, F., Tahmasbi, M.N., Amis, A.A. (1998) Quantitative Study of the Quadriceps Muscles and Trochlear Groove Geometry Related to Instability of the Patellofemoral Joint. Journal of Orthopaedic Research 16, 136-143.

Fox, J.M., Pizzo, W. del (Eds.) (1993) *The Patellofemoral Joint*. McGraw-Hill, New York.

Frobin, W. and Hierholzer, E. (1983) Automatic measurement of body surfaces using raster stereography. Journal of Photogramm. Engng. Remote Sens. 49, 377-384.

Fujikawa, K., Seedhom, B.B. and Wright, V. (1983) Biomechanics of the patello-femoral joint. Part I: a study of the contact and the congruity of the patello-femoral compartment and movement of the patella. Engineering in Medicine 12(1), 3-11.

Fulkerson, J.P., Hungerford, D.S. (1990) *Disorders of the Patellofemoral Joint*. Williams & Wilkins, Baltimore.

Ghosh, S.K. (1979) *Analytical Photogrammetry*. Pergamon, N.Y.

Ghosh, S.K. (1983) A close-range photogrammetric system for 3-d measurements and perspective diagramming in biomechanics. Journal of Biomechanics 16, 667-674.

Goodfellow, J., Hungerford, D.S., and Zindel, M. (1976) Patello-femoral joint mechanics and pathology. 1. Functional anatomy of the patello-femoral joint. Journal of Bone and Joint Surgery 58B, 287-290.

Goodfellow, J., Hungerford, D.S., and Woods, C. (1976) Patello-femoral joint mechanics and pathology. 2. Chondromalacia patellae. Journal of Bone and Joint Surgery 58B, 291-299.

Greenwald, A.S. and O'Connor, J.J. (1971) The transmission of load through the human hip joint. Journal of Biomechanics 4, 507-528.
Grood, E.S., Suntay, W.J. (1983) A joint coordinate system for the clinical description of three-dimensional motions: application of the knee. Journal of Biomechanical Engineering 105, 136-144.

Haut, T.L., Hull, M.L., Howell, S.M. (1998) A high-accuracy three-dimensional coordinate digitizing system for reconstructing the geometry of diarthrodial joints. Journal of Biomechanics 31, 571-577.

Heegaard, J., Leyvraz, P.-F., Kampen, A. van, Rakotomanana, L., Rubin, P.J., Blankevoort, L. (1994) Influence of soft structures on patellar three-dimensional tracking. Clinical Orthopaedics and Related Research 299, 235-243.

Hefzy, M.S., Jackson, W.T., Saddemi, S.R., Hsieh, Y.-F. (1992) Effects of tibial rotations on patellar tracking and patello-femoral contact areas. Journal of Biomedical Engineering 14, 329-343.

Hille, E., Schulitz, K.P., Henrichs, C., Schneider, T. (1985) Pressure and contact surface measurements within the femoropatellar joint and their variations following lateral release. Archieves Orthopedic Trauma Surgery 104:275-282.

Huberti, H.H. and Hayes, W.C. (1984) Patellofemoral contact pressures - the influence of Q-angle and tendofemoral contact. Journal of Bone and Joint Surgery 66A, 715-724.

Huberti, H.H. and Hayes, W.C. (1988) Contact pressures in chondromalacia patellae and the effects of capsular reconstructure procedures. Journal of Orthopedic Research 6, 499-508.

Huiskes, R., Kremers, J., Lange, A. de, Woltring, H.J., Selvik, G., Rens, Th. J.G. van (1985) Analytical stereophotogrammetric determination of three-dimensional knee-joint geometry. Journal of Biomechanics 18, 559-570.

Kaufer, H. (1979) Patellar biomechanics. Clinical Orthopaedics and Related Research 144, 51-54.

Kettelkamp, D.B. and Jacobs, A.W. (1972) Tibiofemoral contact area: determination and implications. Journal of Bone and Joint Surgery 54A, 349-356.

Kralovic, B., Boyd, S., Ronsky, J. (1999) Dynamic in-situ measurements of

patellofemoral joint congruence. Proceedings of the International Society of Biomechanics XVIIth Congress, Calgary, AB, Aug 8-13, 615.

Kralovic, B., Boyd, S., Ronsky, J. (1998) Curvature characteristics of the patellofemoral joint surfaces. NACOB '98. Proceedings of the Third North American Congress on Biomechanics, Waterloo, ON, Aug. 14-18, 61-62.

Koh, T.J., Grabiner, M.K., Swart, R.J. de (1992) In vivo tracking of the human patella. Journal of Biomechanics 25, 637-643.

Kwak, S.D., Newton, P.M., Setton, L.A., and Grelsamer, R.P. (1993) Cartilage thickness and contact area determination in the canine knee joint. Transcripts in Orthopedic Research Society 18(2), 351.

Kwak, S.D., Colman, W.W., Ateshian, G.A., Grelsamer, R.P., Henry, J.H., Mow, V.C. (1997) Anatomy of the human patellofemoral joint articular cartilage: surface curvature analysis. Journal of Orthopaedic Research 15, 468-472.

Lafortune, M.A. (1984) The use of Intra-Cortical Pins to Measure the Motion of the Knee Joint during Walking. Ph.D. Thesis, The Pennsylvania State University, Pennsylvania.

Lafortune, M.A., Cavanagh, P.R., Sommer III, H.J., Kalenak, A. (1992) Three-dimensional kinematics of the human knee during walking. Journal of Biomechanics 25, 347-357.

Lancaster, P. Salkauskas, K. (1986) *Curve and Surface Fitting: An Introduction.* Academic Press Ltd., Toronto.

Lapin, L. (1990) *Probability and Statistics for Modern Engineering.* PWS-KENT Publishing Company, Boston.

Lichti, D.D. (1996) Constrained finite element method self-calibration. M.Sc. thesis. University of Calgary Press, Calgary.

Luo, Z.-P., Niebur, G.L., An, K.-N. (1996) Determination of the proximity tolerance for measurement of surface contact areas using a magnetic tracking device. Journal of Biomechanics 29, 367-372.

Matthews, L.S., Sonstegard, D.A., Henke, J.A. (1977) Load bearing characteristics of the patello-femoral joint. Acta Orthop Scand 48, 511-516.

Maquet, P.G., Van de Berg, A., Simonet, J. (1975) Femorotibial Weight-Bearing Areas. Journal of Bone Joint Surgery 57A, 766-771.

Moran, J.M., Hemann, J.H., Greenwald, A.S. (1985) Finger Joint Contact Areas and Pressures. Journal of Orthopedic Research 3, 49-55.

Mortenson, M.E. (1985) Geometric modelling. John Wiley and Sons, Inc. Toronto.

Mow, V.C., Ateshian, G.A., Spilker, R.L. (1993) Biomechanics of diarthrodial joints: a review of twenty years of progress. Journal of Biomechanical Engineering 115, 460-467.

Nagamine, R., Otani, T., White, S.E., McCarthy, D.S., Whiteside, L.A. (1995) Patellar tracking measurement in the normal knee. Journal of Orthopaedic Research 13, 115-122.

Nigg, B.M. and Herzog, W. (1994) Biomechanics of the Musculo-skeletal System. John Wiley & Sons Ltd., Toronto.

Norkin, C. and Levangie, P. (1983) Joint Structure and Function-A Comprehensive Analysis. F.A. Davis Company, Philadelphia.

Powers, M.J., Ronsky, J.L., Barnes, K., Bray, R. (1998) In-vivo quantification of dynamic three-dimensional patellar tracking. NACOB '98. The Third North American Congress on Biomechanics, Waterloo, Canada, Aug 14-18, 134-5.

Powers, M.J., Ronsky, J.L., Paulson, D.K. (1999) Effects of axial loading on patella tracking kinematics - A cadaver model. Proceedings of the International Society of Biomechanics XVIIth Congress, Calgary, AB, Aug 8-13, 616.
Rehder, U. (1983) Morphometrical studies on the symmetry of the human knee joint: femoral condyles. Journal of Biomechanics 16, 351-361.

Reider, B., Marshall, J.L., Ring, B. (1981) Patellar tracking. Clinical Orthopaedics and Related Research 157, 143-148.

Reinschmidt, C. (1996) Three-dimensional tibiocalcaneal and tibiofemoral kinematics during human locomotion - measured with external and bone markers. PhD. Thesis, University of Calgary Press, Calgary.

Ronsky, J.L. (1994) In-vivo Quantification of Patellofemoral Joint Contact Characteristics, Ph.D. Thesis, Calgary, University of Calgary.

Ronsky, J.L., Bogert, A.J. van den, Nigg, B.M., Wallace, C. (In press) Application of magnetic resonance imaging for non-invasive quantification of joint contact surface areas. Medical Engineering and Physics.

Ronsky, J.L., Boyd, S.K., Lichti, D.D., Chapman, M.A., Salkauskas, K. (1999) Precise measurement of cat patellofemoral joint surface geometry with multistation digital photogrammetry. Journal of Biomechanical Engineering 121, 196-205.

Ronsky, J.L., Herzog, W., Brown, T.D., Pedersen, D.R., Grood, E.S., Butler, D.L. (1995) In vivo quantification of the cat patellofemoral joint contact stresses and areas. Journal of Biomechanics 28, 977-983.

Rushfeldt, P.D., Mann, R.W. and Harris, W.H. (1981) Improved techniques for measuring in vitro the geometry and pressure distribution in the human acetabulum - I. Ultrasonic measurement of acetabular surface, sphericity and cartilage thickness. Journal of Biomechanics 14, 253-260.

Scherrer, P.K., Hillberry, B.M., Sickle, D.C. van (1979) Determining the in-vivo areas of contact in the canine shoulder. Journal of Biomechanical Engineering 101, 271-278.

Seedhom, B.B., Longton, E.B., Wright, V. and Dowson D. (1972) Dimensions of the knee. Ann. Rheum. Dis. 31, 54-58.

Seedhom, B.B. and Tsubuku, M. (1977) A technique for the study of contact between visco-elastic bodies with special reference to the patellofemoral joint. Journal of Biomechanics 10, 253-260.

Sheehan, F.T., Rebmann, A.J., Posh, J.C., Buchanan, T.S. (1999) A comparison of 3D in vivo kinematics in the unimpaired and ACL-deficient knee. Proceedings of the International Society of Biomechanics XVIIth Congress, Calgary, AB, Aug 8-13, 342.

Sikorski, J.M., Peters, J., Watt, I. (1979) The importance of femoral rotation in chondromalacia patellae as shown be serial radiography. Journal of Bone and Joint Surgery (Br) 61, 435-442.

Singerman, R.J., Pedersen, D.R. and Brown, T.D. (1987) Quantitation of pressure-sensitive film using digital image scanning. Exp. Mech 27, 99-103

Soderkvist, I., Wedin, P.-A. (1993) Determining the movements of the skeleton using well-configured markers. Journal of Biomechanics 26, 1473-1477.

Soslowsky, L.J., Flatow, E.L., Bigliani, L.U., Pawluk, R.J., Ateshian, G.A., Mow, V.C. (1992) Quantitation of in situ contact areas at the glenohumeral joint: a biomechanical study. Journal of Orthopaedic Research 10, 524-534.

Steindler, A., (1955) *Kinesiology of the Human Body*, Charles C. Thomas Publisher, Springfield, Illinois.

Van Kampen, A., Huiskes, R. (1990) The three-dimensional tracking pattern of the human patella. Journal of Orthopaedic Research 8, 372-382.

Veress, S.A., Lippert, F.G., Hou, M.C.Y., Takamoto, T. (1979) patellar tracking patterns measurement by analytical X-ray photogrammetry. Journal of Biomechanics 12, 639-650.

Walker, P.S. and Hajek, J.W. (1972) The load bearing area in the knee joint. Journal of Biomechanics 5, 581-592.

Wiberg, G. (1941) Roentgenographic and anatomic studies on the femoro-patellar joint. Acta Orthop. Scand. 12, 319-410.

Wijk, M.C. van (1980) Moire contourgraph - an accuracy analysis. Journal of Biomechanics 13, 605-613.

Wismans, J. (1980) A three-dimensional mathematical model of the human knee joint. Dissertation, Eindhoven University of Technology, The Netherlands.

Woltring, H.J. (1994) 3D attitude representation of human joint: a standardization proposal. Journal of Biomechanics 27, 1399-1414.

Woltring, H. (1990) Model and measurement error influences in data processing in *Biomechanics of Human Movement: Applications in Rehabilitation*, Sports and Ergonomics. (Ed. Berme, N. and Cappozzo, A.) Bertec Corporation: Worthington, Ohio, 203-237.

Yao, J.Q., Seedhom, B.B. (1991) A new technique for measuring contact areas in human joints - the '3S technique.' Proceedings - Institution of Mechanical Engineers 205, 69-72.

Yao, J.Q., Seedhom, B.B. (1993) Mechanical conditioning of articular cartilage to prevalent stresses. British Journal of Rheumatology 32, 956-965.